DEFENCE **RₐD** DÉFENSE

An Investigation in Interference Suppression for HF Surface Wave Radar

Hing C. Chan and Eric K.L. Hung
Defence Research Establishment Ottawa

DEFENCE RESEARCH ESTABLISHMENT OTTAWA

DISTRIBUTION STATEMENT A
Approved for Public Release
Distribution Unlimited

■✦■ National Défense
Defence nationale

Canadä

20001113 139

RESTRICTIVE LEGEND

DEFENCE **R&D** DÉFENSE

An Investigation in Interference Suppression for HF Surface Wave Radar

Hing C. Chan and Eric K.L. Hung
Ground Based Radar Group
Surface Radar Section

DEFENCE RESEARCH ESTABLISHMENT OTTAWA

TECHNICAL REPORT
DREO TR 2000-028
December 1999

Project
05AB11

ABSTRACT

An evaluation of the performance of the coherent sidelobe cancellation (CSLC) techniques in suppressing nighttime co-channel communications interference and ionospheric clutter in HF surface wave radars operating in coastal regions was carried out. In particular, the optimum order of execution among the three signal processing functions: (i) Doppler processing, (ii) digital beamforming and (iii) interference cancellation was of interest, in terms of signal-to-interference-plus-noise ratio (SINR) improvement and angular accuracy. The optimum order of execution between the above mentioned operations depends on the characteristics of the interference. In terms of ionospheric clutter, there is insufficient information to arrive at definitive conclusions. A preliminary examination of the temporal, spatial and spectral characteristics of ionospheric clutter was carried out to aid in the development of mitigating algorithms.

RÉSUMÉ

On a évalué la performance de techniques d'annulation cohérente des lobes latéraux (CSLC) pour la suppression des interférences nocturnes des communications radio dans le même canal et du clutter ionosphérique des radars à onde de surface HF exploités dans les régions côtières. En particulier, il s'agissait de déterminer l'ordre optimal d'exécution de trois fonctions de traitement des signaux, soit (i) le traitement Doppler, (ii) la conformation numérique du faisceau et (iii) l'annulation des interférences, à partir de l'amélioration du rapport signal/interférence plus bruit (SINR) et de la précision angulaire. L'ordre optimal d'exécution de ces fonctions dépend des caractéristiques des interférences. En ce qui a trait au clutter ionosphérique, il n'existe pas suffisamment d'information pour qu'on puisse tirer des conclusions définitives. Un examen préliminaire des caractéristiques temporelles, spatiales et spectrales du clutter ionosphérique a été effectué dans le but d'aider à établir des algorithmes d'atténuation.

EXECUTIVE SUMMARY

High frequency radars rely heavily on digital signal processing to improve target-detection performance. Central to the signal processing suite employed in HF radars are Doppler processing and digital beam-forming operations. In a practical operating environment, however, an HF radar must be able to function in the presence of severe interference that is orders of magnitude higher than the target return of interest. For high frequency radars operating in coastal regions, nighttime co-channel communications interference and direct over-head ionospheric clutter are of particular concern.

Co-channel communications interference is the dominant source of interference at nighttime. Occasionally it is present during day-light hours. Ionospheric clutter is a self-induced interference. Its effects are very much dependent on the system parameters such as operating frequency, antenna pattern, etc, and environmental parameters such as time-of-day, sun-spot cycle, etc.

Because both of these interferences possess some directional characteristics, they can be reduced by cancellation techniques. These techniques require a number of auxiliary antennas, the signals from which provide a means to estimate and subtract the interference from the main antenna outputs. These are collectively referred to as coherent sidelobe cancellation (CSLC) techniques. The basic structures of the cancellation schemes used against ionospheric clutter and communications interference are similar. The major difference lies in the way the correlation properties are estimated. The process of interference cancellation modifies the gain and phase responses of the array elements. A natural question that arises is whether there is a difference in the bearing estimate of a target as a result of changing the order of execution of Doppler processing, interference cancellation and digital beamforming. The work carried out in this report is aimed at obtaining some quantitative answers to the above question.

The results of the analysis indicated that performing CSLC before Doppler processing yielded the best result, both in SINR (signal-to-interference-plus-noise ratio) improvement and in angle-estimate accuracy, under the condition of a single dominant interference source. Performing CSLC after Doppler processing yielded the best result when the requirement is to suppress a weaker interference signal in the presence of a more dominant interference source such as sea clutter or a stronger interference signal from another direction.

Because ionospheric clutter is a self-induced interference and is isolated in both range and Doppler, certain techniques that are effective with communications interference in extracting the correlation properties among the main and auxiliary array antennas are ineffective against ionospheric clutter. A preliminary investigation of the temporal, spatial and spectral properties of ionospheric clutter was carried out. The results showed that the ionospheric clutter does originate from a finite number of directions and there appeared to be short-term stability in its correlation properties. Because of the available data were collected from a linear array, it was not possible to systematically evaluate various schemes. Consequently, it can only be conjectured that time-domain cancellation is probably more effective than Doppler-domain cancellation, although this is by no means certain.

The observed characteristics of ionospheric clutter are highly dependent on the operating radar frequency and time-of-day. The strong ionospheric clutter was observed to migrate in range on a relatively short time scale (tens of minutes). Because the range extent of the ionospheric clutter is relatively narrow, it may be possible to mitigate the effects of ionospheric clutter by a judicious use of frequency agility and advance tracking techniques.

High frequency surface radar has the potential to be an important wide area coastal surveillance sensor for Canada. The results of this work contribute to the continuing effort at DREO to improve the performance of this type of radars. Raytheon Systems Canada Limited (RSCL) has been an industrial partner of DND in the research and development of HF radars. This work was partially supported by RSCL through a contract with DREO.

Chan, Hing C., "An investigation in interference suppression for HF surface Wave Radar", DREO TR2000-028, Defence Research Establishment Ottawa.

SOMMAIRE

Les radars haute fréquence reposent largement sur le traitement numérique des signaux pour améliorer la détection des cibles. Les opérations de traitement Doppler et de conformation numérique du faisceau sont essentielles au traitement des signaux par les radars HF. Dans un environnement pratique, un radar HF doit toutefois être à même de fonctionner en présence d'interférences intense, plusieurs fois supérieures à l'écho d'une cible d'intérêt. Les interférences nocturnes des communications radios dans le même canal et le clutter ionosphérique revêtent une importance particulière pour les radars haute fréquence exploités dans les régions côtières.

Le principal type d'interférences durant la nuit est celui des communications radios dans le même canal. Il arrive également qu'il se produise durant le jour. Le clutter ionosphérique est un type de d'interférences auto-induit. Ses effets dépendent beaucoup des paramètres des systèmes, comme la fréquence de fonctionnement et le diagramme d'antenne, ainsi que des paramètres environnementaux, comme l'heure et le cycle des taches solaires.

Possédant tous deux certaines caractéristiques directionnelles, ces types d'interférences peuvent être réduits à l'aide de techniques d'annulation. Ces techniques exigent un certain nombre d'antennes auxiliaires dont les signaux permettent d'estimer et de soustraire les interférences des sorties d'antenne principales. On les appelle collectivement techniques d'annulation cohérente des lobes latéraux (CSLC). Les structures de base des techniques d'annulation utilisées sont semblables pour le clutter ionosphérique et les interférences radios. La principale différence réside dans la façon dont les propriétés de corrélation sont estimées. Le processus d'annulation des interférences modifie les réponses en gain et en phase des éléments du réseau. La question se pose naturellement de savoir s'il existe une différence de relèvement estimé d'une cible par suite d'un changement apporté à l'ordre d'exécution du traitement Doppler, de l'annulation des interférences et de la conformation numérique du faisceau. Les travaux décrits dans ce rapport visent à obtenir certaines réponses quantitatives à la question ci-dessus.

Les résultats de l'analyse ont indiqué que l'exécution de la CSLC avant le traitement Doppler donnait les meilleurs résultats, tant pour ce qui est de l'amélioration du rapport signal/interférence plus bruit (SINR) que de la précision angulaire, en présence d'une seule source d'interférence dominante. L'exécution de la CSLC après le traitement Doppler donnait les meilleurs résultats lorsqu'il fallait supprimer un signal d'interférence plus faible en présence d'une source d'interférence dominante, par exemple du clutter de mer ou des interférences plus intenses en provenance d'une autre direction.

Comme le clutter ionosphérique est un type d'interférence auto-induit, isolé quant à la distance et à l'effet Doppler, certaines techniques d'extraction des propriétés de corrélation d'antennes réseaux principales et auxiliaires, efficaces pour le traitement des interférences radios, s'avèrent peu performantes contre le clutter ionosphérique. On a effectué une étude préliminaire des propriétés temporelles, spatiales et spectrales du clutter ionosphérique. Les résultats ont révélé que le clutter ionosphérique ne provient pas d'un nombre fini de directions et que ses

configurations. On doit donc se limiter à supposer que l'annulation dans le domaine temporel est probablement plus efficace que l'annulation dans le domaine Doppler, bien que cela ne soit aucunement confirmé.

Les caractéristiques observées du clutter ionosphérique dépendent fortement de la fréquence de fonctionnement du radar et de l'heure. On a observé que du clutter ionosphérique intense pouvait se déplacer en distance sur une période de temps relativement courte (de l'ordre des dizaines de minutes). Comme les limites de distance du clutter ionosphérique sont relativement étroites, il pourrait être possible d'atténuer les effets du clutter ionosphérique en faisant un usage judicieux des techniques d'agilité en fréquence et de poursuite anticipée.

Le radar de surface haute fréquence peut devenir un important outil de surveillance de larges régions côtières canadiennes. Les résultats des travaux décrits contribuent aux efforts permanents du CRDO en vue d'améliorer les performances de ce type de radar. Raytheon Systems Canada Limited (RSCL) est un des partenaires industriels du MDN en matière de recherche et développement de radars HF. RSCL contribue partiellement à ces travaux dans le cadre d'un marché conclu avec le CRDO.

Chan, Hing C.,"Une étude sur la cancellation d'interférence pour les radars décamétrique à onde de surface," CRDO TR2000-028, Centre de Recherches et Développement Ottawa.

TABLE OF CONTENTS

TABLE OF CONTENTS (CONTINUE)

LIST OF FIGURES

LIST OF FIGURES (Continue)

LIST OF TABLES

1. INTRODUCTION

High frequency radars rely heavily on digital signal processing to improve target-detection performance. Central to the signal processing suite employed in HF radars are Doppler processing and the beam-forming operations. In a practical operating environment, however, an HF radar must be able to function in the presence of severe interference that is orders of magnitude higher than the target of interest. To minimize the detrimental effects of interference, cancellation techniques are used to exploit the directional characteristics of the interference signals. These techniques require a number of auxiliary antennas, the signals from which provide a means to estimate and subtract the interference from the main antenna outputs. This subtraction modifies the gain and phase responses of the array elements. A natural question that arises is whether there is a difference in the bearing estimate of a target as a result of changing the order of execution of Doppler processing, interference cancellation and digital beamforming. The work carried out in this report is aimed at obtaining some quantitative answers to the above question.

For high frequency radars operating in coastal regions, there are four major sources of interference, namely, sea clutter, ionospheric clutter, meteor clutter and co-channel communications interference. For sea clutter, there have been many attempts at its cancellation. Most of the techniques that have been reported [1,2] attempt to suppress the sea clutter in the Doppler domain. At the present time, there is no consensus as to what the most effective technique is regarding sea-clutter suppression. Consequently, sea clutter will not be included in this study.

Meteor clutter is a transient phenomenon in that the duration of the echoes from meteoroid trails is short compared with the coherent integration time (CIT) interval. Because meteoroids are isolated both temporally and in range, it is very difficult to obtain reliable correlation properties of the array samples before the interference vanishes. A reasonably effective means of reducing the effects of meteor clutter is impulse excision.

For the remaining two interference sources, there are effective cancellation techniques that can be employed. The basic structures of the cancellation schemes against ionospheric clutter and communications interference are very similar. The major difference lies in the way the correlation properties are estimated.

Ionospheric clutter is a self-generated interference. The ionosphere is a region of ionized gas layers (D, E and F) above the surface of the earth. The echoes from these ionized layers comprise both a specular and a diffuse component. The specular component is confined to a small number of range and Doppler bins. The diffuse component, on the other hand, could occupy a large extent both in Doppler and in range. Figure 1 shows the signal received from an HFSWR in the range-Doppler domain. In this figure, the radar look direction was at boresight. The radar transmits a frequency modulated interrupted continuous waveform (FMICW) with a sweep-bandwidth of 125 kHz at a radar frequency of 5.8 MHz. Two clusters of ionospheric interference can be seen: (i) from around 100 km to over 150 km (associated with reflections from the E-layer), and (ii) from about 210 km to beyond 300 km (associated with reflections from the F-layer). The Doppler extent of the ionospheric interference was a few Hertz.

1

CAPE RACE

DATE: 27-OCT-1994
TIME: 12:11:15

FREQ. =   5.81 MHz
WAVEFORM = FMICW
BW = 125.0 kHz
WRF =   9.18 Hz
BEAM No.1 (Boresight)

INTEGRATION TIME =   27.89 sec.

300 km

200 km

100 km

1.2 km

230 km

-230 km

RANGE

VELOCITY

-50 dB
-60 dB
-70 dB
-80 dB
-90 dB
-100 dB
-110 dB

MAGNITUDE
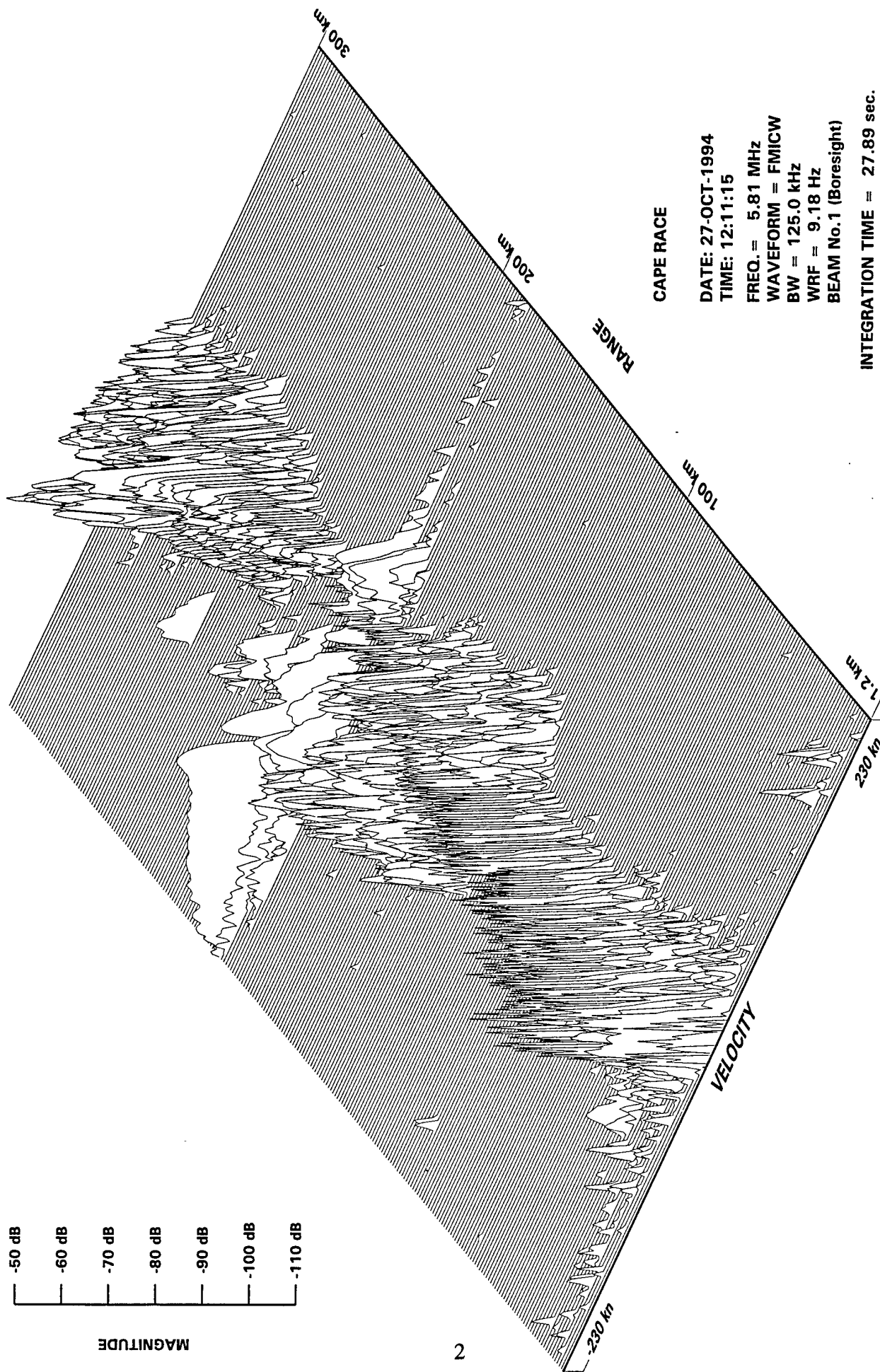
Figure 1. Typical ionospheric clutter in range-Doppler (velocity) space.

An important characteristic of ionospheric clutter is that it is range specific, and its statistical properties may be estimated more reliably using time-averaging of the sample from the same range bin.

Co-channel communications interference is the dominant source of interference at nighttime. Occasionally it could be present during day-light hours. Figure 2 shows the received signal from one of the receiver channels of the Cape Bonavista HFSWR at about 1800 hour in the Doppler-range domain after which the transmitter was turned off. There are six plots in Figure 2, corresponding to six contiguous CITs of 20-second duration. It can be seen that during the last two CITs the noise level had risen significantly. In this figure, the Doppler axis has 200 points, and the Doppler increment was 0.049 Hz. Hence the Doppler domain was about 9.8 Hz, centred about 0 Hz. Figure 3 shows the bearing-Doppler profile of the signal received by the radar for a particular range bin. The plots in Figure 3 were obtained by forming beams pointing at different directions using the antenna array samples. These plots show that there was a distinct directional characteristic to this interference. More importantly, it is observed that the directional characteristic of the interference was more or less range independent. This permits the use of range-averaging to extract the statistical parameters of the interference components required for cancellation.

2.   METHODOLOGY

The objectives of this study are to evaluate quantitatively the accuracy of the bearing estimate in the presence of interference and to determine whether there is a difference in the accuracy of the bearing estimate resulting from changing the order of operations among Doppler processing, interference cancellation and digital beamforming. On the basis of the above analysis we shall recommend an optimal order of processing.

To achieve the above objectives, the following steps will be followed: (i) select the appropriate data set, (ii) inject synthesized target samples in the experimental data, (iii) select the appropriate interference cancellation scheme, (iv) carry out Doppler processing, interference cancellation and digital beamforming in various orders of execution, and (iv) compare the accuracy of the target bearing estimate and the improvement achieved by various processing schemes.

2.1   Interference cancellation algorithms

Interference suppression or cancellation algorithms exploit the directional characteristics of the interfering signals by applying a set of optimum weights to the radar receiver samples such that the contribution of the interference components to the array output is minimized. These techniques were originally developed for communications systems in which both the desired signal and the interference are present over an extended period of time. For radars, the desired signal is the echo from a target, which is present only for a short duration (the length of the transmit pulse). The interference, on the other hand, would be present over a much longer period of time.

3
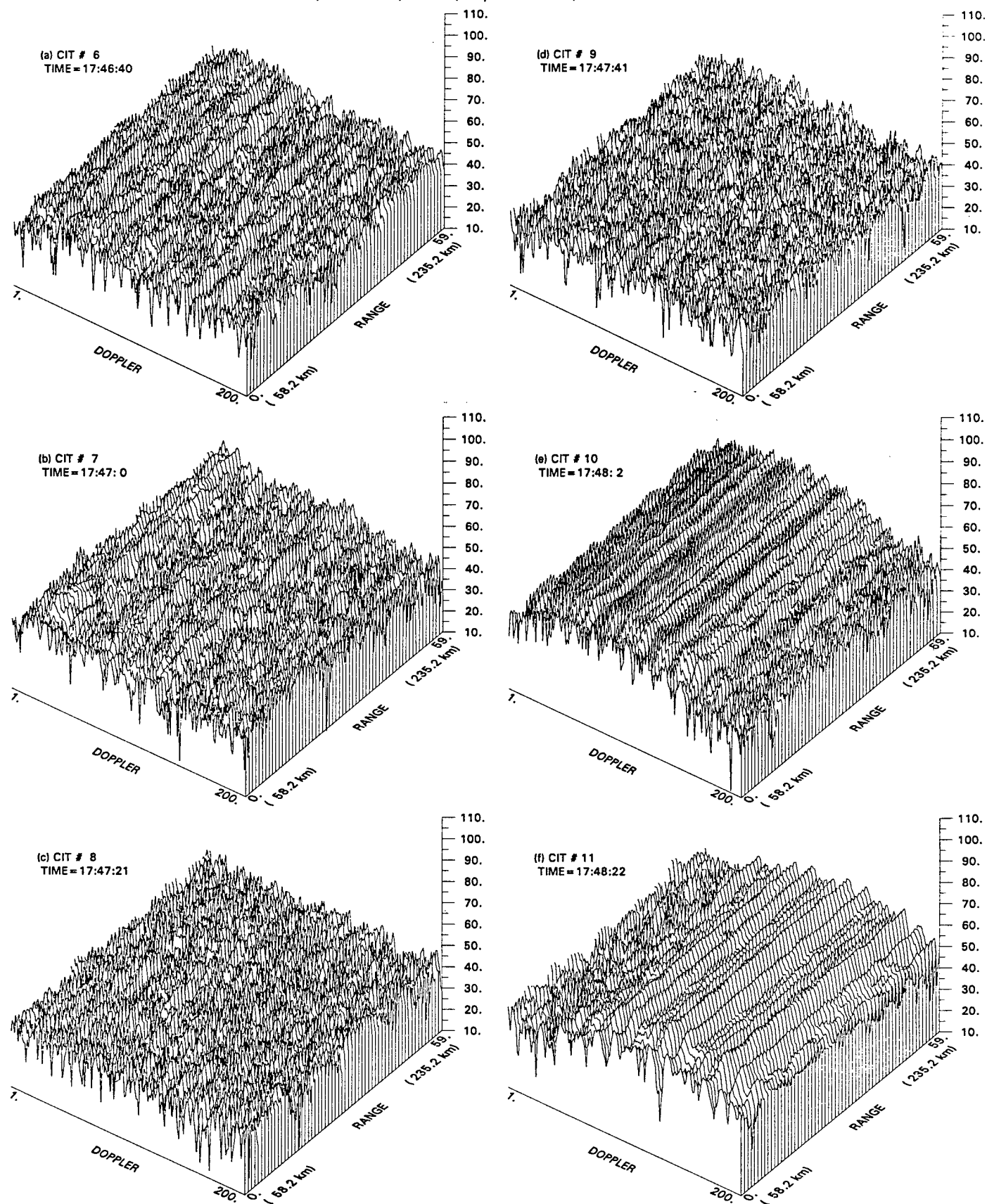
Figure 2. Variation of noise and interference levels with time.

0923-12; AIR-DOP. DATA; Cape Bonavista; RNG.#30(148.2 km); FREQ. = 3.7 MHz
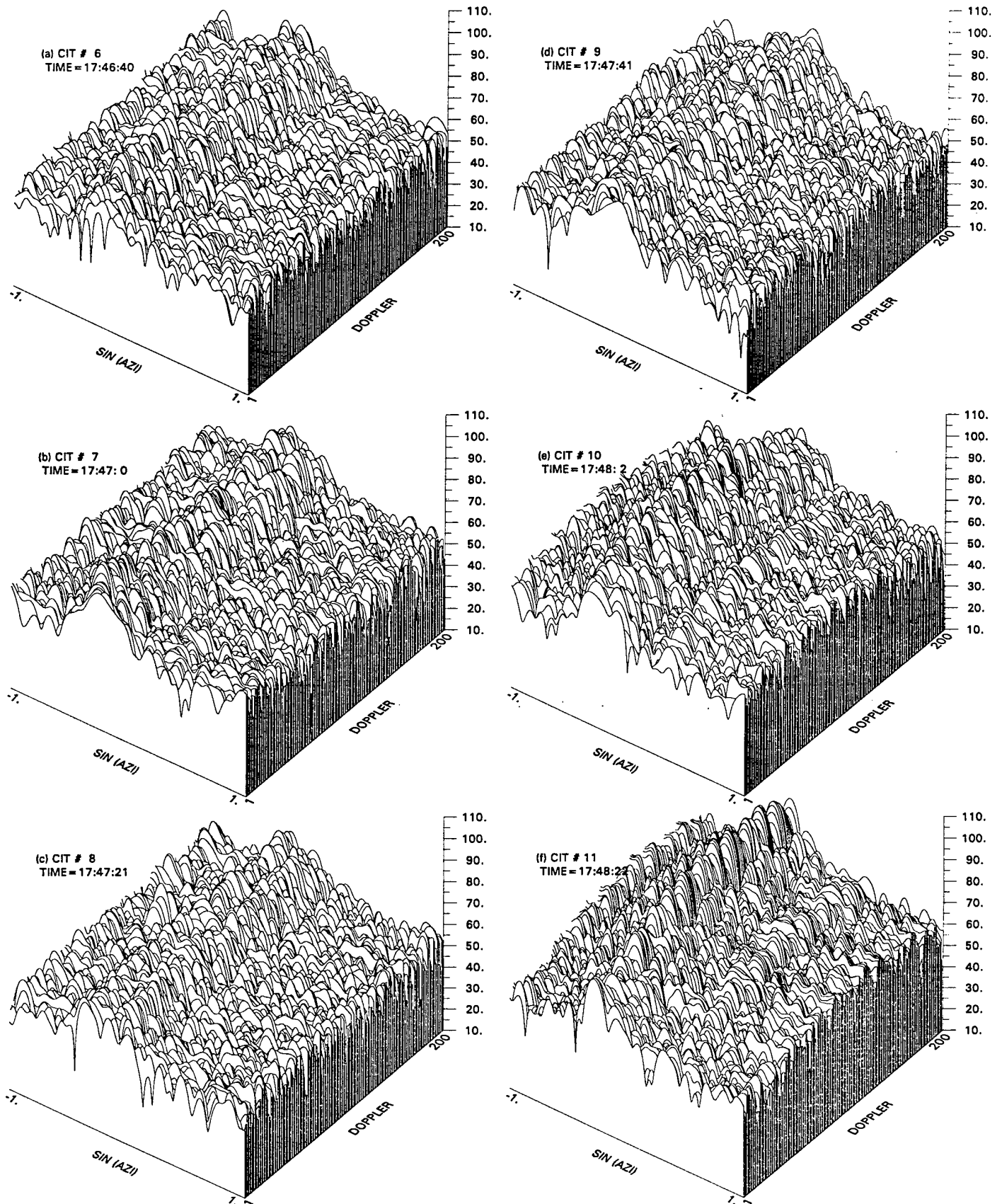
Figure 3. Directional characteristics of interference signal.

5

There are many different interference suppression algorithms available. In this study we shall consider a particular method based on coherent side-lobe cancellation (CSLC) [3,4] because this method is most suited for the signal processing hardware architecture implemented in the radar developed for surveillance of the east coast of Canada.

The general schematic diagram of the coherent sidelobe cancellation algorithms is shown in Figure 4. There are N main-array antennas, arranged in a linear array, which are used to form beams pointing at various directions. In addition there are M auxiliary-array antennas, which may or may not be collinear with the main-array antennas, used exclusively for deriving the parameters used in the interference cancellation schemes. Each antenna element is coupled to an independent coherent receiver from which time series for each range bin can be obtained. The interference cancellation is carried out for each range bin.

The derivation of the basic cancellation algorithm is well documented. We shall quote references and describe the algorithm below.

Referring to Figure 4, the signals from the main and auxiliary antennas for a given range bin are represented by vectors $\underline{x} = [x_0, x_1, \ldots x_{N-1}]^T$ and $\underline{y} = [y_0, y_1, \ldots, y_{M-1}]^T$, respectively, where the subscript is the channel (or antenna element) index, and the superscript, T, denotes transpose. We shall refer to $\underline{x}$ and $\underline{y}$ as the main-array snapshot and auxiliary-array snapshot, respectively.

An estimate of the interference component in $\underline{x}$ is given by $\underline{z}$, where

$$\underline{z} = [z_0, z_1, \ldots, z_{N-1}]^T \tag{1}$$

and

$$z_n = \underline{w}_n^H \underline{y}_c \tag{2}$$

Vector $\underline{w}_n$ is the set of optimal weights for the n-th main-array element. The superscript H denotes complex conjugate transpose. Vector $\underline{y}_c$ is the auxiliary array snapshot corresponding to the main array snapshot from which the interference estimate is to be subtracted. It is not to be confused with $\underline{y}$ which are used to compute the covariance matrix and the correlation vectors.

The interference estimates are subtracted from the main-array snapshot, and the resulting signal vector is $\underline{\tilde{x}} = [\tilde{x}_0, \tilde{x}_1, \ldots, \tilde{x}_{N-1}]^T$, where

$$\tilde{x}_n = x_n - \underline{w}_n^H \underline{y}_c \tag{3}$$

The modified snapshot is then fed to the beamformer, yielding:
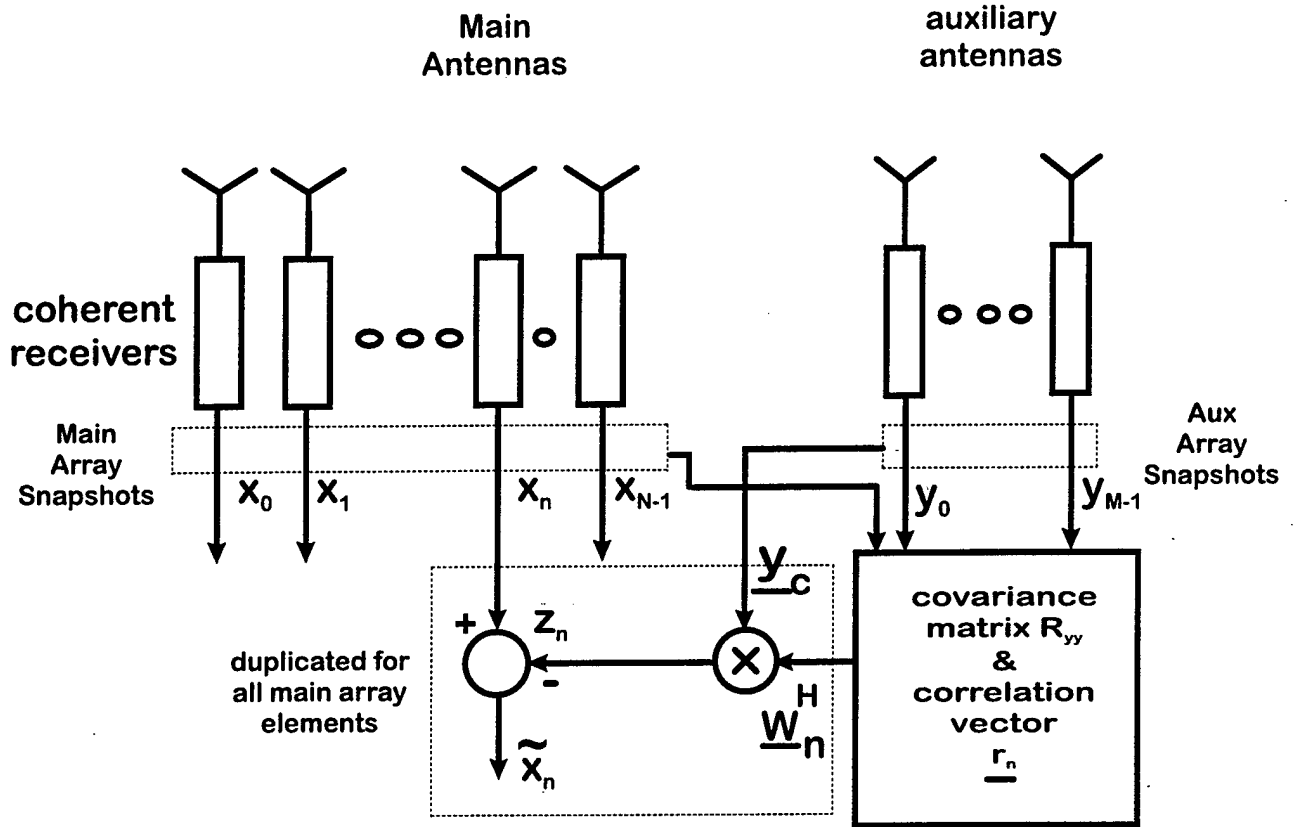
Figure 4. Schematic diagram of an interference cancellation algorithm .

$$u(\theta) = \underline{v}^H \underline{\tilde{x}} \qquad (4)$$

where $\underline{v}$ is the main array beam steering vector given by:

$$\underline{v} = [1, e^{j\frac{2\pi d}{\lambda}\sin\theta}, \ldots, e^{j\frac{2\pi(N-1)d}{\lambda}\sin\theta}]^T. \qquad (5)$$

Here, λ is the radar wavelength, d is the antenna element spacing and θ is the beam steering angle.

In (5) the following conventions are adopted: (a) element n=0 is the left-most antenna and (b) θ is measured clockwise from boresight.

The optimum weight vector $\underline{w}_n$ is obtained from the product between the inverse of the covariance matrix R_{yy} and the correlation vector, $\underline{r}_n$:

$$\underline{w}_n = R_{yy}^{-1} \underline{r}_n \tag{6}$$

The covariance matrix and the correlation vectors are defined as:

$$R_{yy} = E[\underline{y} \, \underline{y}^H] \tag{7}$$

and

$$\underline{r}_n = E[\underline{y} \, x_n^*] \tag{8}$$

for n = 0,1,2,..,N-1,

respectively, where E denotes expected value.

The correlation vector represents the correlation between the elements of the main array and those of the auxiliary array.

Depending on the type of interference to be cancelled, there is a variety of ways in which the covariance matrix and the correlation vectors can be computed. The most common ones are (a) time-averaging and (b) range averaging. The array snapshots are samples of the radar returns corresponding to a particular range bin. Consequently there is one snapshot for each transmitted waveform per range bin. Denoting the time and range dependencies of the snapshots by indices i and j, respectively, we have:

$$\underline{x}(i,j) = [x_0(i,j), \, x_1(i,j), \, ..., \, x_{N-1}(i,j)]^T \tag{9}$$

and

$$\underline{y}(i,j) = [\, y_0(i,j), \, y_1(i,j), \, . \, . \, . \, . \, , \, y_{M-1}(i,j)]^T \tag{10}$$

2.1.1 Time-averaging.

The covariance matrix and the correlation vectors can be obtained by fixing the range index j and averaging over a number of preceding snapshots, i.e.

$$
R_{yy} = \frac{1}{I}\sum_{i=1}^{I}
\begin{bmatrix}
y_0(i,j)y_0^*(i,j) & y_0(i,j)y_1^*(i,j) & .. & .. & y_0(i,j)y_{M-1}^*(i,j) \\
y_1(i,j)y_0^*(i,j) & & .. & .. & .. & y_1(i,j)y_{M-1}^*(i,j) \\
.. & & .. & .. & .. & .. \\
.. & & .. & .. & .. & .. \\
y_{M-1}(i,j)y_0^*(i,j) & & .. & .. & .. & y_{M-1}(i,j)y_{M-1}^*(i,j)
\end{bmatrix}
\tag{11}
$$

and

$$
\underline{r}_n = \frac{1}{I}\sum_{i=1}^{I}\left[y_0(i,j)x_n^*(i,j) \quad y_1(i,j)x_n^*(i,j) \quad .. \quad .. \quad y_{M-1}(i,j)x_n^*(i,j)\right]^T
\tag{12}
$$

where I is the number of time samples used in the averaging.

2.1.2 Range-averaging.

Alternatively, if there is a high degree of correlation in the interference components among snapshots that are far apart in range, the covariance matrix and the correlation vectors can be obtained by fixing the snapshot index i and averaging over a number of range samples, i.e.

$$
R_{yy} = \frac{1}{J}\sum_{j=1}^{J}
\begin{bmatrix}
y_0(i,j)y_0^*(i,j) & y_0(i,j)y_1^*(i,j) & .. & .. & y_0(i,j)y_{M-1}^*(i,j) \\
y_1(i,j)y_0^*(i,j) & & .. & .. & .. & y_1(i,j)y_{M-1}^*(i,j) \\
.. & & .. & .. & .. & .. \\
.. & & .. & .. & .. & .. \\
y_{M-1}(i,j)y_0^*(i,j) & & .. & .. & .. & y_{M-1}(i,j)y_{M-1}^*(i,j)
\end{bmatrix}
\tag{13}
$$

and:

$$r_n = \frac{1}{J} \sum_{j=1}^{J} \left[y_0(i,j)x_n^*(i,j) \quad y_1(i,j)x_n^*(i,j) \quad .. \quad .. \quad y_{M-1}(i,j)x_n^*(i,j) \right]^T \qquad (14)$$

where J is the number of range samples used in the averaging.

2.2   Order of execution.

The order in which the three operations, (a) interference suppression, (b) Doppler processing and (c) digital beam-forming, are executed will have some effect on the over-all performance in terms of target detection and bearing estimate. The relative merits of various orders of execution will also influence the choice of methods for computing the covariance matrix and the correlation vectors. We shall consider each case and determine whether they should be investigated in detail. The possible combinations are the following:

(i)   Interference suppression; Doppler processing; digital beamforming,
(ii)   Interference suppression; digital beamforming; Doppler processing,
(iii)   Doppler processing; interference suppression; digital beamforming,
(iv)   Doppler processing; digital beamforming; interference suppression,
(v)   Digital beamforming; interference suppression; Doppler processing,
(vi)   Digital beamforming; Doppler processing; interference suppression.

Obviously, cases (i) and (ii) should yield identical results, because both Doppler processing and digital beamforming are performed using FFTs. Since the FFT is a linear operation, the order of execution is interchangeable. The same argument applies to cases (iv) and (vi). Generally, array processing will alter the relative amplitude and phase relationships among the elements and may produce different results if the order of execution is interchanged between interference suppression and digital beamforming. This would be the case if the main array elements are also used in the computation of the covariance matrix. For the interference cancellation schemes employed in this study, case (ii) and case (v) should yield identical results. The reasons follow.

In case (v) the main-array snapshot is first multiplied by the beam-steering vector $\underline{v}$ to form a beam in direction:

$$u'(\theta) = \underline{v}^H \underline{x} \qquad (15)$$

The result can then be considered as the output of a single antenna element, and interference cancellation as defined in (1) and (2) can be applied, yielding:

10

$$z' = \underline{w}^H \underline{y}_c = \left(R_{yy}^{-1}\underline{r}'\right)^H \underline{y}_c \qquad (16)$$

and

$$\underline{r}' = \underline{y}\,(u')^* = \underline{y}\left(\underline{v}^H\underline{x}\right)^* \qquad (17)$$

Subtracting the interference estimate z' from (14) yields

$$u' - z' = \underline{v}^H\,(\underline{x}-\underline{z}) = u \qquad (18)$$

In subsequent discussions, we shall refer to the class of interference suppression schemes that are based on coherent sidelobe cancellation as "interference cancellation". For this class, there are only two distinct cases that need to be considered:

- Interference suppression in the time-domain (i.e. before Doppler processing), followed by Doppler processing and beamforming;
- Interference suppression in the Doppler domain (i.e. Doppler processing followed by interference cancellation and digital beamforming).

For each of the above cases, there are the options of using time-averaging or range-averaging to compute the covariance matrix and the correlation vectors. For the case of interference cancellation in Doppler domain, there is a concern in the appropriateness of using time-averaging to calculate the covariance matrix and correlation vectors because a large number of pulses is required to form the Doppler spectrum. Hence, a significant amount of time would have elapsed if a number of spectra is to be used, making decorrelation of the samples highly likely.

We shall investigate the following cases:

(a)   perform interference cancellation in the time domain (i.e. pulse by pulse) using time-averaging for the computation of the correlation estimates.

(b)   perform interference cancellation in the time domain using range-averaging for the computation of the correlation estimates.

(c)   perform interference cancellation in the Doppler domain (i.e. Doppler by Doppler) using the range-averaging method to compute the correlation estimates.

11

2.2.1 Various configurations

Figure 5 shows a schematic diagram of the basic coherent sidelobe cancellation algorithm. For a particular implementation of the interference cancellation, the appropriate samples from each antenna element (both main and auxiliary) are placed in a data buffer. A segment of the data in the buffer, starting from sample $\#I_1$ and ending at sample $\#I_2$, is used for the calculation of the covariance matrix and correlation vectors. The inverted covariance matrix and the correlation vectors are used to derive the weight vector $\underline{w}_n$. To perform cancellation on a particular data sample in the buffer, say the i-th sample of the n-th main antenna element $(x_n(i))$, the corresponding sample of auxiliary array data vector is multiplied with the weight vector $\underline{w}_n$ and subtracted from the main antenna sample $x_n(i)$.

The calculation of the covariance matrix and the correlation vectors is essentially a process of extracting the correlation properties of the interference process among antenna elements. Hence we shall refer to these, collectively, as correlation estimates. There is a variety of ways to obtain the correlation estimates, depending on what type of data are placed in the data buffers in Figure 5 and how they are utilized.

For interference processes that are isolated in range, such as ionospheric clutter, the use of time averaging of samples from a fixed range bin to get the correlation estimates is more appropriate.

The disadvantage in employing time averaging for the correlation estimates is that it requires a number of snapshots to obtain the results. If the time between the estimation process and the application of the results exceeds the decorrelation time of the interference process, poor cancellation will result. Consequently, it is necessary to employ a sliding window so that the time lag between the estimate and cancellation process is minimized.

Another disadvantage is that, since data samples used for the correlation estimates also come from the range bin to which cancellation is to be applied, there is a possibility that the estimates includes the target component, thereby cancelling some of the target component as well. This cannot be avoided. However, in most cases the interference energy is significantly higher than the target energy and improvement can still be obtained.

The following is a list of different configurations whose interference suppression performance will be investigated.

(a)   Time-domain cancellation with sliding-time-window averaging

Figure 6 shows the type of data and boundaries of the data used for the calculation of the correlation estimates for the case of time-domain cancellation with sliding-time-window averaging. In this case, the data to be stored in the data buffer are time samples (either individual channel or beam-formed) of a fixed range bin over a number (NFFT + NAVG) of consecutive pulses. It is assumed that a Doppler processor follows operating on NFFT cancelled samples. For each time sample to be cancelled, NAVG preceding samples are used for the computation of the

12
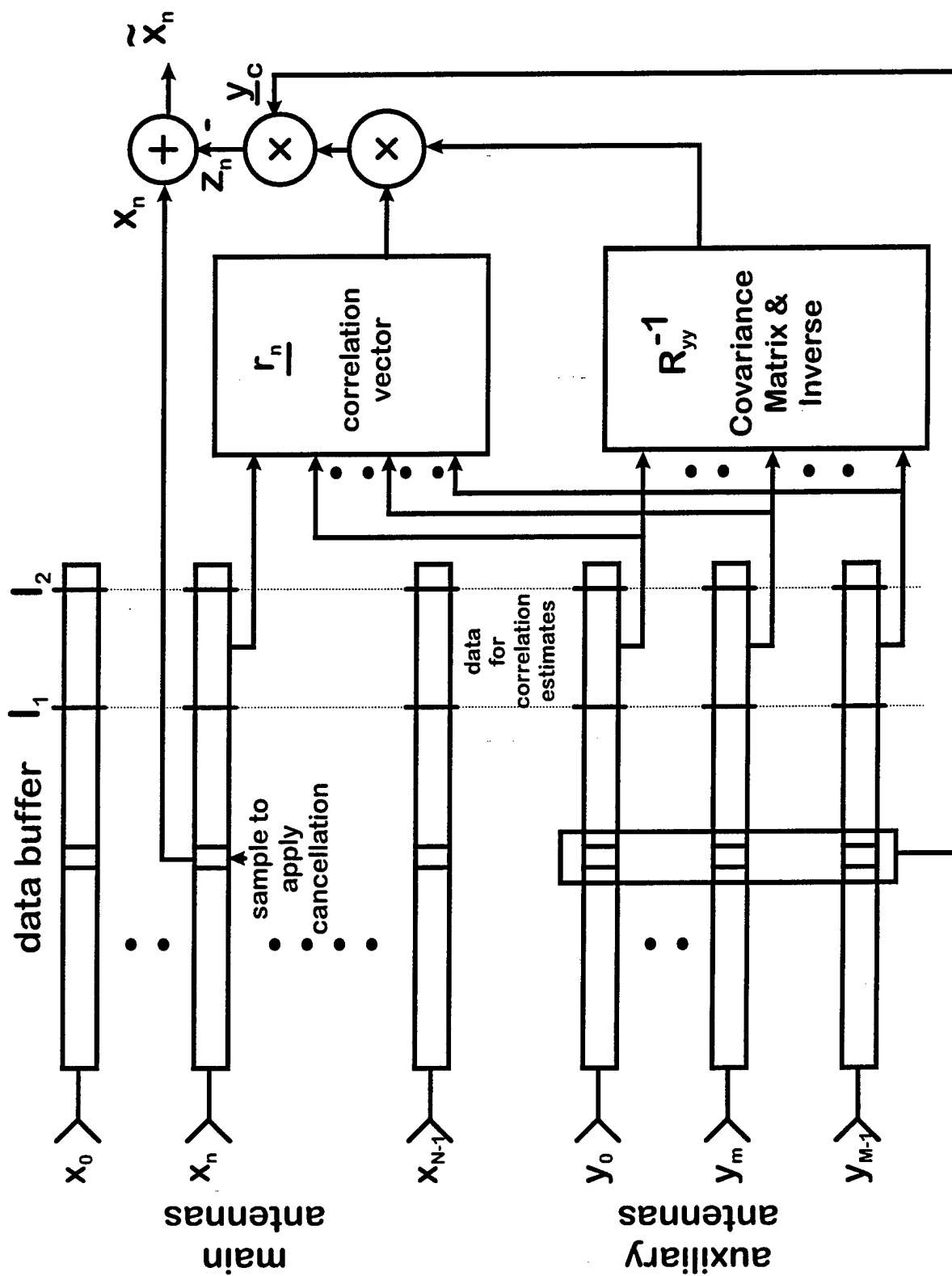
Figure 5. Schematic diagram of a coherent side-lobe canceller.

13
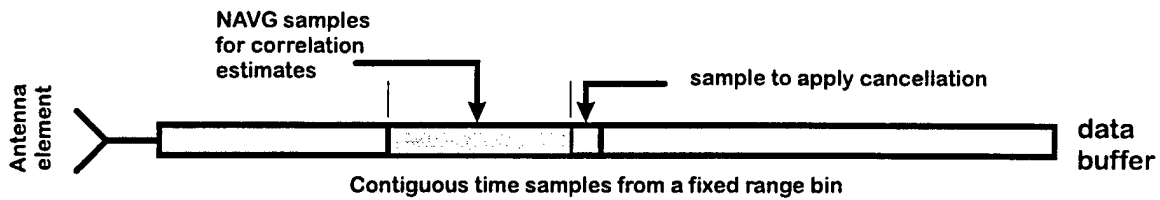
Figure 6. Time-domain cancellation with sliding-time- window averaging.
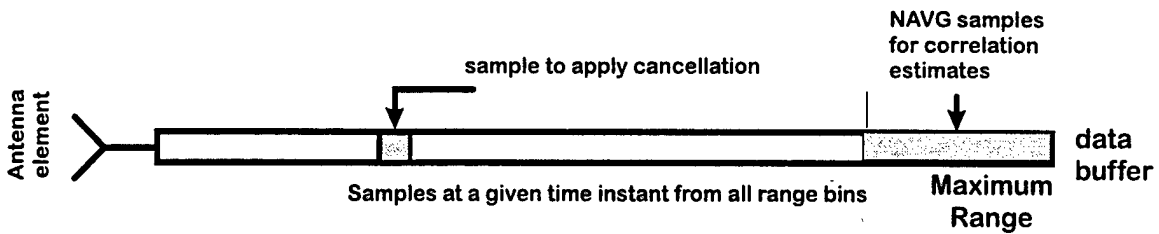
Figure 7. Time-domain cancellation with fixed-range-window averaging.
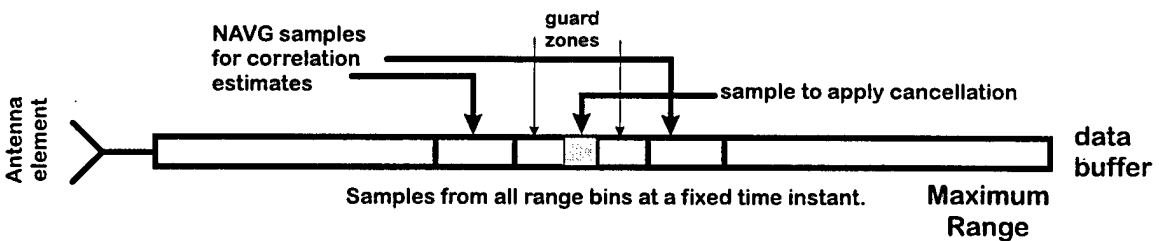
Figure 8. Time-domain cancellation with sliding-range-window averaging.
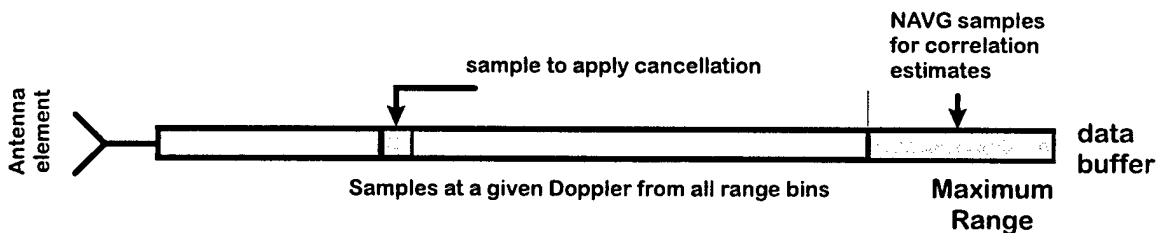
Figure 9. Doppler-domain cancellation with fixed-range-window averaging.
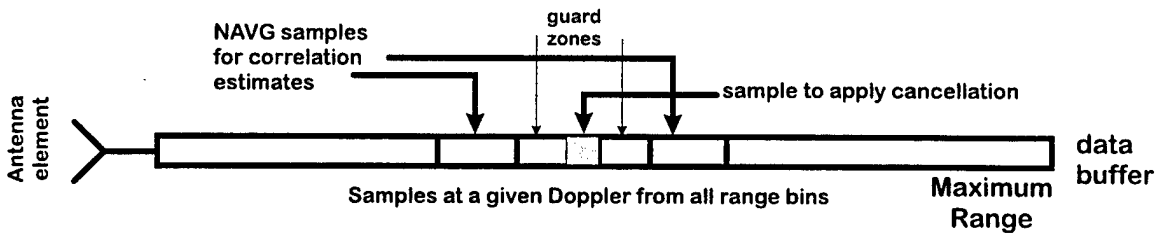
Figure 10. Doppler-domain cancellation with sliding-range- window averaging.

14

correlation estimates (hence the number NFFT + NAVG).

(b)   Time-domain cancellation with fixed-range-window averaging.

Figure 7 shows the type of data and the boundaries of the data used for calculating the correlation estimates for the case of "Time-domain cancellation with fixed window range averaging". In this case, the data to be stored in the data buffer are time samples (either individual channel or beam-formed) of a given snapshot for all the range bins. The last NAVG range samples are used to calculate the correlation estimates.

(c)   Time-domain cancellation with sliding-range-window averaging.

Figure 8 shows the type of data and the boundaries of the data used for calculating the correlation estimates for the case of "Time-domain cancellation with sliding-range-window averaging". In this case, the data to be stored in the data buffer are time samples (either individual channel or beam-formed) of a given snapshot for all the range bins. The data samples used for the calculation of the correlation estimates are divided into two parts, separated by a guard zone on either side of the sample to be cancelled. The guard zones are used to ensure that the target component will be excluded from the correlation estimates.

(d)   Doppler-domain cancellation with fixed-range-window averaging.

A similar scheme as described in (b) may be used to perform cancellation on Doppler samples. Figure 9 shows the type of data and the boundaries of the data used for calculating the correlation estimates for the case of "Doppler-domain cancellation with fixed-range-window averaging". In this case, the data to be stored in the data buffer are samples of a particular Doppler of a given snapshot for all range bins. A number (NAVG) of samples (usually near the maximum range) are used to calculate the correlation estimates. The results are used to cancel the interference component of the samples at other range bins.

(e)   Doppler-domain cancellation with sliding-range-window averaging.

A similar scheme as that described in (c) may be used to perform cancellation on Doppler samples. Figure 10 show the type of data and the boundaries of the data used for calculating the correlation estimates for the case of "Doppler-domain cancellation with sliding-range-window averaging".

2.3   Types of interference

In this study we shall consider the cancellation of ionospheric clutter and co-channel communications interference only.

2.3.1 Ionospheric clutter.

Ionospheric clutter is present in groups of range bins corresponding to altitudes of the E and F layers of the ionosphere. One would not expect that there is much correlation between the

snapshots from two range bins that are far apart. Consequently, it may not be appropriate to use range-averaging to calculate the covariance matrix and the correlation vectors. On the other hand, if the range bins used in the calculation of the covariance matrix and the correlation vectors are reasonably close to the range bin for which interference cancellation is being applied, there may be sufficient correlation among these samples to permit cancellation. The analysis will be confined to those range bins which contain ionospheric clutter, and the range bins used for computing the covariance matrix and the correlation vectors are those close to the range bin for which cancellation is to be applied.

2.3.2   Co-channel communications interference.

For communications interference, the snapshots contain the samples of the interference at time instants that are separated by only a small time interval. For examples, if the waveform repetition frequency (WRF) of the radar is 100 Hz, then the snapshot of the maximum range is separated from that of the minimum range by only 10 milli-seconds. Since the interference signal is usually comprised of continuous signals that last over a time much longer than the radar's waveform repetition interval (WRI), it would be present in all range bins, and there would be a high degree of correlation among the samples taken from range bins that are far apart. Consequently the correlation properties can be estimated using samples from one group of range bins and the resulting weights can be used to cancel the interference at other ranges.

2.4   Performance criteria

Some care must be exercised in defining the performance criteria. Our objectives are to determine (a) whether, and to what degree, the various interference suppression schemes introduce errors in the target-bearing estimate, and (b) which of the interference suppression schemes is optimum. The evaluation must be carried out under a common set of conditions such as SINR.

2.4.1   Accuracy of the bearing estimate.

The measure of bearing-estimate accuracy is relatively straightforward. We use the mean bearing error and its standard deviation as measures. Synthesized target samples with given Doppler and angle-of-arrival can be generated and embedded in experimental data that contain interference. The data can then be processed with the various interference suppression schemes. Since the true target bearing is known, the error in target bearing can be evaluated. The mean error and standard deviation are obtained over a number of trials with independent sets of data samples.

There is one problem, and that is the interference level is not constant, either in time, or in Doppler. This means that a SINR cannot be specified independent of the data. Figure 11 shows the Doppler spectrum of the radar returns from a particular range bin (range = 60 km). The data were taken from file AIR_ONE (3 November 1995), and the CIT interval was approximately 28 seconds. Interference is observed in a band of Doppler frequencies centred at about -0.7 Hz;

16
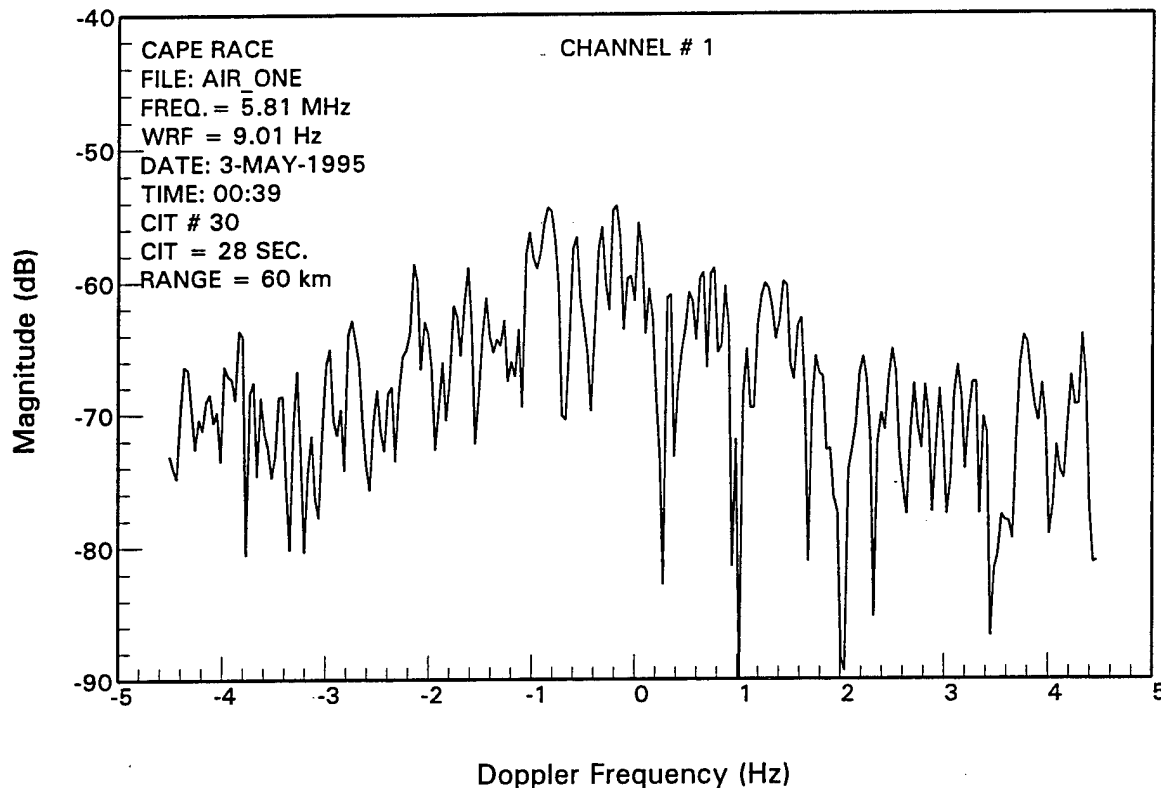
Figure 11. Spectrum of radar returns with a high level of communications interference.

however, there is a significant amount of fluctuation of the interference level over the Doppler band. Ultimately the SINR that counts is the one specified at the target Doppler shift. Obviously, the SINR would depend on the target Doppler.

The approach we adopted is the following. The data to be analyzed were divided into blocks, each of which comprises a number of time samples in a CIT interval. The angle-of-arrival of the interference component was estimated from the data. Synthesized target samples were generated at a number of angle-of-arrivals and Doppler shifts. The bearing estimates were compared among various cases that include (a) no interference cancellation and (b) with interference cancellation. The analysis was repeated for a number of SINR values (e.g. +5, 0, and -5 dB, etc). This implies that the actual target magnitude is dependent on the interference level at the specified Doppler in a CIT. The mean and standard deviation of the error in bearing estimated were obtained over the number of CITs analyzed.

2.4.2 Improvement factor

To arrive at a figure-of-merit for interference suppression schemes requires some thought. One possible performance criteria is the improvement factor usually defined as the ratio between

17

the SINR after and before the application of interference suppression. This requires that the signal magnitude be known. In defining the signal level, it is preferable that a fixed reference be used. However, this is not always possible since it is data dependent.

As stated earlier, the composite signal of an HFSWR comprises sea-clutter, external noise, ionospheric clutter and possibly co-channel interference. At close-in ranges, the sea clutter is dominant. However, the Bragg lines could still be a significant part of the total radar return even at very long range. Ionospheric clutter is present in specific ranges and has essentially a low-pass spectrum. The same problem discussed in Section 2.4.1 is also present here.

In radar, because of the constant-false-alarm-rate (CFAR) requirement, the detection performance depends not only on the SINR at the target Doppler and range, but also on the relative magnitudes of the noise and interference in neighbouring range and Doppler bins. A high level of noise and interference in neighbouring Doppler and range bins results in a high detection threshold setting, thereby lowering the probability of detection.

There are two problems in using the conventional definition of improvement factor. These are (a) the SINR is dependent on the target's Doppler shift and (b) the improvement depends not only on how much the interference is suppressed, but also on how much the signal is reduced by the interference-suppression algorithm. Since there is no a priori knowledge regarding the target Doppler and angle of arrival, an input SINR can only be defined with respect to a particular set of data.

For the interference suppression schemes considered in this study, the amount of reduction in the target-signal magnitude is inversely proportional to the angular distance between the target and the interference. The reason is that the interference-suppression algorithm attempts to place a null on the antenna pattern, in the direction of the interference. If the bearing of the target coincides with that of the interference, it will be completely cancelled, thereby yielding no improvement or even degradation. On the other hand, if the bearing of the target is well separated from that of the interference (say, more than one beamwidth), there is generally a negligible amount of reduction in the target-signal magnitude. Consequently, a reasonable alternative definition of the improvement factor is as follows:

$$I = \frac{\text{Average interference power before suppression}}{\text{Average interference power after suppression}} \qquad (19)$$

where the average is over Doppler, range or both.

The above definition of the improvement factor is only valid for the case where the target bearing is sufficiently separated from that of the interference. In evaluating the improvement factor, some times it is necessary to exclude other components such as sea clutter because these may be the dominant component in the signal on which the interference suppression algorithm may not have any effect. More will be said about this in Section 3 which describes the data analysis.

2.5 Test data

Data collected in experimental trials conducted at Cape Bonavista and Cape Race have been analyzed to determine their suitability for this study.

2.5.1 Cape Bonavista data

Most of the data obtained from Cape Bonavista trials were collected during daylight hours. The few data sets that were collected at nighttime contain system artifacts that make them unsuitable for this study. In particular, data from four out of the eight channels contain an injected calibration tone. A considerable amount of effort would be required to remove this component from the data which is necessary for the case of time-domain interference cancellation. Consequently, the Cape Bonavista data will not be used in this study.

2.5.2 Cape Race data

Three sets of data collected from Cape Race will be used in this study. Table 1 tabulates the essential parameters of these data files.

File Name	Date	Time	Frequency	Waveform	PRF (Hz)	No. of channels
AIR_ONE	3-May 1995	00:39	5.81	FMICW	9.01	10
AIR_FIVE	27-Oct 1994	11:57	5.81	FMICW	9.18	10
AIR_SEVEN	28-Oct 1994	18:06	5.81	FMICW	9.18	10

Table 1. Cape Race data sets used in this study.

The Cape Race data has the following characteristics. First, the ten receiver channels were connected to ten sub-arrays comprising four receive-antenna elements. The element separation is 22.22 m which is equalled to half a wavelength at 6.75 MHz. Hence the effective spacing of the sub-arrays is 88.88 m. This results in grating lobes in the receive-antenna pattern. However, because the performance of the various processing schemes is evaluated on a relative basis, it is not considered to be a serious problem. Second, there exist range-ambiguity responses arising from the sub-optimal pulse-compression algorithm used in the Cape Race radar. These anomalies could corrupt the covariance matrix and correlation vector calculations. Fortunately the range-ambiguity responses were isolated in range and their locations were known. Consequently those samples corresponding to the range-ambiguity response were excluded in the calculations. In the analysis that follows, Channels 1 and 10 were used as auxiliary antennas. Channels 2 to 9 forms an eight-element main array.

Data file AIR_ONE was collected around midnight. These data had a high external noise level as well as communications interference. This file was used to comparatively evaluate the various interference suppression schemes and their effects on the accuracy of bearing estimate.

Date file AIR_FIVE was collected at mid day. The data in a number of range bins contain strong ionospheric clutter. This file was used to test algorithms for possible ionospheric clutter suppression.

Data file AIR_SEVEN was collected at dusk. The data in this file contained echoes of a controlled target as well as some communications interference. This file was used to compare various interference suppression schemes under practical conditions.

3. ANALYSIS RESULTS.

The Cape Race Radar had ten receiver channels. Unless otherwise stated, the results presented in this section were obtained under the following conditions.

(i) Main array comprised channels 2 - 9.
(ii) Auxiliary array comprised channels 1 and 10
(iii) No. of snapshots used for the evaluation of correlation properties = 64.

3.1 Communications interference.

3.1.1 Case where the communications interference is dominant.

Data file AIR_ONE listed in Table 1 were collected in a trial on May 1995 around midnight. At this time, the external noise level was very high. Figure 12 shows the range-Doppler profile of the radar samples in AIR_ONE at boresight over one CIT. It shows that sea clutter (Bragg lines) was visible out to only about 70 km. The external noise floor was at approximately -90 dB, and there was interference around the centre of the Doppler band that was more or less range independent.

Figure 13 shows the results of applying time-domain cancellation to the same data as in Figure 12, using sliding-time-window averaging to calculate the correlation estimates. Each time sample was cancelled using the correlation estimates computed from 64 preceding snapshots. It shows that the results were worse than in Figure 12 where no cancellation was applied.

Figure 14 shows the results of applying time-domain cancellation to the data, using fixed-range-window averaging to calculate the correlation estimates. The time sample in each range bin was cancelled using the correlation estimates computed from 64 range samples positioned near the maximum range. The interference level had been reduced.

20

MAGNITUDE (dB)

-40 dB
-50 dB
-60 dB
-70 dB
-80 dB
-90 dB
-100 dB

RANGE

300 km
200 km
100 km
1.2 km

DOPPLER

4.51 Hz
-4.51 Hz

FILE = AIR_ONE
          CIT No.30

DATE: 3-MAY-1995
TIME: 00:53:36

FREQ. = 5.81 MHz
WAVEFORM = FMICW
BW = 125.0 kHz
WRF = 9.01 Hz
BEAM No.1 (Boresight)

INTEGRATION TIME = 28.40 sec.
(NO INTERFERENCE CANCELLATION)
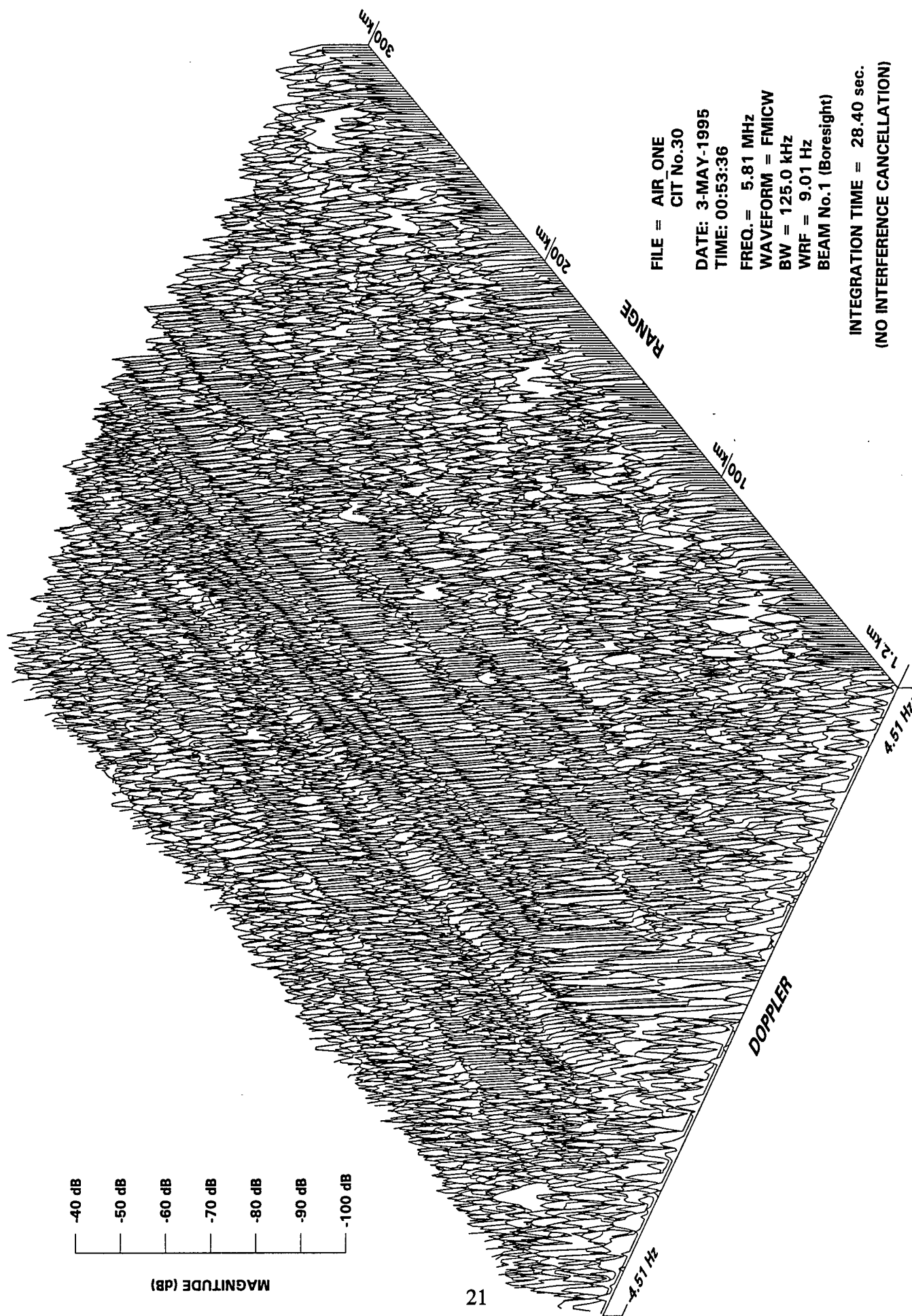
Figure 12. Range-Doppler profile of radar returns with no interference cancellation.

21

Figure 13.   Range-Doppler profile of radar returns with time-domain cancellation using sliding-time-window averaging.

FILE = AIR_ONE
       CIT No.30

DATE: 3-MAY-1995
TIME: 00:53:36

FREQ. = 5.81 MHz
WAVEFORM = FMICW
BW = 125.0 kHz
WRF = 9.01 Hz
BEAM No.1 (Boresight)

INTEGRATION TIME = 28.40 sec.
(TIME-DOMAIN CANC.; NAVG = 64)

FIXED-RANGE-WINDOW AVG.

Figure 14.   Range-Doppler profile of radar returns with time-domain cancellation using fixed-range-window averaging.

23

Figure 15 shows the results of applying time-domain cancellation to the data, using sliding-range-window averaging to calculate the correlation estimates. Sixty four range samples near the sample to be cancelled were used to calculate the correlation estimates. The guard zones contain one range bin. This was sufficient for the Cape Race Radar because its range resolution was one range samples. The results show that the interference level had been suppressed.

Figure 16 shows the results of applying Doppler-domain cancellation to the data, using fixed-range-window averaging to calculate the correlation estimates. The correlation estimates were obtained the same way as that for Figure 14, except that the time samples were first Doppler processed. Cancellation was applied to the Doppler samples, and the interference level was reduced.

Figure 17 shows the results of applying Doppler-domain cancellation to the data, using sliding-range-window averaging to calculate the correlation estimates. The correlation estimates were obtained the same way as that for Figure 15, except that Doppler samples were used. Reduced interference level was obtained.

The relative merits of the various processing schemes can be evaluated by comparing the averaged interference levels after cancellation was applied. Because the communications interference was dominant and was more or less range independent, the Doppler spectra can be averaged over all the range bins. The results are shown in Figure 18a through 18f, for the spectra in Figures 12-17, respectively. It can be seen in Figure 18a that, before cancellation was applied, the interference occupied a Doppler domain from -2 Hz to about +1 Hz.

The result in Figure 18b shows that the performance was worse using time-domain cancellation with sliding-time-window averaging. The reasons for this performance degradation will be discussed in Section 4.2.

Results in Figures 18c through 18f showed that, qualitatively, time-domain cancellation with sliding-range-window averaging yields the best performance. The improvement factor may be derived from the results of Figures 18a. The two peaks around zero Doppler were those of the ground clutter at close ranges and the Bragg components. The spectra in Figure 18 can be averaged over the Doppler domain, with the samples around zero Doppler excluded. The results are shown in Table 2.

3.1.2 Case where the communications interference is not dominant.

Data file AIR_SEVEN listed in Table 1 was collected in a trial on 28 October, 1994 at dusk. At that time, the external noise level had begun to increase, and there was some communications interference. Figure 19 shows the range-Doppler profile of the radar samples over one CIT. It shows that the noise floor was at approximately -115 dB. The centre portion of the Doppler spectrum was occupied by the sea clutter which extended out to beyond 300 km. In the Doppler region between 2.3 Hz and 4.0 Hz, there was a band of interference which appears in all range bins. The level of this interference was substantially below that of the sea clutter.

24

FILE = AIR_ONE
CIT No.30

DATE: 3-MAY-1995
TIME: 00:53:36

FREQ. = 5.81 MHz
WAVEFORM = FMICW
BW = 125.0 kHz
WRF = 9.01 Hz
BEAM No.1 (Boresight)

INTEGRATION TIME = 28.40 sec.
(TIME-DOMAIN CANC.; NAVG = 64)
SLIDING-RANGE-WINDOW AVG.

Figure 15. Range-Doppler profile of radar returns with time-domain cancellation using sliding-range-window averaging.

25

FILE = AIR_ONE
        CIT No.30

DATE: 3-MAY-1995
TIME: 00:53:36

FREQ. = 5.81 MHz
WAVEFORM = FMICW
BW = 125.0 kHz
WRF = 9.01 Hz
BEAM No.1 (Boresight)

INTEGRATION TIME = 28.40 sec.
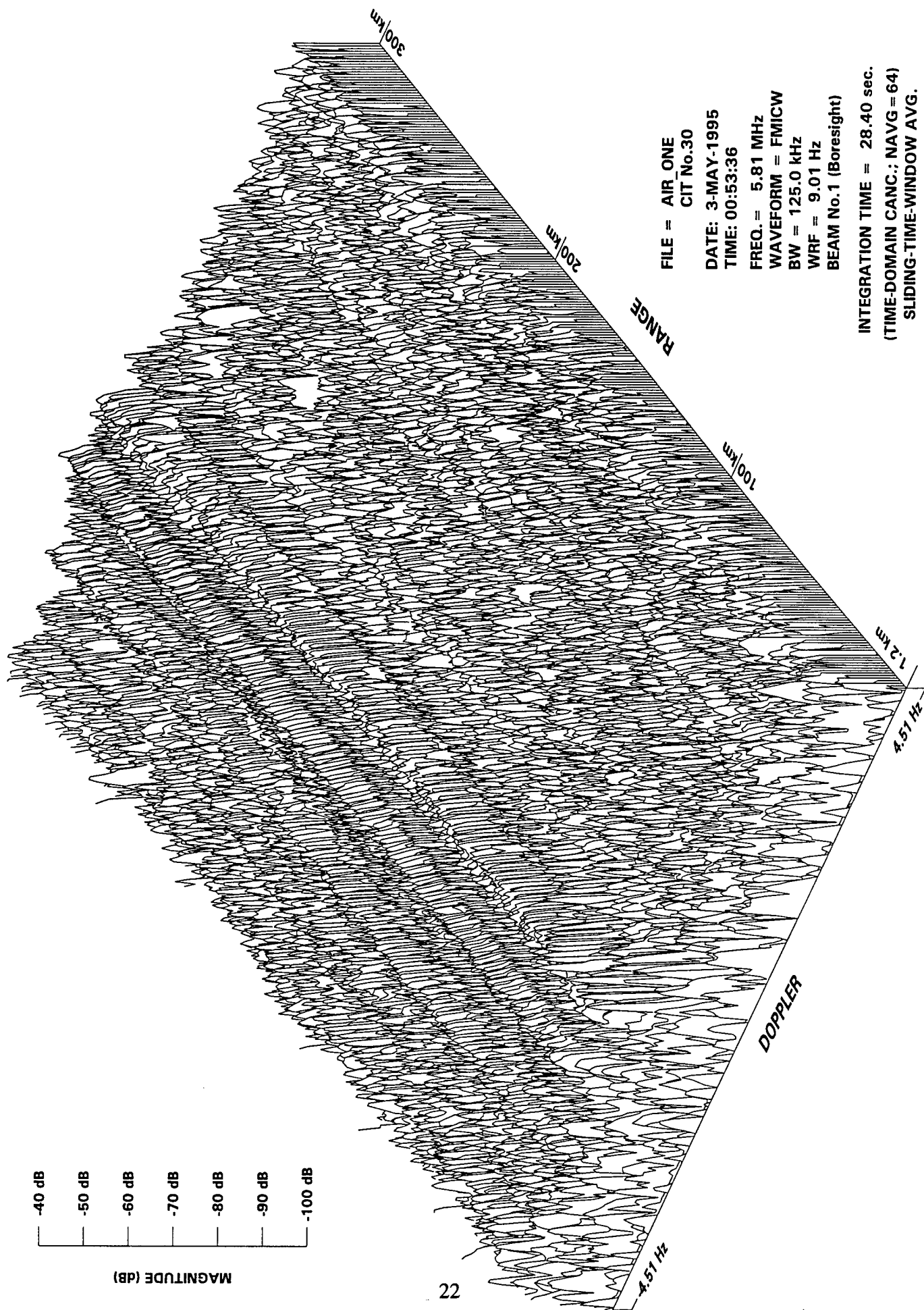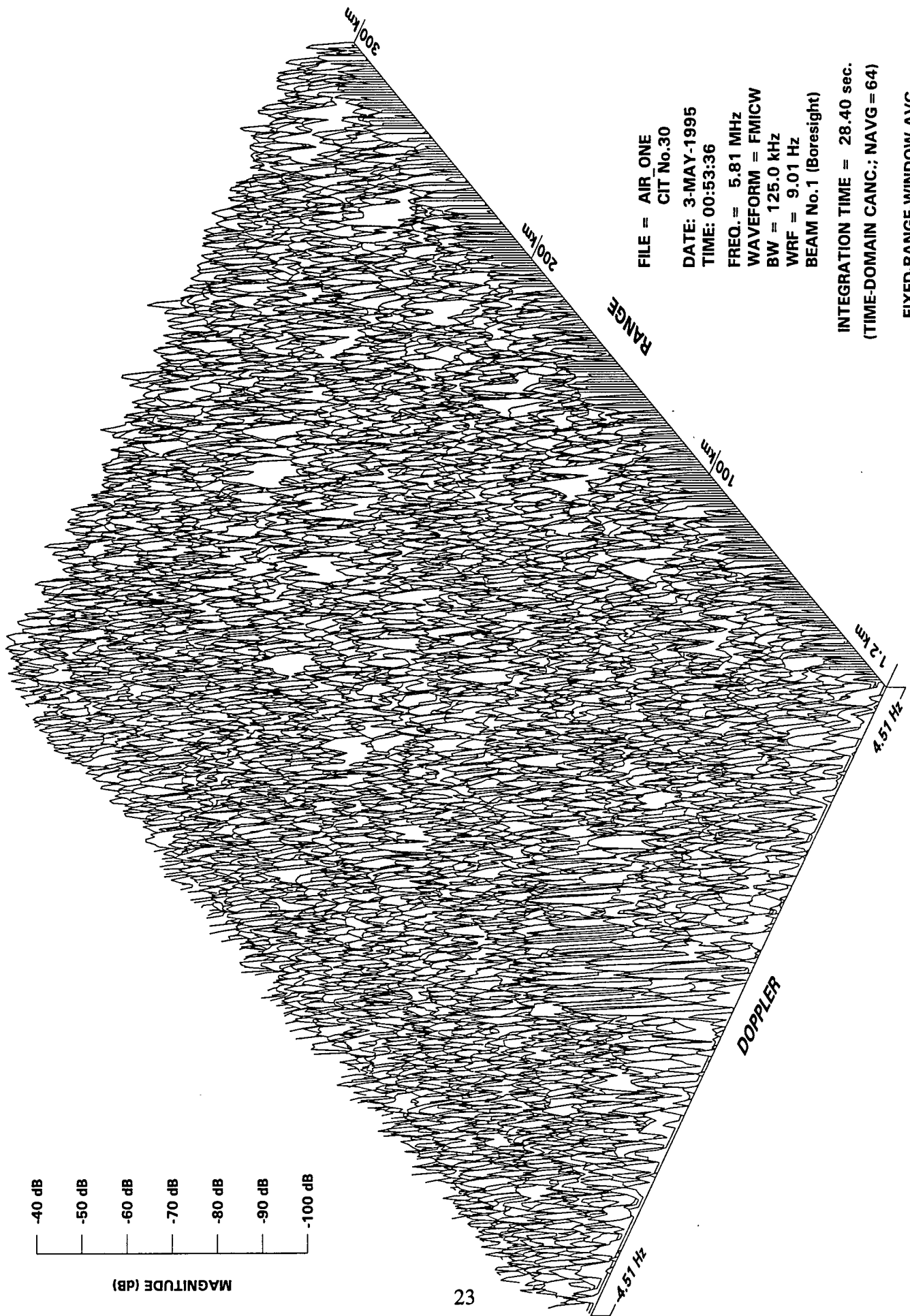(DOPPLER-DOMAIN CANC.; NAVG = 64)
FIXED-RANGE-WINDOW AVG.

Figure 16.   Range-Doppler profile of radar returns with Doppler-domain cancellation, using fixed-range-window averaging.

Figure 17. Range-Doppler profile of radar returns with Doppler-domain cancellation, using sliding-range-window averaging.

FILE = AIR_ONE
CIT No.30

DATE: 3-MAY-1995
TIME: 00:53:36

FREQ. = 5.81 MHz
WAVEFORM = FMICW
BW = 125.0 kHz
WRF = 9.01 Hz
BEAM No.1 (Boresight)

INTEGRATION TIME = 28.40 sec.
(DOPPLER-DOMAIN CANC.; NAVG = 64)
SLIDING-RANGE-WINDOW AVG.

RANGE

300 km

200 km

100 km

1.2 km

4.51 Hz

4.51 Hz

DOPPLER

MAGNITUDE (dB)

-40 dB
-50 dB
-60 dB
-70 dB
-80 dB
-90 dB
-100 dB

27

FILE: AIR_ONE; FREQ. = 5.81 MHz; WRF = 9.01 Hz; CIT # 30; CIT = 28 sec.
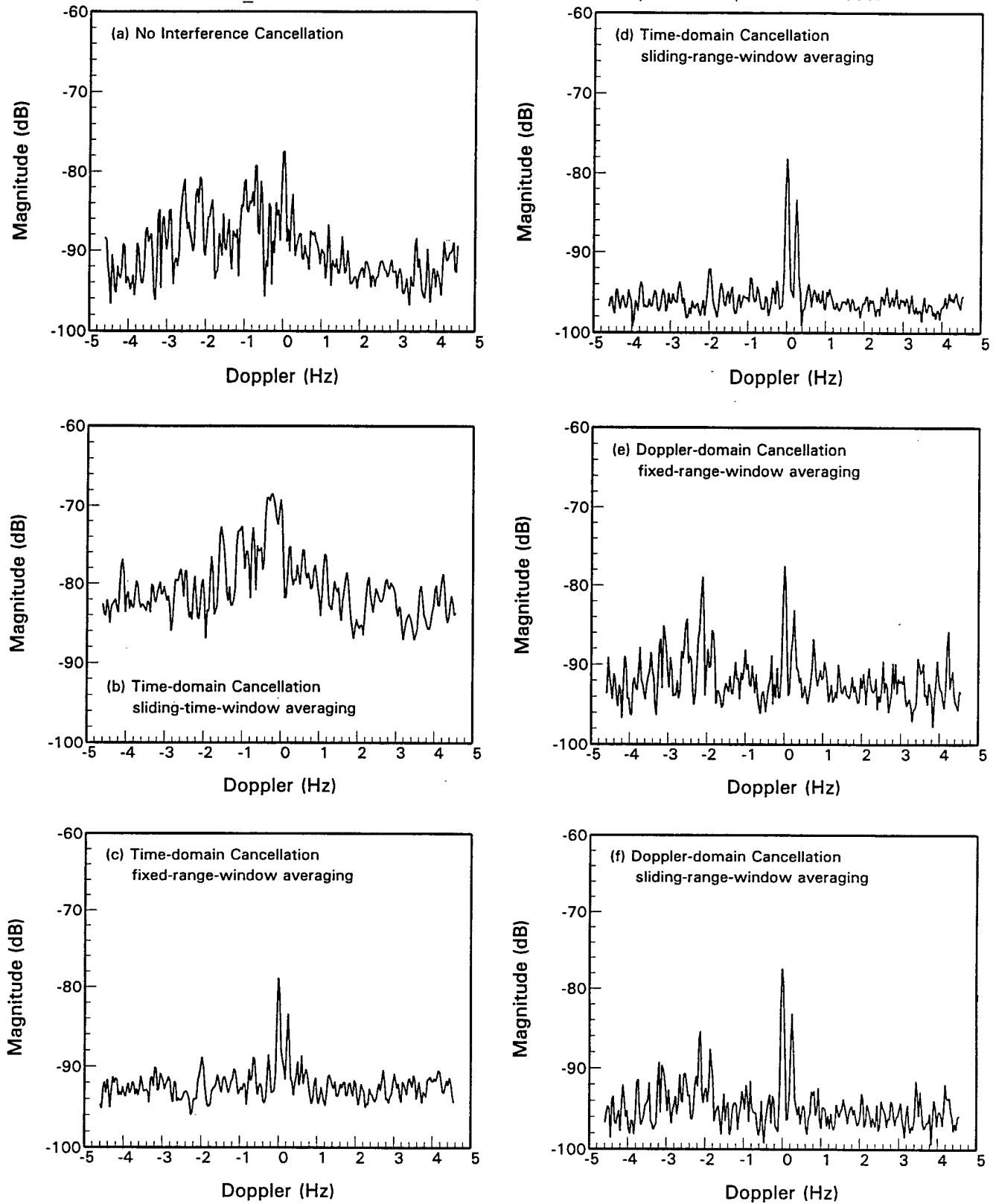
Figure 18. Averaged spectra before and after interference cancellation.

28

	Avg. Interference level	Improvement Factor (AIR_ONE)
(a) No interference cancellation	-88.41	-
(b) time-domain cancellation using sliding-time-window averaging	-79.64	-8.77
(c) time-domain cancellation using fixed-range-window averaging	-92.39	3.98
(d) time-domain cancellation using sliding-range-window averaging	-96.07	7.66
(e) Doppler-domain cancellation using fixed-range-window averaging	-90.45	2.04
(f) Doppler-domain cancellation using sliding-range-window averaging	-94.41	6.00

Table 2:   Comparison of Improvement Factor among various schemes, for the case where the communications interference is dominant.

At the time this data set was collected, there was a Challenger 601 aircraft flying towards the Cape Race radar along boresight. The speed of the aircraft was about 178 knots. The corresponding target Doppler fell in the region occupied by the interference, and the aircraft was not detected. Figures 20 through 24 show the range-Doppler profiles of the radar samples after interference cancellation was applied.

Figures 20, 21 and 22 are for cases of time-domain cancellation with (i) sliding-time-window averaging, (ii) fixed-range-window averaging and (iii) sliding-range-window averaging, respectively. These results show that time-domain cancellation failed to suppress the communications interference.

Figures 23 and 24 are for cases of Doppler-domain cancellation, with (i) fixed-range-window averaging and (ii) sliding-range-window averaging, respectively. These results show that Doppler-domain cancellation is capable of suppressing the communications interference, and the aircraft target emerged after cancellation.

The spectra in Figures 20 through 24 were averaged over all range bins, and the results are shown in Figure 25. In cases where time-domain cancellation was used, the result was generally worse than the case where no cancellation was used. In the case of time-domain cancellation, with sliding-range-window averaging, artifacts in the response can result (see Figure 25d).

29

FILE = AIR_SEVEN
CIT No.71

DATE: 28-OCT-1994
TIME: 18:39:16

FREQ. = 5.81 MHz
WAVEFORM = FMICW
BW = 125.0 kHz
WRF = 9.18 Hz
BEAM No. 1

INTEGRATION TIME = 27.89 sec.
(NO INTERFERENCE CANCELLATION)
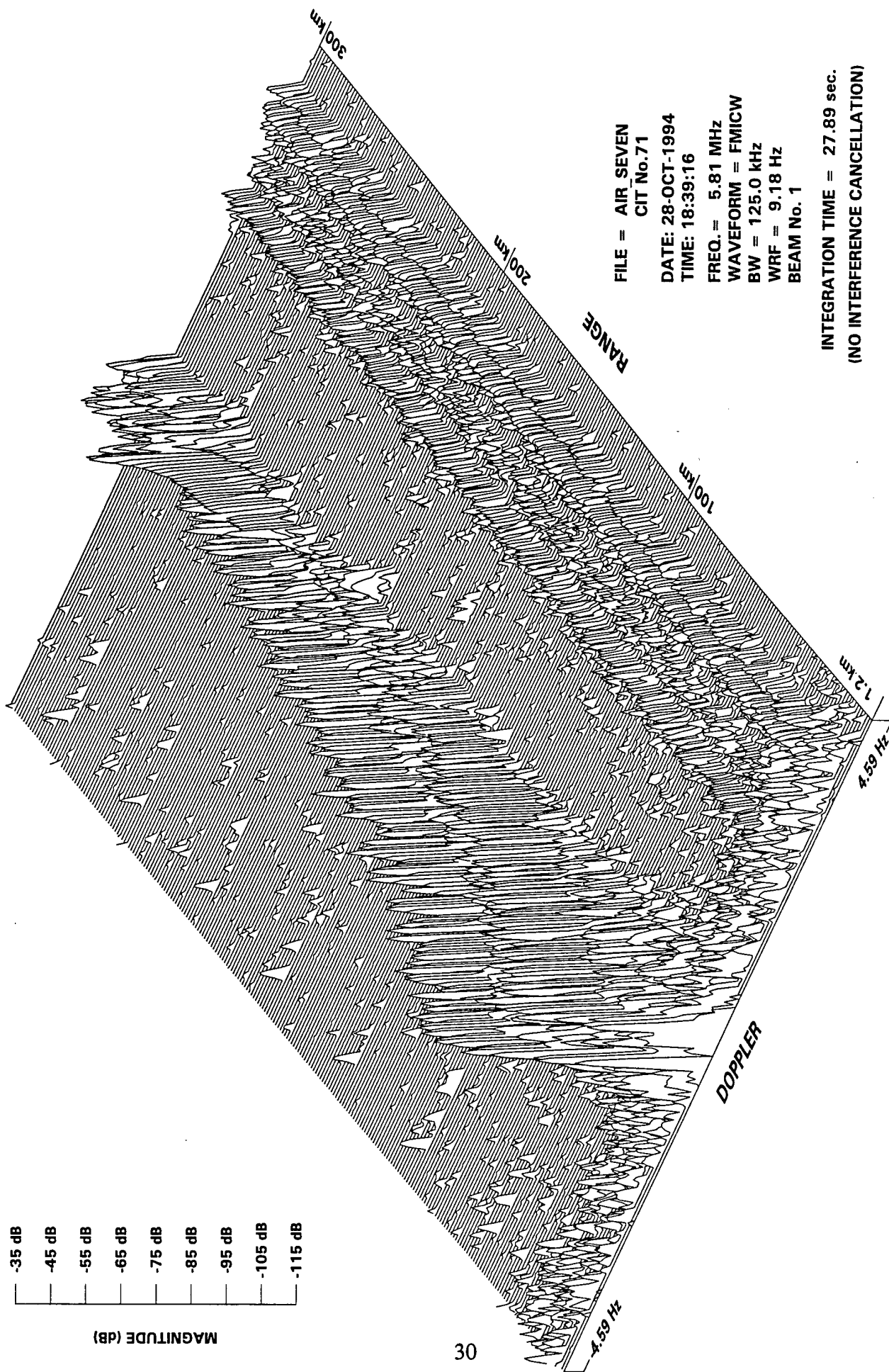
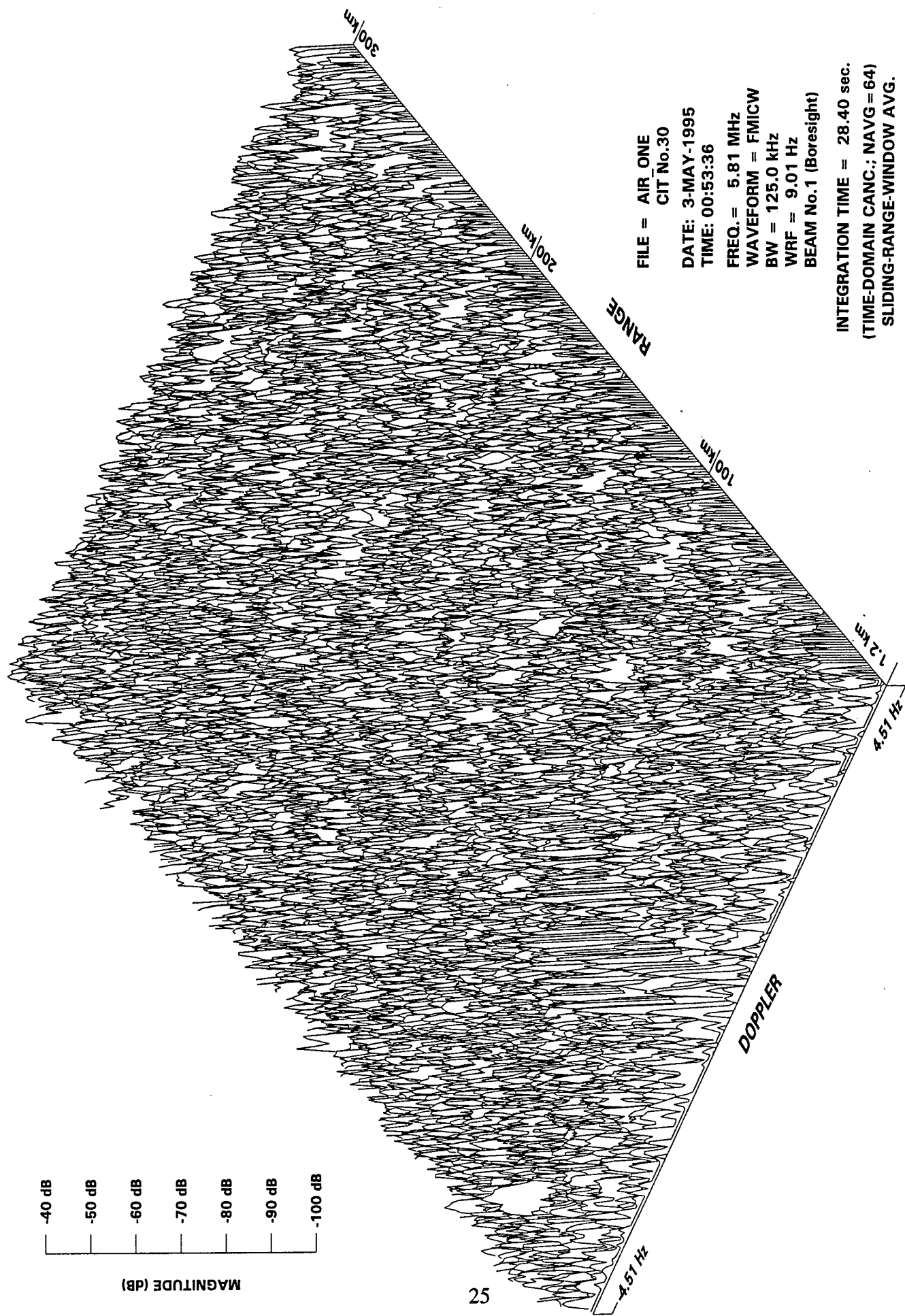Figure 19. Range-Doppler profile of radar returns with no interference cancellation.
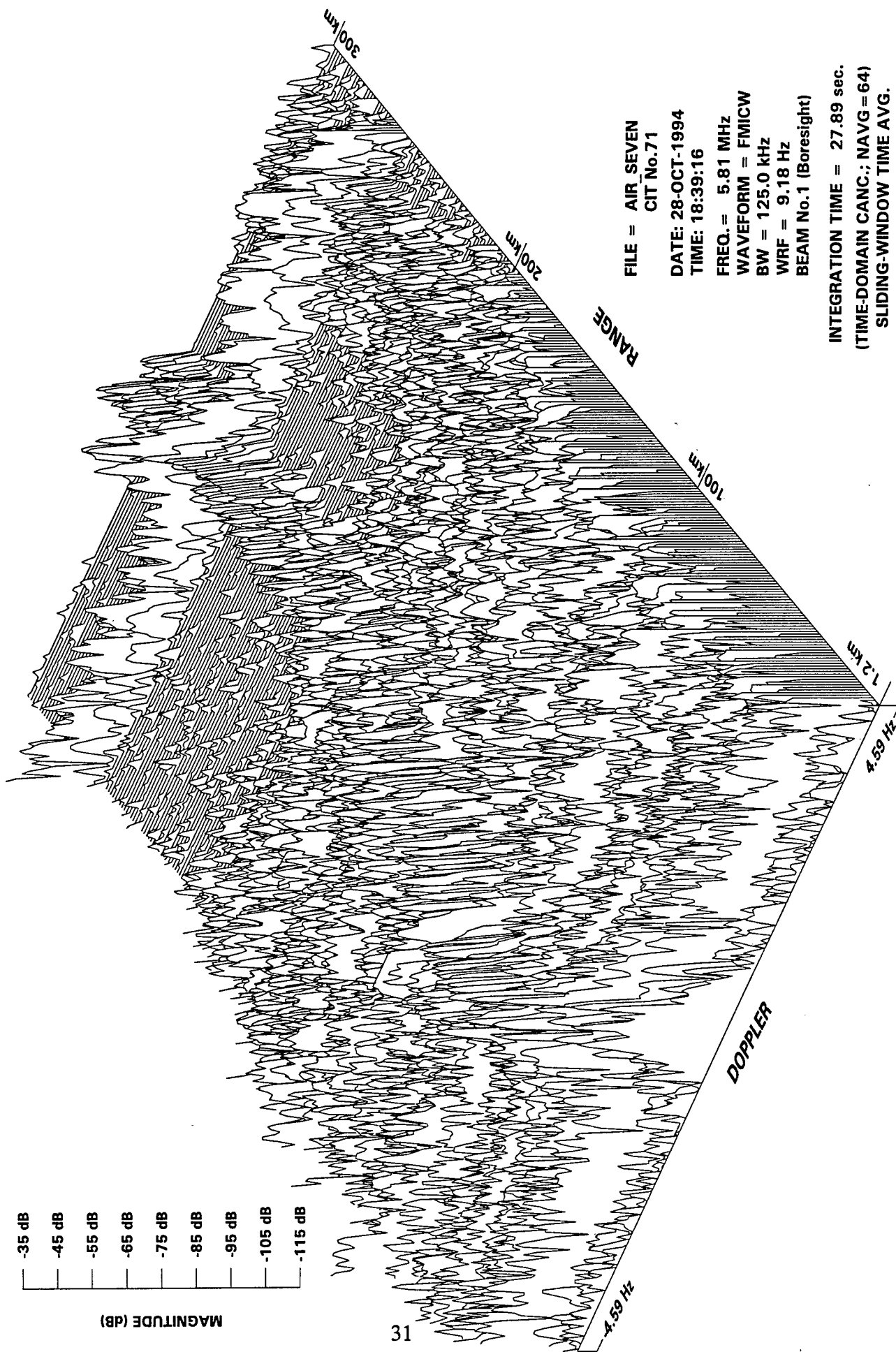
Figure 20. Range-Doppler profile of radar returns with time-domain cancellation using sliding-time-window averaging.

FILE = AIR_SEVEN
CIT No.71

DATE: 28-OCT-1994
TIME: 18:39:16

FREQ. = 5.81 MHz
WAVEFORM = FMICW
BW = 125.0 kHz
WRF = 9.18 Hz
BEAM No.1 (Boresight)

INTEGRATION TIME = 27.89 sec.
(TIME-DOMAIN CANC.; NAVG=64)
SLIDING-WINDOW TIME AVG.

300 km

200 km

RANGE

100 km

1.2 km

4.59 Hz

DOPPLER

4.59 Hz

-35 dB
-45 dB
-55 dB
-65 dB
-75 dB
-85 dB
-95 dB
-105 dB
-115 dB

MAGNITUDE (dB)

31
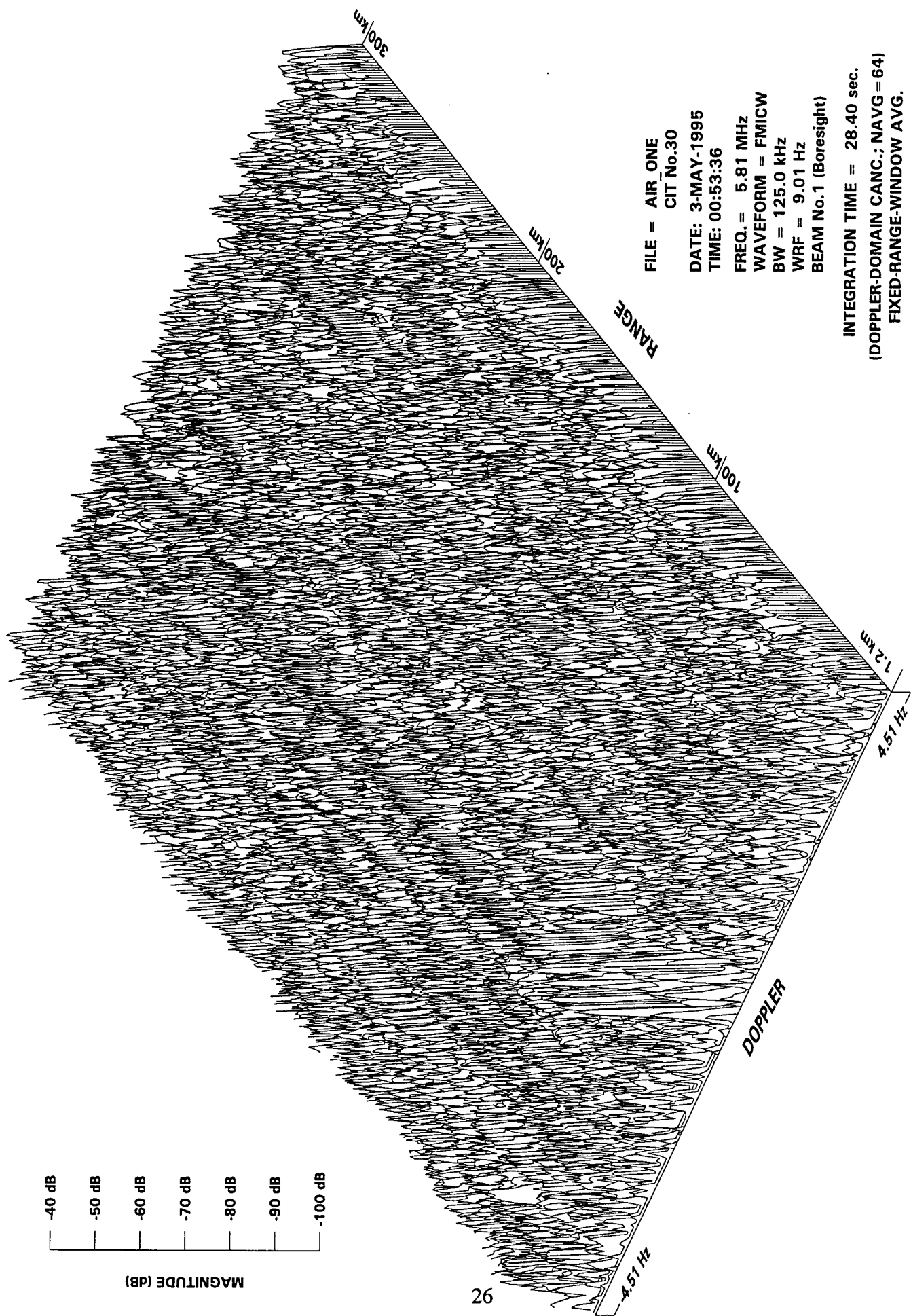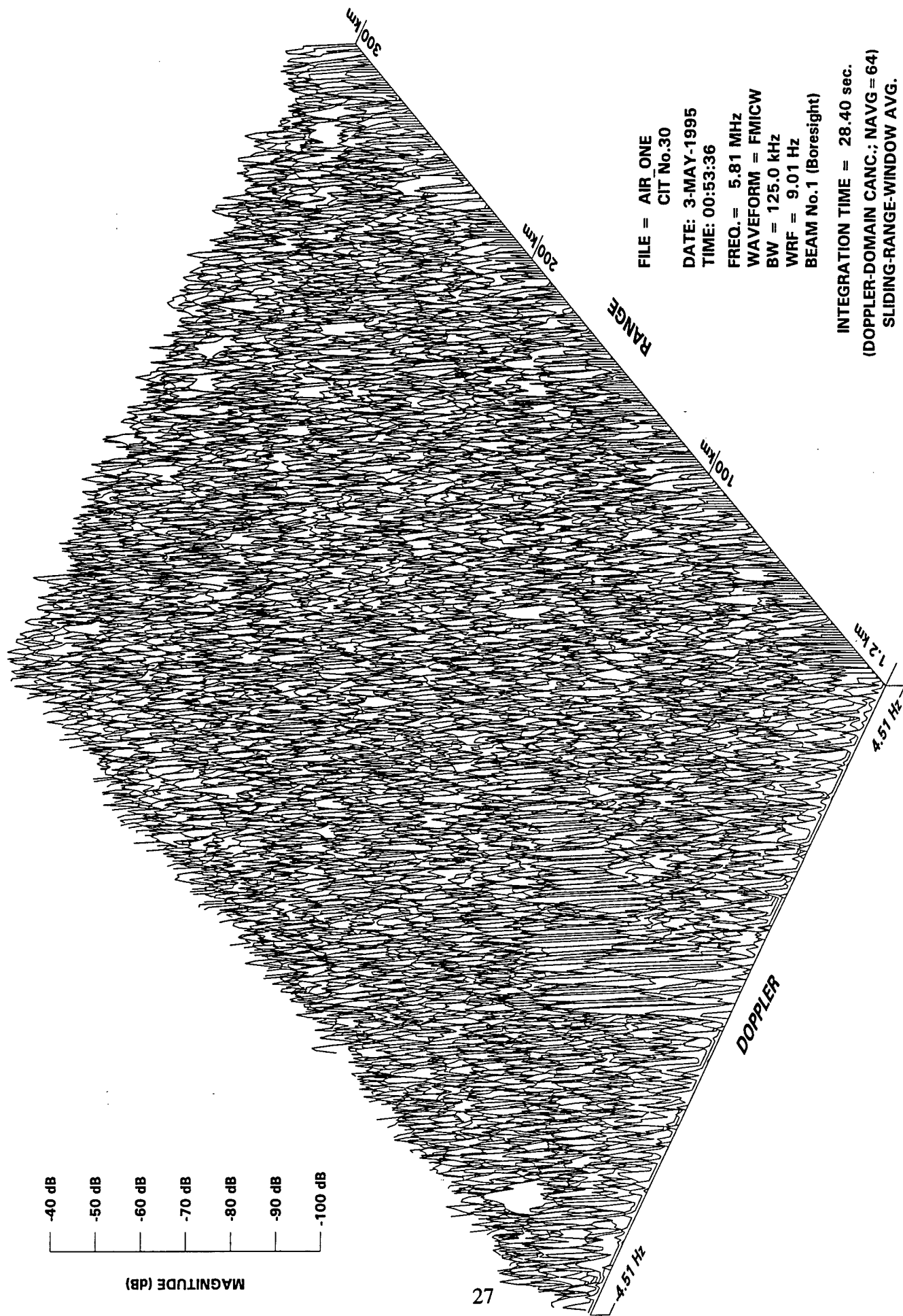
Figure 21. Range-Doppler profile of radar returns with time-domain cancellation using fixed-range-window averaging.

FILE = AIR_SEVEN
CIT No.71

DATE: 28-OCT-1994
TIME: 18:39:16

FREQ. = 5.81 MHz
WAVEFORM = FMICW
BW = 125.0 kHz
WRF = 9.18 Hz
BEAM No.1 (Boresight)

INTEGRATION TIME = 27.89 sec.
(TIME-DOMAIN CANC.; NAVG = 64)
FIXED-WINDOW RANGE AVG.

RANGE

300 km

200 km

100 km

1.2 km

DOPPLER

4.59 Hz

-4.59 Hz

MAGNITUDE (dB)

-35 dB
-45 dB
-55 dB
-65 dB
-75 dB
-85 dB
-95 dB
-105 dB
-115 dB

32

MAGNITUDE (dB)

-35 dB
-45 dB
-55 dB
-65 dB
-75 dB
-85 dB
-95 dB
-105 dB
-115 dB

RANGE

300 km
200 km
100 km
1.2 km

DOPPLER

4.59 Hz
-4.59 Hz

FILE = AIR_SEVEN
        CIT No.71

DATE: 28-OCT-1994
TIME: 18:39:16

FREQ. = 5.81 MHz
WAVEFORM = FMICW
BW = 125.0 kHz
WRF = 9.18 Hz
BEAM No.1 (Boresight)

INTEGRATION TIME = 27.89 sec.
(TIME-DOMAIN CANC.; NAVG = 64)
SLIDING-WINDOW RANGE AVG.

Figure 22. Range-Doppler profile of radar returns with time-domain cancellation using sliding-range-window averaging.

33
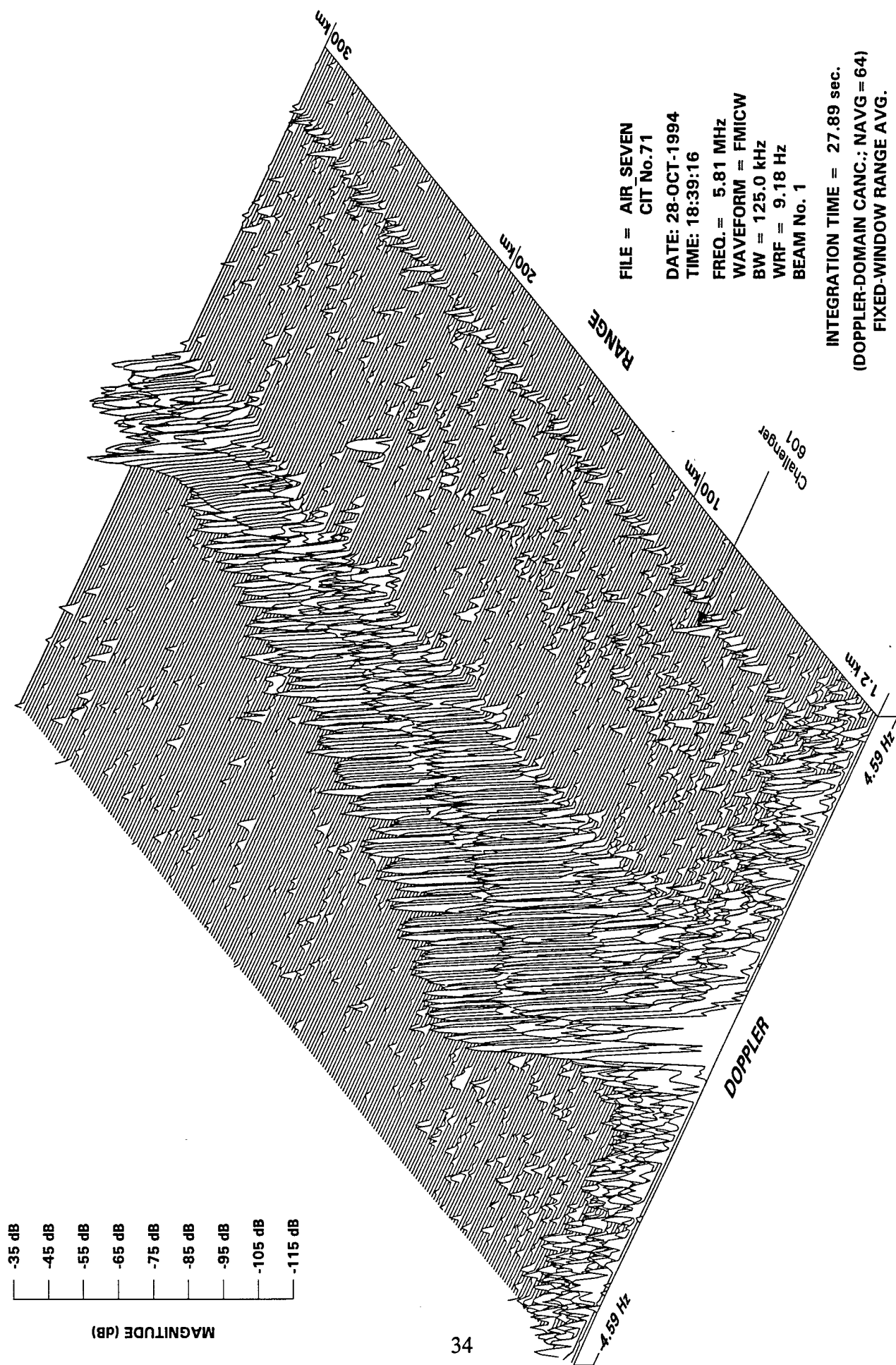
Figure 23. Range-Doppler profile of radar returns with Doppler-domain cancellation, using fixed-range-window averaging.

34

FILE = AIR_SEVEN
CIT No.71

DATE: 28-OCT-1994
TIME: 18:39:16

FREQ. = 5.81 MHz
WAVEFORM = FMICW
BW = 125.0 kHz
WRF = 9.18 Hz
BEAM No. 1

INTEGRATION TIME = 27.89 sec.
(DOPPLER-DOMAIN CANC.; NAVG = 64)
SLIDING WINDOW RANGE AVG.

Figure 24. Range-Doppler profile of radar returns with Doppler-domain cancellation, using sliding-range-window averaging.

35
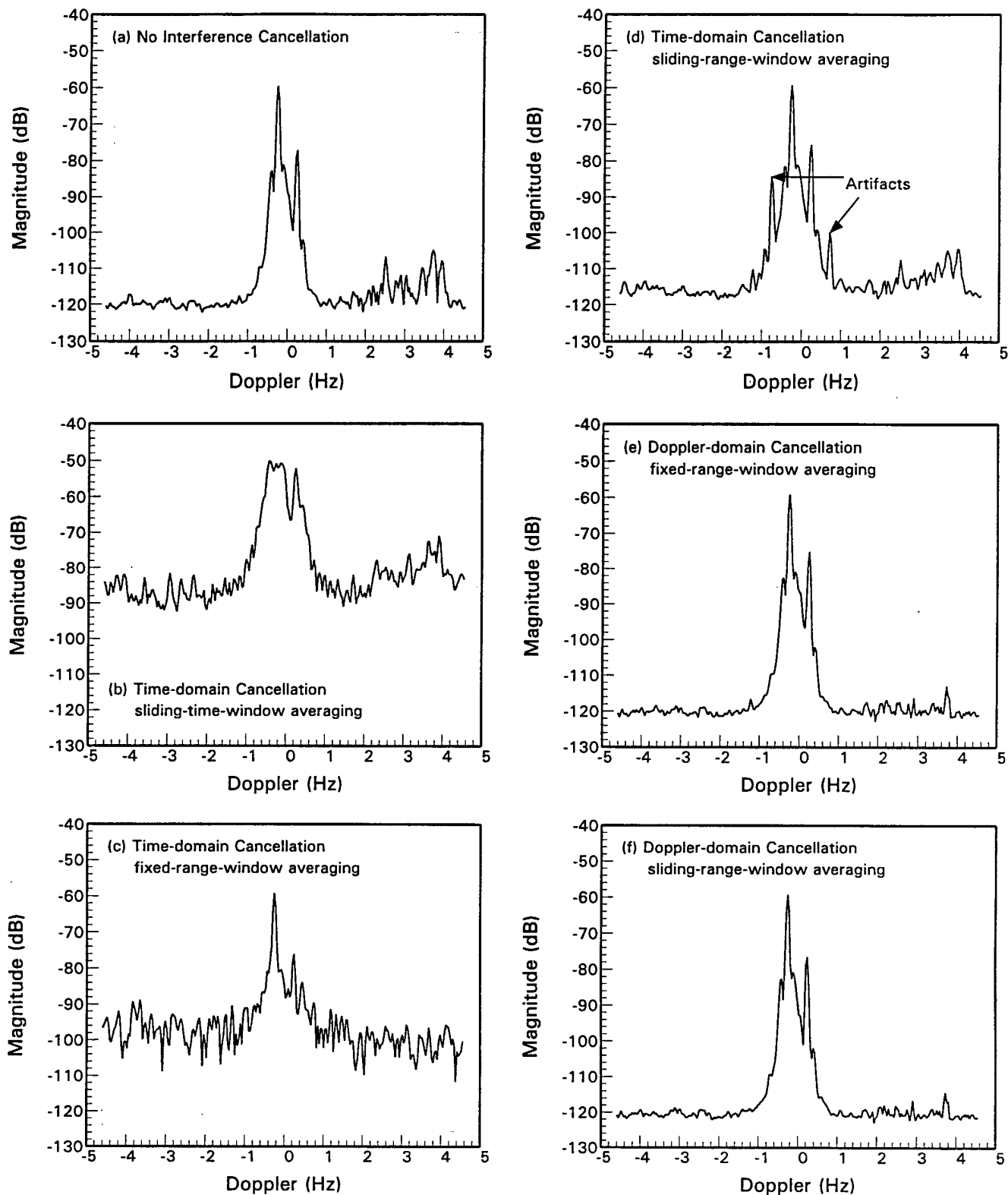
Figure 25. Averaged spectra before and after interference cancellation.

To get an estimate of the improvement factor, the spectra in Figure 25 were averaged over the Doppler domain. In this case, we need to exclude the sea clutter because it is not part of the interference against the target. Hence the spectra were averaged over the Doppler bins from 1 Hz to 4.59 Hz only. The results are shown in Table 3.

For the case where the communications interference was not dominant, Doppler-domain cancellation with sliding-range-window averaging yielded the best result.

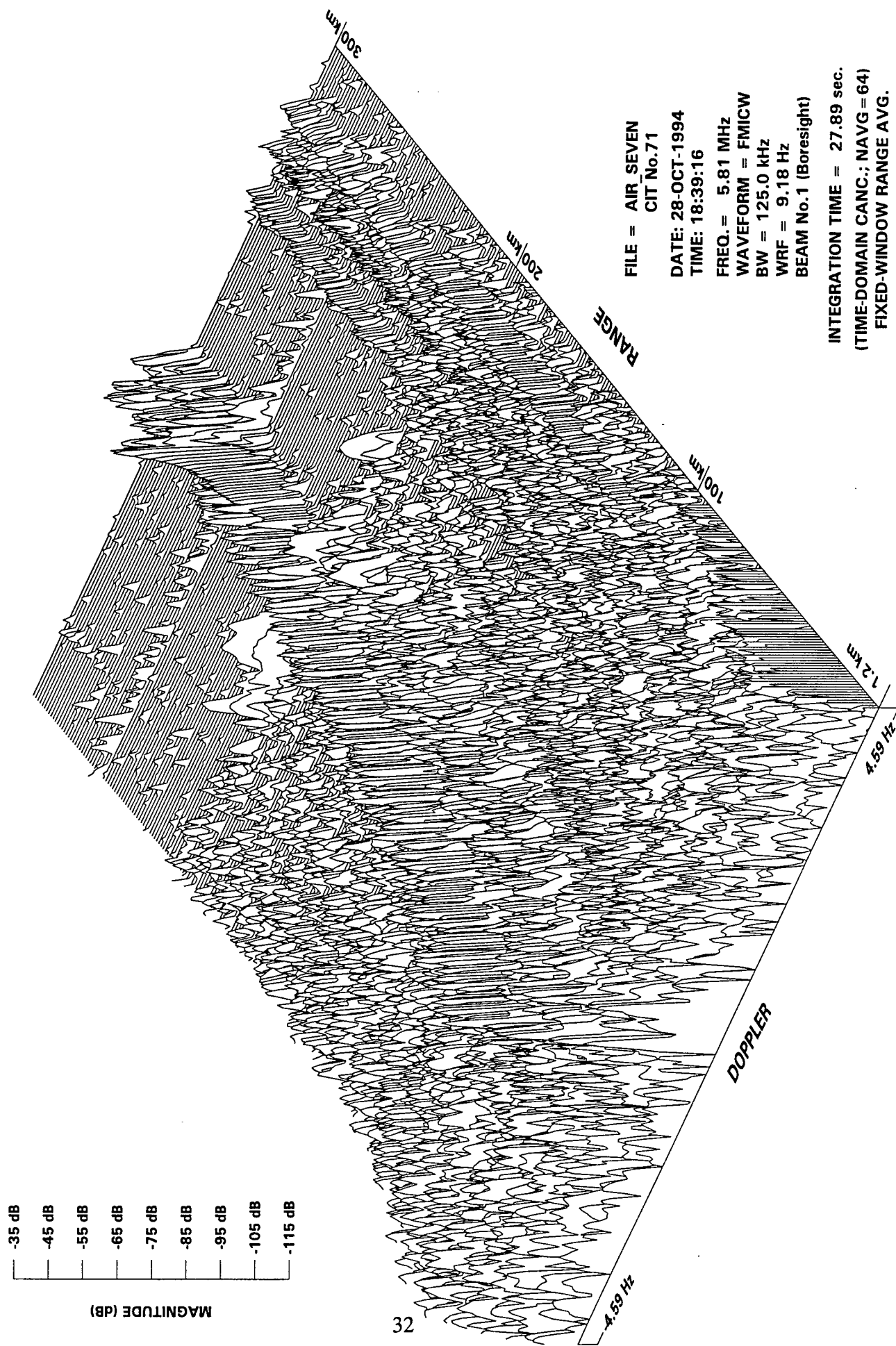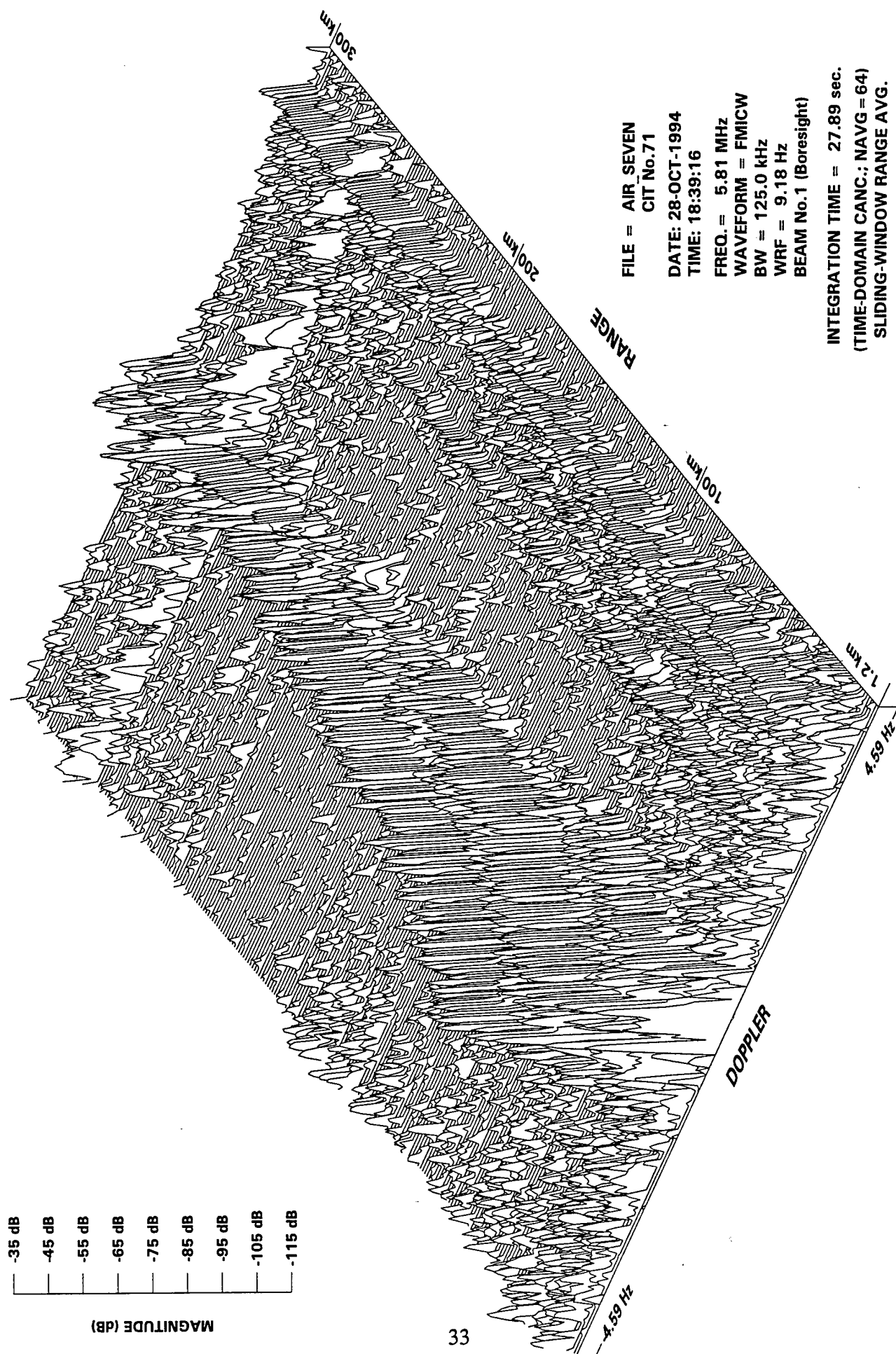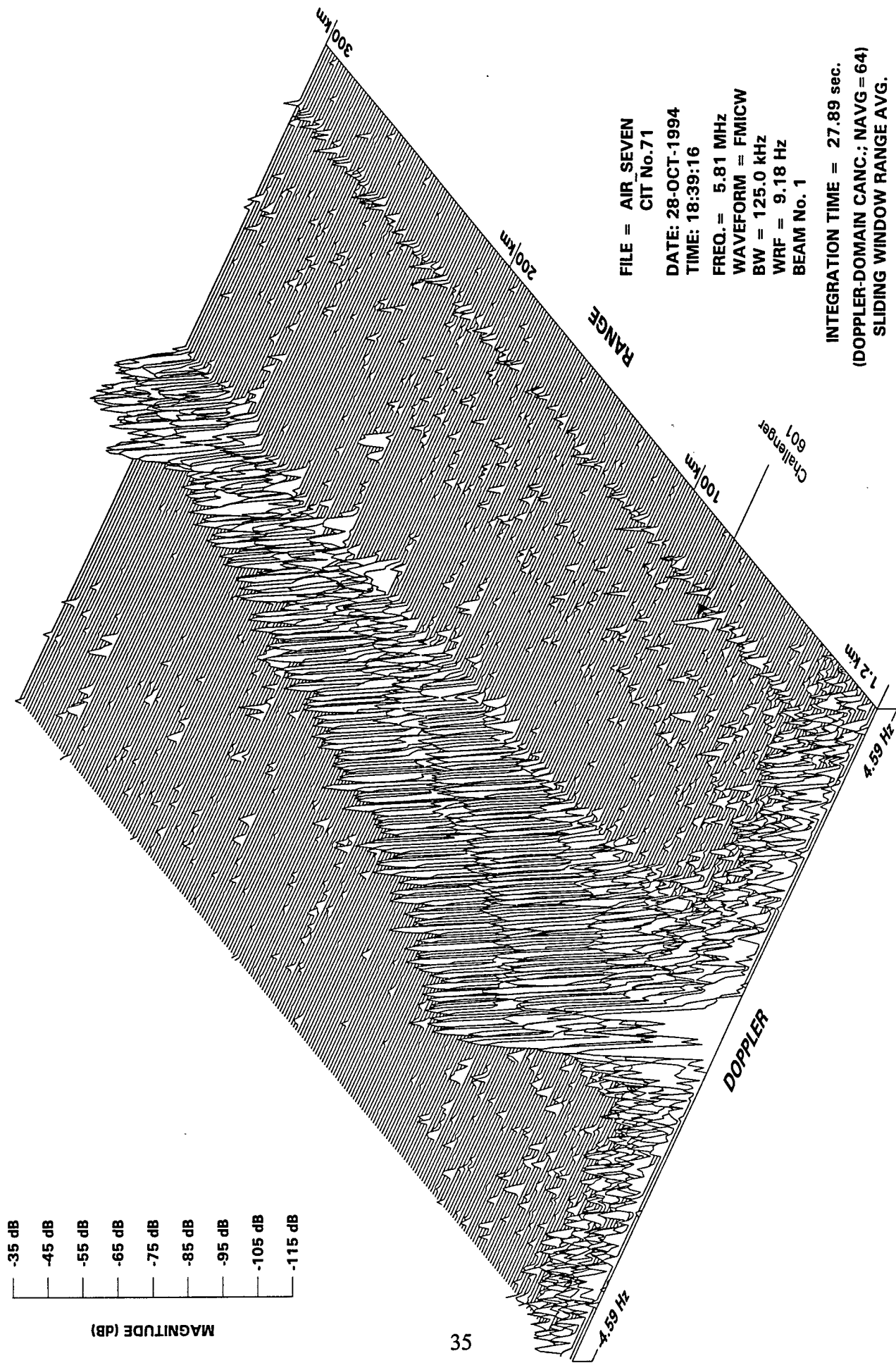|		Avg. Interference level	Improvement Factor (AIR_SEVEN)
(a)	No interference cancellation	-113.95	-
(b)	time-domain cancellation using sliding-time-window averaging	-80.06	-33.89
(c)	time-domain cancellation using fixed-range-window averaging	-99.14	-14.81
(d)	time-domain cancellation using sliding-range-window averaging	-111.32	-2.63
(e)	Doppler-domain cancellation using fixed-range-window averaging	-119.31	5.36
(f)	Doppler-domain cancellation using sliding-range-window averaging	-120.06	6.11

Table 3: Comparison of Improvement Factor among various schemes, for the case where the communications interference is not dominant.

3.1.3 Effect of interference cancellation on accuracy of bearing estimate.

The analysis presented in this subsection is intended to give an indication of the relative accuracy of the bearing estimate between two different interference cancellation procedures. It is not intended as an absolute quantitative measure of accuracy. The difficulty in obtaining an absolute quantitative measure of accuracy arises from the fact that it depends on many factors which are not known a priori. These include the spectral and directional characteristics of the interference signals, and the separation of the target, both in Doppler and in bearing, from the interference. Nevertheless, we shall make an attempt to get some answers with respect to a set of specific conditions.

Three methods of processing radar data were studied:

(a)　No Sidelobe Cancellation (NO_SLC), i.e. Doppler Processing only,
(b)　Doppler Processing followed by Sidelobe Cancellation (DP_SLC), and
(c)　Sidelobe Cancellation followed by Doppler Processing (SLC_DP).

The emphasis was on target detectability and accuracy of direction estimates.

The processing parameters and definitions are briefly described in what follows.

(i)　Each Doppler spectrum has I, where I = 256, amplitudes. It was obtained as the inverse FFT of the output of an array element for a specified range bin in I consecutive data blocks.

(ii)　The frequency bins in the Doppler spectra are identified with i = -I/2 to i = I/2, and the Doppler frequency at the i-th bin is given by:

$$f = PRF \, \frac{i}{I}, \tag{20}$$

where PRF is the pulse repetition frequency. An approaching target produces a positive Doppler frequencies.

(iii)　For the radar frequency of 5.81 MHz, the Bragg lines are at frequencies of -0.2459 and 0.2459 Hz (Doppler bins i = -7 and i = 7), respectively.

(iv)　Each directional spectrum has K, where K = 256, amplitudes. It was obtained as the inverse FFT of a K-point sequence obtained by augmenting the N amplitudes of a processed main array snapshot with K-N zeros. The processing included Doppler processing and, if needed adaptive sidelobe cancellation.

(v)　The bins in the K-point FFT direction spectra are labelled with k = -K/2 to k = K/2. The direction at the k-th bin is given by:

$$\theta_k = \frac{Nk}{K} \quad \text{(beamwidth)} \tag{21}$$

or

$$\theta_k = \sin^{-1}(\frac{k\lambda}{Kd}) \quad \text{(radians)} \tag{22}$$

where N is the number of main-array elements, d is the element spacing and λ is the radar wavelength. All directions are measured clockwise from boresight.

A direction in beamwidths, θ_{bw}, is related to the corresponding direction in radians, θ_{rad}, by:

$$\theta_{bw} = \frac{Nd}{\lambda} \sin\theta_{rad} \; . \tag{23}$$

(vi)   A target direction estimate, denoted by $\hat{\theta}$, is an estimated obtained from a K-point FFT directional spectrum. It is the direction of the spectral peak closest to the true target direction θ. The error in the estimate is defined as:

$$\Delta\theta = \hat{\theta} - \theta \tag{24}$$

A smaller $\Delta\theta$ corresponds to a more accurate direction estimate.

(vii) Let $\underline{x}'$ be a target-absent array snapshot in a specified Doppler bin. The interference-plus-noise power in this bin is calculated as:

$$P_I + P_N = \frac{|\underline{x}'|^2}{N} \tag{25}$$

Let $\underline{x}''$ be the target-only array snapshot at the same Doppler bin. The signal power in the bin is calculated as:

$$P_s = \frac{|\underline{x}''|^2}{N} \tag{26}$$

The composite snapshot, with both target and interference present is defined as:

$$\underline{x} = \underline{x}' + \underline{x}'', \tag{27}$$

the input SINR in $\underline{x}$ is calculated as:

$$SINR_I = \frac{P_S}{P_I + P_N} \tag{28}$$

(viii)   Output SINR in a processed snapshot $\underline{x}$ is calculated as:

$$SINR_O = \frac{|\underline{x}_{\parallel}|^2}{|\underline{x}_{\perp}|^2} \qquad (29)$$

where $\underline{x}_{\parallel}$ and $\underline{x}_{\perp}$ are the components of $\underline{x}$ parallel and orthogonal to the array steering vector $\underline{v}(\theta)$, respectively. A larger $SINR_O$ corresponds to a higher detection probability.

Given a number of pairs of $\{\underline{x}_{\parallel},\underline{x}_{\perp}\}$, the output SINR is calculated as:

$$SINR_o = \frac{Ave(|\underline{x}_{\parallel}|^2)}{Ave(|\underline{x}_{\perp}|^2)} . \qquad (30)$$

Average values were used, because they smoothed out the effect of interaction between the injected and interference signals.

A preliminary examination of the data showed that the night-time interference was present in all range and Doppler bins. For this data set, the interference peaked at Doppler bin $i = 34$, corresponding to 1.2189 Hz. The direction of the peak interference was observed to vary with time between direction bins $k = 32$ and $k = 100$. After Doppler filtering, the highest peak was close to the direction bin $k = 66$ in all Doppler bins. Bins $k = 32$, 100 and 66 corresponded to 1.0, 3.12 and 2.06 beamwidths, respectively, measured clockwise from the boresight direction.

The above characteristic regarding peak position is consistent with the fact that the ionosphere is highly dynamic. This directional characteristic is essentially independent of Doppler and range.

File AIR_ONE was modified by the injection of a target with a specified range, Doppler frequency and direction. One hundred and five non-overlapping sets, each containing I, where I = 256, consecutive array snapshots with the specified range were extracted from the modified file. From each set, an array snapshot $\tilde{x}$ with the specified Doppler frequency was generated, using the methods described in Section 3.13a, b and c. This $\tilde{x}$ was then used to calculate a target direction estimate $\tilde{\theta}$ and a vector pair $\{\tilde{x}_{\parallel},\tilde{x}_{\perp}\}$, where $\tilde{x}_{\parallel}$ and $\tilde{x}_{\perp}$ were the components of $\tilde{x}$ parallel and orthogonal to the array steering vector $\underline{v}(\theta)$, respectively. The 105 values of $\tilde{\theta}$, $\tilde{x}_{\parallel}$ and $\tilde{x}_{\perp}$ were then used to calculate an average error in direction estimate, $Ave\{\Delta\theta\}$, a standard deviation of direction estimates, $Std\{\theta\}$, and an output SINR, $SINR_O$. To facilitate the comparison of results, all directions are expressed in beamwidths (bw) measured clockwise from boresight.

Table 4 contains the values of $Ave\{\Delta\theta\}$, $Std\{\theta\}$ and $SINR_O$ calculated with sixteen target directions spaced 0.5 beamwidth apart. The injected target signal was in range bin 50 and

θ (bw)	NO_SLC			DP_SLC			SLC_DP		
	Ave(Δθ̂) (bw)	Std(Δθ̂) (bw)	SINR$_o$ (dB)	Ave(Δθ̂) (bw)	Std(Δθ̂) (bw)	SINR$_o$ (dB)	Ave(Δθ̂) (bw)	Std(Δθ̂) (bw)	SINR$_o$ (dB)
-4.0	-0.001	0.069	5.66	-0.144	0.092	1.35	-0.134	0.042	4.15
-3.5	-0.007	0.053	5.45	-0.053	0.085	2.90	-0.042	0.037	5.62
-3.0	0.002	0.060	5.30	-0.076	0.065	2.15	-0.068	0.027	5.48
-2.5	0.007	0.051	5.35	0.049	0.114	2.79	0.052	0.076	5.22
-2.0	-0.002	0.049	5.53	-0.004	0.106	1.93	-0.013	0.046	5.60
-1.5	-0.004	0.067	5.48	0.038	0.109	1.01	0.049	0.051	2.75
-1.0	0.001	0.065	5.39	-0.038	0.114	3.24	-0.034	0.084	7.24
-0.5	0.014	0.052	5.47	0.011	0.112	1.56	0.021	0.047	3.71
0.0	0.004	0.061	5.64	0.021	0.094	2.90	0.024	0.074	6.07
0.5	-0.014	0.061	5.59	0.084	0.073	1.75	0.077	0.045	4.68
1.0	0.013	0.145	6.15	0.201	0.193	4.33	0.179	0.120	7.75
1.5	0.018	0.161	8.73	0.226	0.168	5.61	0.194	0.129	10.18
2.0	0.015	0.083	11.87	0.025	0.295	1.72	-0.006	0.195	3.83
2.5	0.000	0.124	9.56	-0.013	0.257	4.19	0.021	0.147	7.96
3.0	-0.024	0.137	7.06	-0.257	0.230	4.84	-0.269	0.110	7.16
3.5	-0.015	0.078	5.78	-0.106	0.169	2.90	-0.081	0.058	5.80

Table 4: Dependence of Ave(Δθ̂), Std(θ̂) and SINR$_o$ on beam direction for SINR$_i$ = 5 dB. The Doppler bin i = 34 and the interference-plus-noise power $P_i + P_N$ = 0.1975E-06.

41

θ (bw)	NO_SLC			DP_SLC			SLC_DP		
	Ave(Δθ̂) (bw)	Std(Δθ̂) (bw)	SINR$_o$ (dB)	Ave(Δθ̂) (bw)	Std(Δθ̂) (bw)	SINR$_o$ (dB)	Ave(Δθ̂) (bw)	Std(Δθ̂) (bw)	SINR$_o$ (dB)
-4.0	-0.001	0.200	-3.29	-0.140	0.142	-0.33	-0.130	0.093	1.77
-3.5	-0.054	0.190	-3.73	-0.054	0.104	0.50	-0.053	0.072	2.27
-3.0	0.010	0.202	-4.20	-0.075	0.086	-0.01	-0.065	0.111	2.17
-2.5	0.030	0.192	-3.96	0.045	0.150	0.61	0.052	0.105	2.42
-2.0	-0.018	0.121	-3.54	-0.019	0.135	-0.18	-0.001	0.076	2.06
-1.5	-0.035	0.136	-3.70	0.032	0.138	-0.76	0.041	0.110	0.52
-1.0	0.007	0.201	-3.93	-0.041	0.163	0.99	-0.042	0.119	3.24
-0.5	0.051	0.191	-3.69	-0.010	0.184	-0.15	0.012	0.101	1.34
0.0	0.018	0.172	-3.37	0.024	0.125	0.41	0.029	0.099	2.15
0.5	-0.022	0.247	-3.31	0.082	0.099	-0.25	0.086	0.067	1.75
1.0	0.100	0.416	-1.56	0.214	0.265	2.07	0.193	0.176	3.99
1.5	0.137	0.328	3.99	0.229	0.221	3.79	0.204	0.182	5.71
2.0	0.003	0.212	6.47	0.045	0.282	1.36	0.051	0.241	2.14
2.5	-0.090	0.298	4.78	-0.043	0.311	2.81	-0.039	0.271	4.23
3.0	-0.101	0.377	0.00	-0.235	0.333	3.27	-0.279	0.235	4.65
3.5	-0.004	0.384	-2.57	-0.124	0.239	0.89	-0.087	0.157	2.12

Table 5: Dependence of Ave(Δθ̂), Std(θ̂) and SINR$_o$ on beam direction for SINR$_i$ = 0 dB. The Doppler bin i = 34 and the interference-plus-noise power $P_i + P_N$=0.1975E-06.

θ (bw)	NO_SLC			DP_SLC			SLC_DP		
	Ave($\Delta\hat{\theta}$) (bw)	Std($\Delta\hat{\theta}$) (bw)	SINR$_o$ (dB)	Ave($\Delta\hat{\theta}$) (bw)	Std($\Delta\hat{\theta}$) (bw)	SINR$_o$ (dB)	Ave($\Delta\hat{\theta}$) (bw)	Std($\Delta\hat{\theta}$) (bw)	SINR$_o$ (dB)
-4.0	-0.001	0.120	0.94	-0.144	0.106	0.87	-0.131	0.057	3.45
-3.5	-0.010	0.115	0.65	-0.053	0.088	2.17	-0.046	0.046	4.49
-3.0	0.002	0.111	0.42	-0.077	0.068	1.50	-0.071	0.035	4.39
-2.5	0.015	0.094	0.51	0.049	0.125	2.15	0.052	0.082	4.39
-2.0	-0.002	0.081	0.74	-0.002	0.110	1.28	-0.010	0.055	4.41
-1.5	-0.022	0.079	0.68	0.031	0.115	0.45	0.047	0.066	2.03
-1.0	0.000	0.114	0.51	-0.038	0.127	2.55	-0.036	0.093	5.86
-0.5	0.030	0.101	0.68	0.002	0.139	1.06	0.018	0.059	3.00
0.0	0.006	0.100	0.93	0.022	0.100	2.14	0.026	0.082	4.72
0.5	-0.024	0.111	0.87	0.084	0.080	1.16	0.082	0.050	3.75
1.0	0.055	0.283	2.13	0.204	0.216	3.58	0.182	0.131	6.44
1.5	0.072	0.251	5.74	0.229	0.179	5.02	0.191	0.146	8.50
2.0	0.030	0.134	8.47	0.058	0.296	1.52	0.028	0.197	3.10
2.5	-0.028	0.223	6.49	-0.026	0.274	3.71	0.012	0.177	6.39
3.0	-0.047	0.238	3.25	-0.242	0.235	4.33	-0.276	0.151	6.35
3.5	-0.061	0.279	1.31	-0.124	0.221	2.31	-0.081	0.076	4.50

Table 6: Dependence of Ave($\Delta\hat{\theta}$), Std($\hat{\theta}$) and SINR$_o$ on beam direction for SINR$_i$ = -5 dB. The Doppler bin i = 34 and the interference-plus-noise power $P_i + P_N = 0.1975E\text{-}06$.

Doppler frequency bin i = 34 and its $SINR_I$ was 5.0 dB. In the last two rows are the averages and standard deviations of the values in the columns. There are several notable observations. Firstly, the values vary with directions and the variation is largest in the range $1.0 \leq \theta \leq 3.0$ bw. Secondly, the direction estimates were the most accurate in the results obtained with NO_SLC, less accurate with SLC_DP and least accurate with DP_SLC. Thirdly, the average $SINR_O$ is 6.5 dB in the NO_SLC results, about 5.8 dB in the SLC_DP results, and less than 3.0 dB in the DP_SLC results. Tables 6 and 7 contain the results obtained by lowering the $SINR_I$ to 0.0 and -5.0 dB, respectively. From the average and standard deviations in the last two rows, it was observed that the SLC_DP method produced the best results.

Table 7 contains the results calculated with sixteen Doppler frequencies spaced 16 bins apart. The injected target signal was in range bin 50 and direction $\theta = 0$. Its $SINR_I$ was 0.0 dB. With the exception of slightly larger values of Ave$\{\Delta\hat{\theta}\}$, it was observed that the SLC_DP produced the best results for all frequencies.

Table 8 contains the results calculated with four different range bins and target directions $\theta = 0.0$, 0.31, and 1.25 bw. The injected target signal was in Doppler bin i = 34 and the $SINR_I$ was 0.0 dB. With the exception of larger values of Ave$\{\Delta\hat{\theta}\}$ for $\theta = 1.25$, it was observed that the SLC_DP procedure produced the best results for all range bins.

The following conclusions are based on the results in Tables 4 to 8:

(i)   The NO_SLC results are the best if $SINR_I = 5$ dB or higher; and

(ii)   The SLC_DP results are the best if $SINR_I = 0$ dB or lower and the target direction θ is not close to the peak direction of the interference. When the two directions are close the magnitude of Ave$\{\Delta\hat{\theta}\}$ is larger than those in the NO_SLC and DP_SLC results.

A few remarks are in order. Firstly, the $SINR_O$ cannot fall below a certain minimum value; otherwise, the target cannot be detected. The minimum value is system dependent and will not be discussed here. Based on this consideration, the SLC_DP method provides the best detection performance when the $SINR_I$ is low.

Secondly, adaptive sidelobe cancellation is unnecessary if $SINR_I$ is high. In this case, one expects the results to be better than those obtained with SLC_DP and DP_SLC, because sidelobe cancellation modifies the gain patterns of the main array. The modification changes the relative magnitudes of the signals and noise and usually adds a bias to the target direction estimate as well.

Thirdly, the SLC_DP results are usually better than the DP_SLC results, because night-time interference is produced by ionospheric reflection of unwanted target signals. The ionosphere is highly dynamic and produces rapid fluctuations in arrival directions of interference signals. The DP_SLC method averages these fluctuations over time and is less effective than the SLC_DP method which works on the instantaneous interference directions. The variation of the parameters in Table 4 with direction agrees with the earlier observation that the interference direction is centred near 2.06 beamwidth off boresight.

Doppler (Bin)	$P_I + P_N$	NO_SLC			DP_SLC			SLC_DP		
		Ave($\Delta\hat{\theta}$) (bw)	Std($\Delta\hat{\theta}$) (bw)	$SINR_o$ (dB)	Ave($\Delta\hat{\theta}$) (bw)	Std($\Delta\hat{\theta}$) (bw)	$SINR_o$ (dB)	Ave($\Delta\hat{\theta}$) (bw)	Std($\Delta\hat{\theta}$) (bw)	$SINR_o$ (dB)
-126	0.7491E-07	-0.029	0.104	0.62	-0.001	0.126	1.15	0.015	0.078	5.85
-110	0.8030E-07	0.004	0.109	0.54	0.015	0.096	1.71	0.022	0.072	5.78
-94	0.7601E-07	0.003	0.135	0.77	0.006	0.118	1.21	0.025	0.080	5.36
-78	0.1057E-06	-0.002	0.111	0.82	0.001	0.124	1.64	0.021	0.079	5.84
-62	0.1685E-06	0.006	0.107	0.87	0.006	0.129	2.36	0.023	0.072	6.25
-46	0.2446E-06	0.009	0.129	0.67	0.001	0.128	2.65	0.023	0.070	·6.57
-30	0.6539E-06	0.012	0.114	0.67	0.018	0.105	3.11	0.022	0.068	6.71
-14	0.1582E-05	0.017	0.097	0.59	0.060	0.092	2.98	0.023	0.071	6.89
2	0.6443E-06	-0.004	0.119	0.73	0.026	0.104	1.86	0.017	0.072	6.75
18	0.3078E-06	0.024	0.119	0.64	0.018	0.121	1.59	0.024	0.076	6.14
34	0.1975E-06	0.006	0.100	0.93	0.022	0.101	2.13	0.024	0.074	6.07
50	0.1277E-06	0.027	0.126	0.62	0.035	0.094	2.12	0.025	0.073	6.02
66	0.9117E-07	0.010	0.127	0.90	0.021	0.104	1.39	0.022	0.084	5.30
82	0.1002E-06	0.027	0.135	0.35	0.034	0.122	1.52	0.025	0.077	5.67
98	0.7957E-07	-0.008	0.100	0.71	0.026	0.115	1.43	0.023	0.083	5.62
114	0.8289E-07	-0.004	0.107	0.56	0.018	0.105	1.37	0.020	0.071	5.77
Average		0.006	0.115	0.69	0.019	0.112	1.89	0.022	0.075	6.04
Standard Deviation		0.014	0.012	0.15	0.015	0.012	0.59	0.003	0.005	0.47

Table 7: Dependence of Ave($\Delta\hat{\theta}$), Std($\hat{\theta}$) and $SINR_o$ on Doppler frequency for a target in range bin 50 and bearing at boresight ($SINR_I = 0$ dB).

θ (bw)	$P_I + P_N$	Range (bin)	NO_SLC Ave(Δθ̂) (bw)	NO_SLC Std(Δθ̂) (bw)	NO_SLC SINR$_o$ (dB)	DP_SLC Ave(Δθ̂) (bw)	DP_SLC Std(Δθ̂) (bw)	DP_SLC SINR$_o$ (dB)	SLC_DP Ave(Δθ̂) (bw)	SLC_DP Std(Δθ̂) (bw)	SLC_DP SINR$_o$ (dB)
0.0	0.1975E-06	50	0.006	0.100	0.93	0.022	0.101	2.13	0.026	0.082	4.72
	0.1904E-06	70	0.001	0.097	0.86	0.016	0.101	2.28	0.018	0.079	5.04
	0.1896E-06	110	0.008	0.120	0.58	0.032	0.108	1.70	0.027	0.086	4.99
	0.1936E-06	170	0.007	0.140	0.70	0.024	0.097	2.64	0.018	0.074	5.74
0.31	0.1975E-06	50	-0.012	0.102	0.93	0.074	0.092	0.89	0.071	0.058	2.82
	0.1904E-06	70	-0.011	0.099	0.82	0.062	0.091	1.04	0.065	0.059	3.27
	0.1896E-06	110	0.010	0.111	0.67	0.076	0.090	0.89	0.067	0.061	3.16
	0.1936E-06	170	-0.001	0.132	0.74	0.073	0.084	1.23	0.068	0.057	3.44
1.25	0.1975E-06	50	0.051	0.275	3.31	0.288	0.182	4.27	0.264	0.108	6.87
	0.1904E-06	70	0.093	0.274	3.68	0.312	0.188	4.89	0.274	0.125	7.26
	0.1896E-06	110	0.044	0.233	3.50	0.282	0.202	4.62	0.278	0.120	7.03
	0.1936E-06	170	0.045	0.258	3.43	0.277	0.193	4.61	0.274	0.113	7.31

Table 8: Dependence of Ave($\hat{\Delta\theta}$), Std($\hat{\theta}$) and SINR$_o$ on range for several target directions at fixed Doppler ($SINR_I = 0$ dB; Doppler bin #34).

46

To gain some insight into the accuracy of the bearing estimate of a real target after interference cancellation, the data segments that contain the echoes of the Challenger 601 and communications interference were analyzed. These data segments correspond to CIT No. 70 to 77 of data file AIR_SEVEN. In these CIT intervals, the target was not detected because of the interference. Figure 26a shows the spectrum of the data in CIT No.71. The Doppler component corresponding to the Challenger is submerged in interference. Figure 26b shows the spectrum of the same data after Doppler-domain cancellation with sliding-range-window averaging is applied. The interference around the target Doppler has been suppressed and the target has emerged.

The Doppler shift of the target in Figure 26 is estimated to be 3.55 Hz which corresponds to a radial velocity of 178.2 knots. The angular response of this Doppler component is obtained by performing digital beam forming on this Doppler component, using a 256-point FFT. The results are shown in Figure 27. In both cases (with and without interference cancellation), the peak response of the target is at 0.39°. This agrees well with the ground-truth data of the target which indicated that the aircraft flew along the aperture boresight towards the radar.

3.2   Ionospheric clutter.

There are more constraints on the cancellation of ionospheric clutter than that of communications interference. Ionospheric clutter is a self-generated interference and not present when the transmit signal or a reflective medium is not present. Consequently, it is not appropriate to use range averaging to calculate the correlation estimates. This leaves time-domain cancellation with sliding-time-window averaging as the only viable solution. However, as demonstrated in Section 3.1, the effectiveness of time-domain cancellation depends on how quickly the correlation estimates are obtained and applied. For low WRF systems such as the Cape Race radar, the time between snapshots is too long for the time-domain cancellation to be effective since it takes at least several tens of snapshots to obtain reliable correlation estimates. By the time the estimation process is completed, several seconds would have elapsed, rendering the cancellation ineffective. Nevertheless, if the WRF is sufficiently high such that the time between snapshots is short, time-domain cancellation will yield good ionospheric clutter suppression.

Since the WRF of the radar was rather low, these data are not suitable for analysis of time-domain cancellation schemes for ionospheric clutter, using either time or range averaging. There is one other scheme which we have not tried up to this point that might work when the WRF is low. That is "Doppler-domain cancellation with Doppler averaging". The rationale is as follows. Assume that the ionospheric clutter is the dominant interference in the returns from a number of range bins and that it has a Doppler spectrum that encompasses a moderate number of Doppler bins. If the clutter is coming from a small number (smaller than the number of auxiliary antennas) of bearings, then the various Doppler components associated with the ionospheric clutter will have similar directional characteristics. And the covariance matrix and the correlation vectors may be estimated by averaging Doppler samples. To examine this approach we use data from the Cape Race radar.
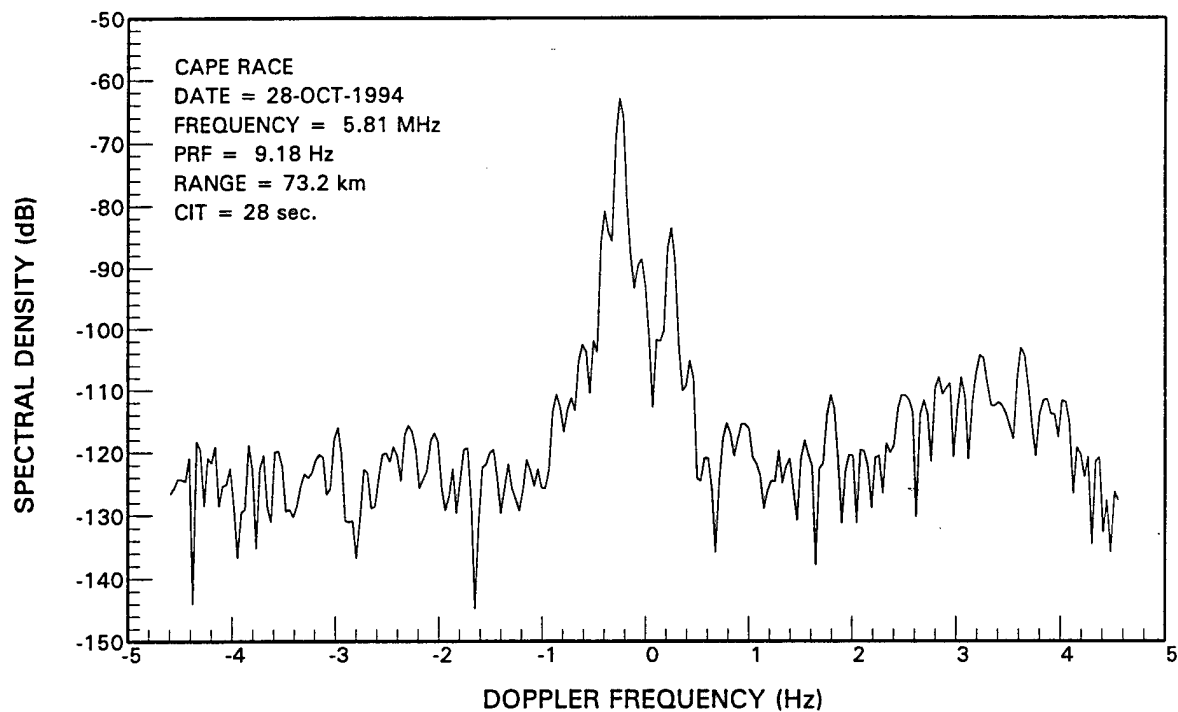
(a) Doppler spectrum with no cancellation.
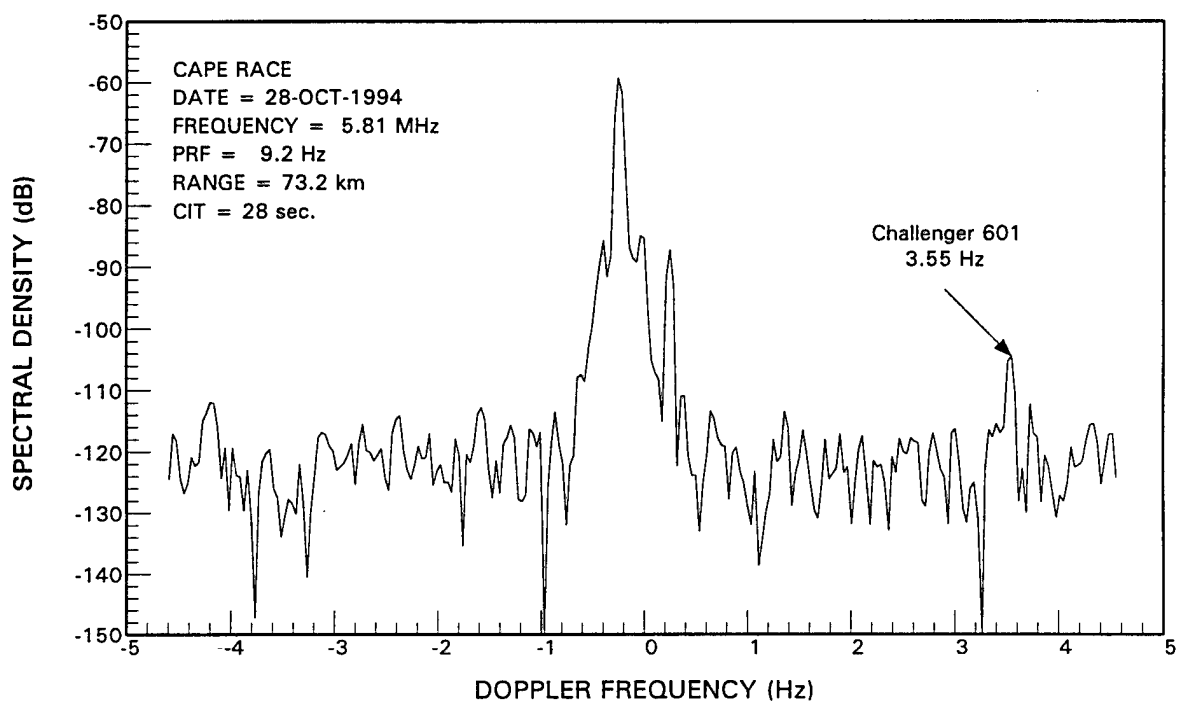
(b) Doppler spectrum after Doppler-domain cancellation.

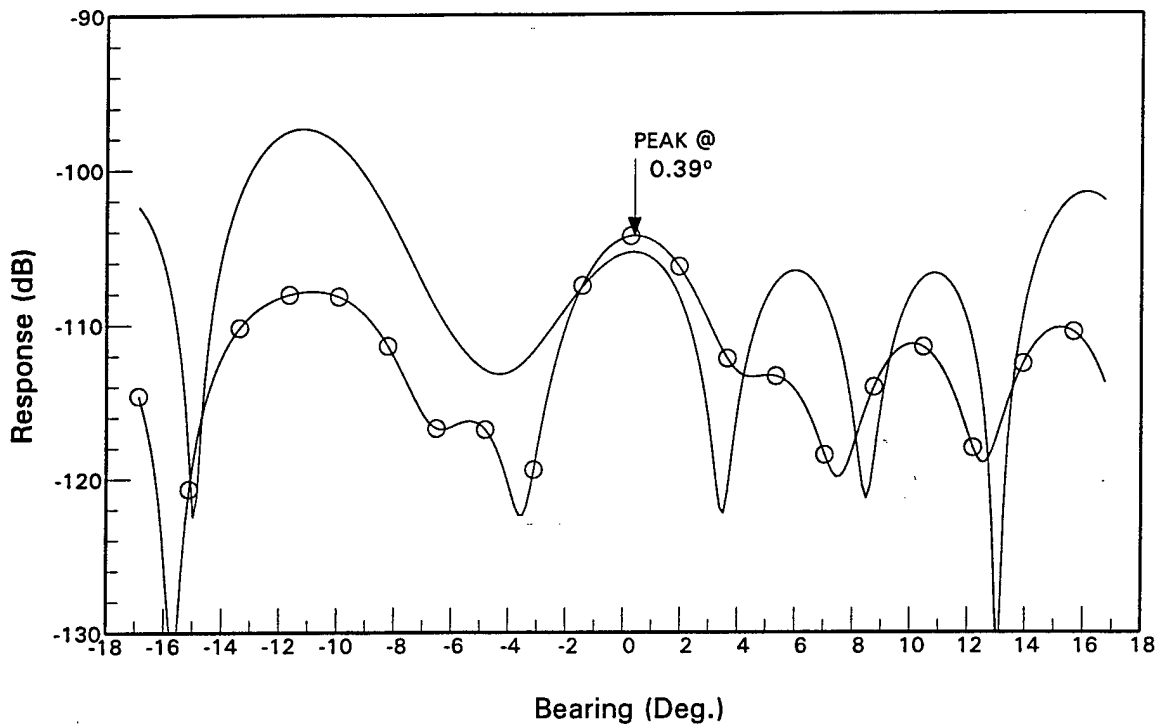Figure 26. Spectra of data containing echoes from a Challenger 601.

48

Figure 27. Angular response of the target Doppler component.

Figure 28 shows the Doppler spectrum of the returns at boresight from range bin no. 200 (about 240 km from Cape Race). The data were taken from file AIR_FIVE, and the spectrum was computed using a 2048-point FFT. This FFT size corresponds to a CIT of 223 seconds which is compatible with ship detection. The spectral components from -0.4 Hz to about +0.9 Hz were those of the ionospheric clutter. Since the WRF of the data was 9.18 Hz, there were about 290 Doppler bins in this region.

A simple scheme that is easy to implement is to use all (except the one to which cancellation is to be applied and a number of neighbouring Doppler bins which serves as a guard zone) the Doppler samples in the region (-0.4 Hz to +0.9 Hz) to compute the covariance matrix and the correlation vectors. An estimate of the interference derived from these correlation estimates is subtracted from each Doppler sample in the region. Since both estimation and cancellation take place within the same range bin at the same time instant, the problem of the long elapsed time between estimation and cancellation is circumvented.

It was conjectured that, if there is no significant variation in the directional characteristics of the ionospheric clutter within a CIT, this scheme could work. Figure 29 shows the resulting spectrum after cancellation was applied to all Doppler samples, using the scheme described above. The ionospheric clutter was suppressed in some of the Doppler components. The average improvement factor in the Doppler region (-0.4 Hz, +0.9 Hz) was about 2 dB.
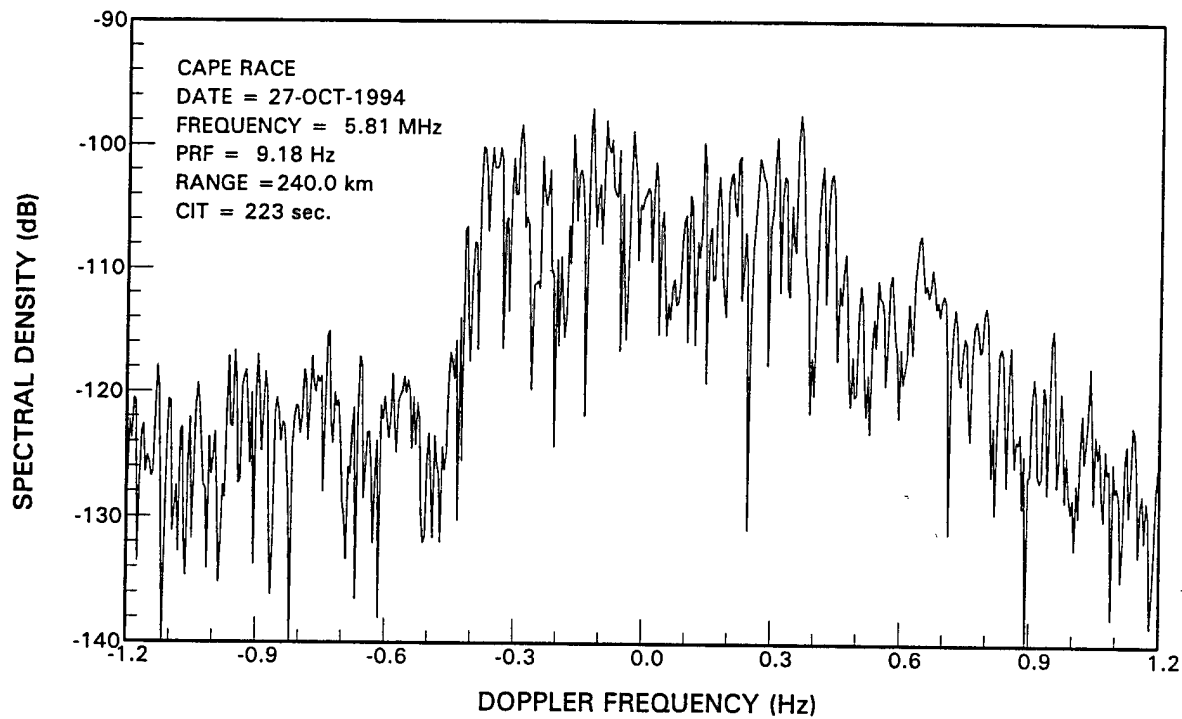
49

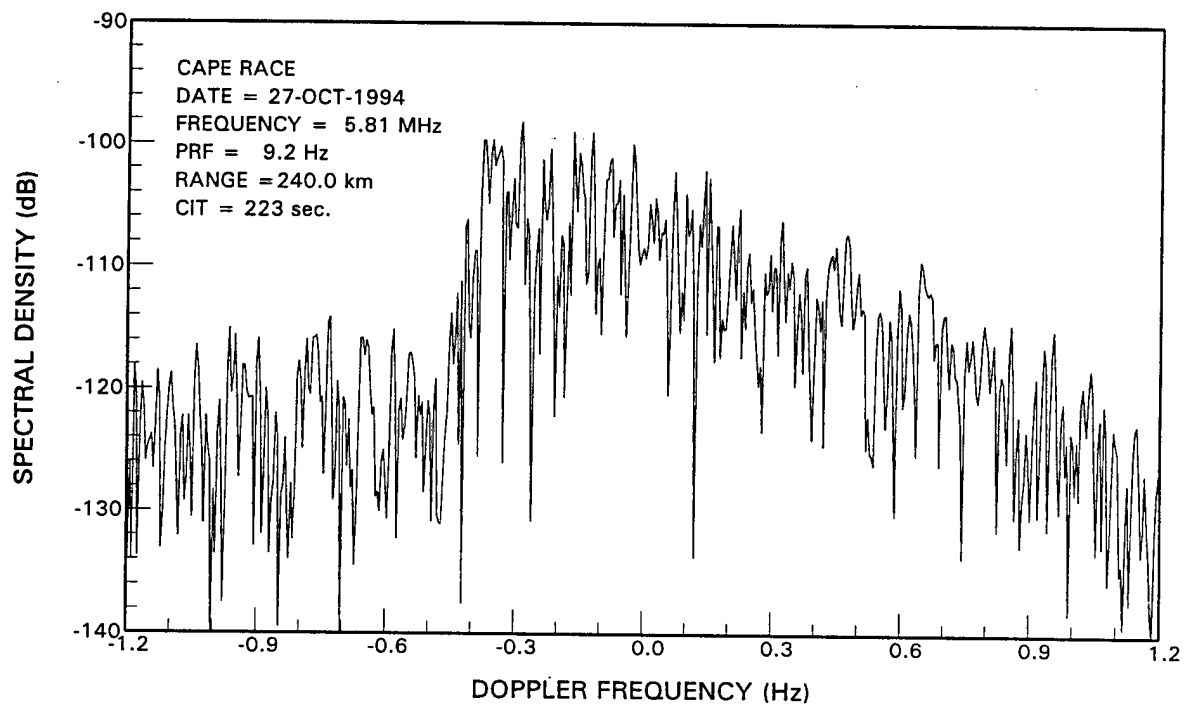Figure 28. Doppler spectrum with no cancellation.

Figure 29. Spectrum of data after Doppler-domain cancellation.

To investigate how this interference cancellation scheme affects a target, synthesized target samples were generated and imbedded in the time series before Doppler processing. The target bearing was at boresight, and the target magnitude was -96 dB. From Figure 29, it can be seen that the suppression was greater on the positive side of the Doppler spectrum. Hence we chose a target Doppler of 0.15 Hz.

Figure 30 shows the spectrum of the time series with the imbedded target without interference cancellation. It is difficult to differentiate the target from the interference. Figure 31 shows the resulting spectrum after interference cancellation had been applied. The target has now emerged from the clutter.

From the above analysis, it is evident that the coherent sidelobe cancellation scheme as implemented for co-channel communications interference is not very effective against ionospheric clutter. The reasons are as follows.

(i)   Ionospheric clutter could come from several directions, and these directions may vary with time. Consequently, the auxiliary antenna array must have a sufficient number of elements to provide the required degrees of freedom to cancel the spatially-distributed clutter.

(ii)   In the ionospheric clutter region, there are frequent occurrences of meteoric clutter. The meteoric clutter alters the temporal and spatial correlation characteristics, rendering their estimation inaccurate.

(iii)   Ionospheric clutter is isolated in range. This means that it is not appropriate the employ range-averaging to estimate the correlation properties needed for coherent sidelobe cancellation.

(iv)   Ionospheric clutter is time varying both in range and Doppler. This means that employing time averaging or Doppler averaging to estimate the correlation properties is likely to be ineffective.

It may be possible to improve the performance of the coherent sidelobe cancellation scheme by a judicious use time-averaging, range averaging and Doppler averaging to obtain the correlation properties. Alternatively, techniques other than the coherent sidelobe cancellation scheme may be employed. The development of these schemes and the verification of their performance is beyond the scope of the current study. Nevertheless, it is important to gain a good understanding of the behaviours of ionospheric clutter in the temporal, spatial and spectral domains. In Appendix A, we present the analysis of some available ionospheric clutter data in terms of its temporal, spatial and spectral behaviours.

Based on the results presented in Appendix A, it appears that the ionospheric clutter arising from overhead reflection off the E-region is less of a problem at higher frequencies (about 4 MHz) where ship detection is concerned. The reason for this is that the magnitude of the ionospheric clutter from the E region, at higher frequencies, is significantly lower than the Bragg lines. It is most pronounced during the morning hours. Since the apparent range of the E-region
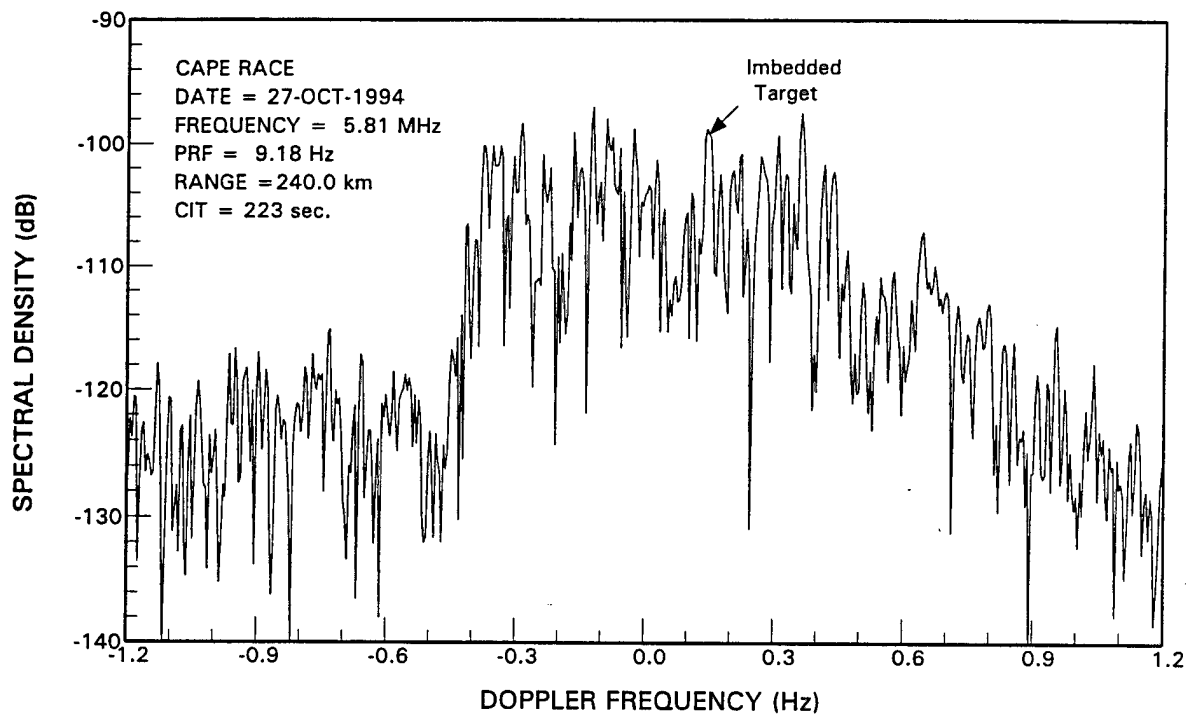
51

Figure 30. Doppler spectrum of data with an imbedded synthetic target with no cancellation.
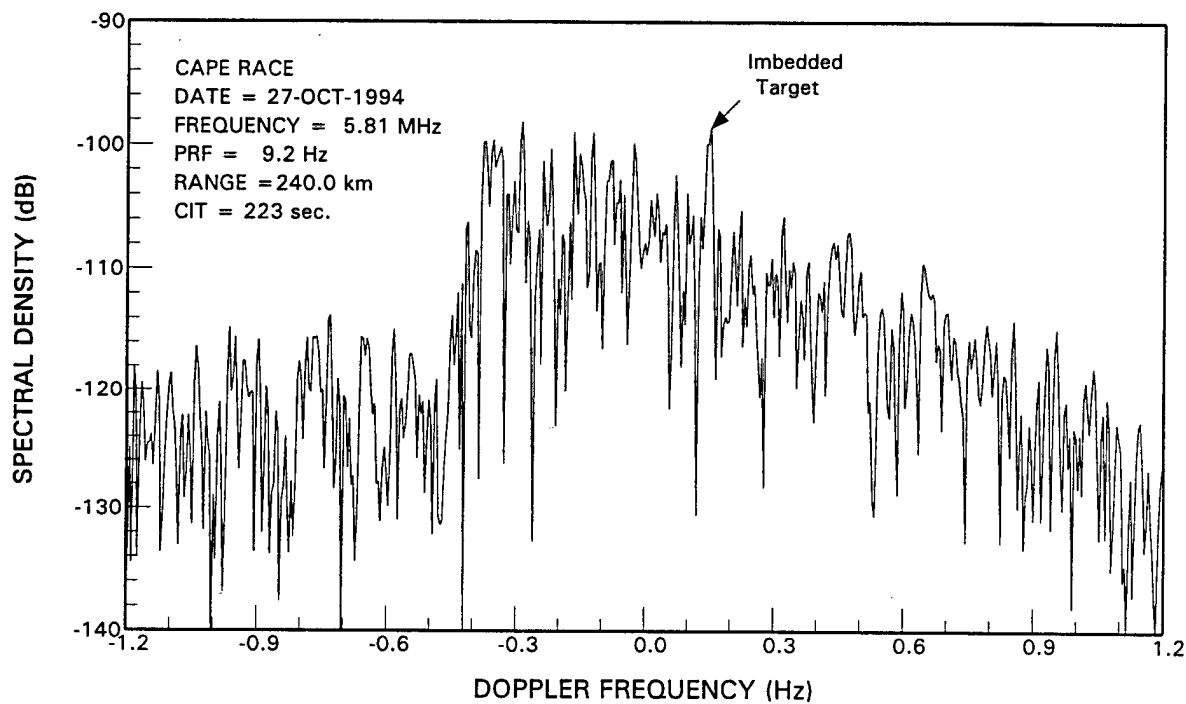

Figure 31. Doppler Spectrum of data with an imbedded synthetic target after Doppler-domain cancellation using Doppler averaging.

is around 100 km, vessels with a moderately large RCS would still yield sufficient signal-to-clutter ratio for detection.

At longer ranges (250 km to 350 km), ionospheric reflection presents a bigger problem. The magnitude of the F-region ionospheric clutter at higher frequencies is higher than that for the E-region. In addition, at long ranges, the target magnitude would be attenuated, resulting in a much lower signal-to-clutter ratio. For long-range ship detection in the F-region ionospheric clutter zone, the radar should operate at frequencies below 4 MHz.

4.   CONCLUSIONS AND DISCUSSION.

4.1   Conclusions

From analyses presented in Section 3, the following conclusions can be drawn.

(a)   For interference suppression schemes based on coherent sidelobe cancellation techniques, there are only two distinct cases in which different results will be produced as a consequence of changing the order of execution among interference suppression, Doppler processing and digital beam forming. These are (i) interference cancellation before Doppler processing and (ii) interference cancellation after Doppler processing. Changing the order of execution between Doppler processing and digital beamforming either in the time domain or the Doppler domain does not affect the outcome.

(b)   For the case where co-channel communications interference is dominant, the optimum processing procedures are as follows.

(i)   Interference cancellation on each time sample using sliding-range-window averaging for computation of the correlation estimates;
(ii)   Doppler processing
(iii)   Digital beamforming.

Steps (ii) and (iii) may be interchanged.

(c)   For the case where co-channel communications interference is not dominant, the optimum processing procedures are as follows.

(i)   Doppler processing;
(ii)   Interference cancellation on each Doppler sample using sliding-range-window averaging for calculation of the correlation estimates;

(iii)   Digital beamforming.

Steps (ii) and (iii) may be interchanged.

(d)   For ionospheric-clutter cancellation, using range averaging for the computation of the covariance matrix and the correlation vectors is not appropriate. The reason for this is that

ionospheric clutter is present in a small number of range bins only, and there is very little correlation among samples from range bins that are far apart. At this time, the recommended processing procedures is:

(i)   Interference cancellation in the time-domain (i.e. before Doppler processing); using sliding-time-window averaging for the computation of the covariance matrix and the correlation vectors; use a small number of samples for the average to minimize decorrelation;

(ii)   Doppler processing and beamforming or vice versa.

(e)   In terms of the effects of interference suppression on the accuracy of bearing estimates, refer to Section 3.1.3.

4.2   Discussion.

The effectiveness of any interference suppression scheme based on coherent sidelobe cancellation using array antennas depends on several factors. The first is that there must be some directivity in the interference. The second is the number of angles-of-arrival of the interference signal. This dictates the number of degrees of freedom the system must have to yield an effective cancellation.

The third is that the time between the estimation of the correlation properties of the interference process among various antenna elements and the application of cancellation must be much shorter than the decorrelation time of the interference process. For example, in the data analyzed in this study, the WRF was about 9 Hz and thus the time between two contiguous snapshots is about 110 msec. If the interference process occupies a Doppler domain of a few Hz, the decorrelation time is in the order of a few hundred milli-seconds. If time-averaging is used to calculate the correlation estimates, it will take several tens of snapshots to get the results. By the time the estimates are obtained, several seconds would have elapsed, and poor cancellation is likely to result. This is supported by the analysis results. Table 9 compares the elapsed time for calculating the correlation estimates and the improvement factor (when applied to data set AIR_ONE) among three different schemes. Progressively improving cancellation results are obtained as the elapsed time decreases.

Decorrelation, in itself, does not present problems if the interference originates in one spatial location only. In reality, however, interference comes from many directions. Because it takes different amount of time for the various interference signals to arrive at the antenna elements, the relative amplitude and phase relationships among various antenna elements could change significantly with time due to decorrelation.

Although cancellation in the Doppler-domain does not always yield the most improvement, there are, however, several advantages when the overall performance is considered.

54

Correlation estimation scheme	Elapsed time	Improvement factor (AIR_ONE) (dB)
Sliding-time-window averaging (64 snapshots)	6.9 sec.	-8.99
Fixed-range-window averaging (using 64 samples near the maximum range)	~110 msec	3.98
Sliding-range-window averaging (64 range samples)	~hundreds of μsec.	7.66

Table 9:   Comparison of improvement factor as a function of elapsed time between correlation estimates and cancellation.

The first is that it provides a means for isolating the various interference sources, thereby allowing the algorithm to operate on weaker interferences. The second is that the computation load is greatly reduced. For example, cancellation is not required for Doppler components that are outside the range of expected target-Doppler shifts. In addition, the available time for the required processing is measured in terms of tens of seconds (depending on the size of the FFT), rather than milli-seconds, as in the case of pulse-by-pulse cancellation. The third is that it preserves the information contained in the data. For example, time-domain interference suppression distorts the relative magnitude of the sea-clutter components, rendering it useless for monitoring the ocean-surface conditions. Finally, it can be implemented without disturbing the basic signal-processing structure. Because the output of the Doppler processor is near the end of the signal processing chain, the interference-suppression module can be implemented as a self-contained module inserted between the Doppler process and the digital beam former.

For improved low-altitude aircraft detection against communications interference, suppression in the Doppler domain is the most appropriate scheme. The reason for this is that the range of interest is within 150 km where the sea clutter is dominant. Doppler-domain suppression permits the isolation of the sea clutter from the interference.

Concerning the suppression of ionospheric clutter, however, there is insufficient information at present to draw the conclusion as to whether time-domain or Doppler-domain suppression yields a better performance. Because the ionospheric clutter is isolated in range, it precludes the use of Doppler-domain cancellation using range-averaging for the correlation estimates. From the limited analysis presented in Appendix A, it appears that the dominant ionospheric clutter comes from a small number of directions, perhaps 3 to 4. Consequently, given a sufficient number of auxiliary antenna elements, these can be cancelled effectively. The difficulty is in attempting to cancel the ionospheric clutter continuum. The clutter can originate from a large number of directions and thus requiring a prohibitively large number of auxiliary antennas. Furthermore, because the amplitude of the clutter continuum is significantly lower than the specular component, it would be difficult to estimate its correlation properties precisely in the presence of the much larger specular components.

There is one other property that we should examine. That is the true angle- of-arrival of the ionospheric clutter in the elevation plane. This requires a planar array or a cross array. If it can be established that the angle-of-arrival of the ionospheric clutter in elevation is confined to a narrow region, then it may be possible to cancel it with a finite number of auxiliary antenna elements configured to yield nulls in elevation. More experiments and analyses are required before a definite conclusion can be drawn.

5.   REFERENCES.

[1]   R. H. Khan, "Ocean-Clutter Model for High-Frequency Radar," IEEE Journal of Ocean Engineering, Vol. 62, pp. 181-188, April 1991.

[2]   M.W.Y. Poon, R.H. Khan and S. Le-Ngoc, "A Singular Value Decomposition based Method for Suppressing Ocean Clutter in High Frequency Radar", IEEE Trans on Signal Processing, Vol.41, No.3, March 1993, pp.1421-1425.

[3]   Howells, "Intermediate Frequency Sidelobe Canceller," U.S. Patent 3 202 990, August 1965.

[4]   S.P. Applebaum, "Adaptive Arrays," IEEE Transactions on Antennas and Propagation, AP-24, September 1976, pp. 585-598.

[5]   L. Petrie, private communication, Petrie Telecommunication, October 1999.

[6]   W.R. Pigott and K. Rawer, Ed., "URSI Handbook of Ionogram Interpretation and Reduction," Amsterdam, New York: Elsevier, 1961.

[7]   J. Capon, R.J.Greenfield and R.J. Kolker, "Multidimensional Maximum Likelihood processing of a large aperture seismic array", Proceedings of the IEEE, Vol.55, No.2, February 1967, pp. 192-211.

6.   ACKNOWLEDGEMENTS.

7.   Appendix A: A cursory look at the temporal, spatial and spectral behaviours of ionospheric clutter.

To develop effective algorithms to combat ionospheric clutter in HFSWR, a thorough understanding of its behaviour is essential. Ideally, one would like to observe ionospheric clutter in terms of its strength, Doppler spread, spread in range, angles of arrival, temporal correlation, spatial correlation. In addition, it is also desirable to observe any change in behaviour as functions of time-of-day, season as well as radar-system parameters such as frequency, bandwidth, waveform, etc. This would entail a long period of data collection and analysis. In this appendix we present a preliminary examination of the characteristics of ionospheric clutter. This examination is limited in scope because of the limited amount of available data. It is understood that these observations were site-specific and that only a limited number of frequencies were used. Consequently, no generalization of these results should be made. Nevertheless, some insight may be gained from these observations that could tell us the probable effectiveness of a particular algorithm. For example, if it is observed that the ionospheric clutter originates from many directions (both in azimuth and elevation), then sidelobe cancellation techniques would require too many degrees of freedom to be effective.

Data collected from the April 1995 iceberg-tracking trial at Cape Bonavista were used. The Cape Bonavista radar employed a simple pulsed waveform with the following parameters.

Frequency   = 4.1 MHz.
PRF   = 12.5 Hz.
Waveform   = 50 μsec, raised cosine shaping.
Transmit array   = 5 element log-periodic array, Beamwidth ≈ 100°.
Receive array   = 8 element doublet array, element spacing = 38.46 m.
                   (the two monopole antennas in a doublet was spaced nominally
                   a quarter wavelength apart at 3.9 MHz)

A.1   Range-Doppler views of ionospheric clutter.

Figure A.1 shows the range-Doppler characteristics of the ionospheric clutter observed by the Cape Bonavista HFSWR. The data are taken from the April 1995 iceberg tracking trial. The radar parameters are shown in the figure. The look direction was at boresight (Beam No. 1, 110° true). Since the radar frequency was 4.1 MHz, the Bragg lines were at $f_B = \pm 0.206$ Hz, where f_B is the Bragg resonance frequency given by:

$$f_B = \pm \sqrt{\frac{g}{\pi \lambda}}$$

where $g = 9.81$ m/sec^2 is the gravity acceleration, and λ is the radar wavelength.
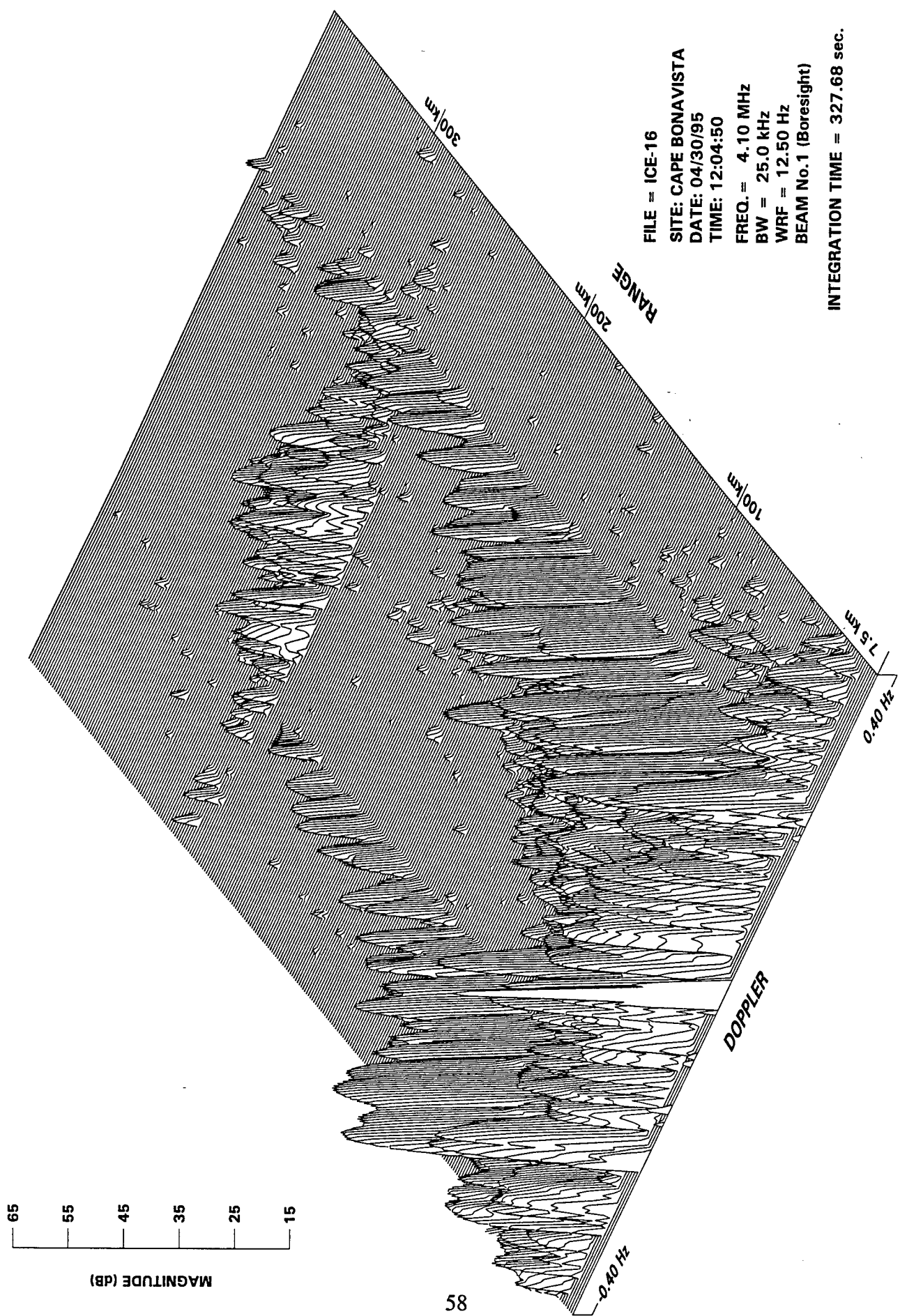
57

Figure A.1 A typical range-Doppler profile of ionospheric clutter.

FILE = ICE-16
SITE: CAPE BONAVISTA
DATE: 04/30/95
TIME: 12:04:50

FREQ. = 4.10 MHz
BW = 25.0 kHz
WRF = 12.50 Hz
BEAM No.1 (Boresight)

INTEGRATION TIME = 327.68 sec.

RANGE

300 km
200 km
100 km
7.5 km

0.40 Hz

DOPPLER

-0.40 Hz

MAGNITUDE (dB)

65
55
45
35
25
15

The Bragg lines are shown in the figure as two relatively large Doppler components around f_B that extend out to beyond 300 km. The CIT interval was 327.68 seconds (4096 pulses), a value suitable for ship detection. At approximately 270 km, a spectral components can be observed between the two Bragg lines with a range extent of about 20 to 30 km. This component is attributed to the backscatter from the ionosphere, probably the F region. Depending on the season and the time-of-day, the altitude of the F region may vary between 250 km to beyond 400 km. Since the waveform used in this radar had a nominal bandwidth of 20 kHz, the range resolution cell was approximately 7.5 km. Hence the thickness of the region that gives rise to this ionospheric clutter component was relatively small, perhaps no more than 15 to 20 km. For the data set, ionospheric reflection around 100 km range (nominally the E region) was observed only intermittently, and its magnitude was small compared with those observed at ranges beyond 250 km (nominally the F region).

The Doppler spectrum of the 270-km range bin in Figure A.1 is shown in Figure A.2. The ionospheric clutter occupied a Doppler region between ±0.4 Hz. It can be observed that, even though there was a peak in the spectrum, it was not significantly higher than its neighbours. Figure A.3 shows the spectrum of another time series, taken at 1400 hour, of a range bin in which the peak ionospheric clutter was observed. A dominant spectral peak was observed at 0.067 Hz, with a magnitude close to 20 dB greater than the next highest peak. This peak could be the result of specular reflection from some specific regions of the ionosphere. Thus the peak of the ionospheric clutter drifted in range by 36 km in about two hours.

Examining additional data, it was observed that the location of the peak ionospheric clutter in both range and Doppler, as well as its magnitude, varied as a function of the time-of-day. Figure A.4 shows the apparent height (range) of the spectral peak as a function of Newfoundland local time. It shows that the ionospheric clutter was at the greatest range (apparent height) in the afternoon and was at the closest range just before midnight. In addition, it was observed that, during daylight hours, there was a greater short-term variation (i.e., from one CIT to the next) in the range of the peak ionospheric clutter.

The magnitude of the peak ionospheric-clutter component also varied as a function of the time-of-day. Figure A.5 shows the relative magnitude of the spectral peak as a function of Newfoundland local time. It shows that the ionospheric clutter was at the lowest level around noon and the highest after dusk but before midnight. Again, during daylight hours, a greater short-term variation in the magnitude of the peak was observed. The magnitudes spanned a range of about 30 dB between midday and midnight.

No significant variation in the Doppler shift of the peak component was observed as a function of the time-of-day. Figure A.6 shows that Doppler shift of the peak ionospheric component as a function of Newfoundland local time. The Doppler shift of the peak varied between ±0.2 Hz. There was, however, a slight bias towards the positive Doppler.

The assumption that the observed ionospheric clutter was that reflected from the F-region was corroborated by calculations carried out by Petrie [5,6]. He produced prediction of the apparent height of the reflection and the relative signal strength as a function of time based on
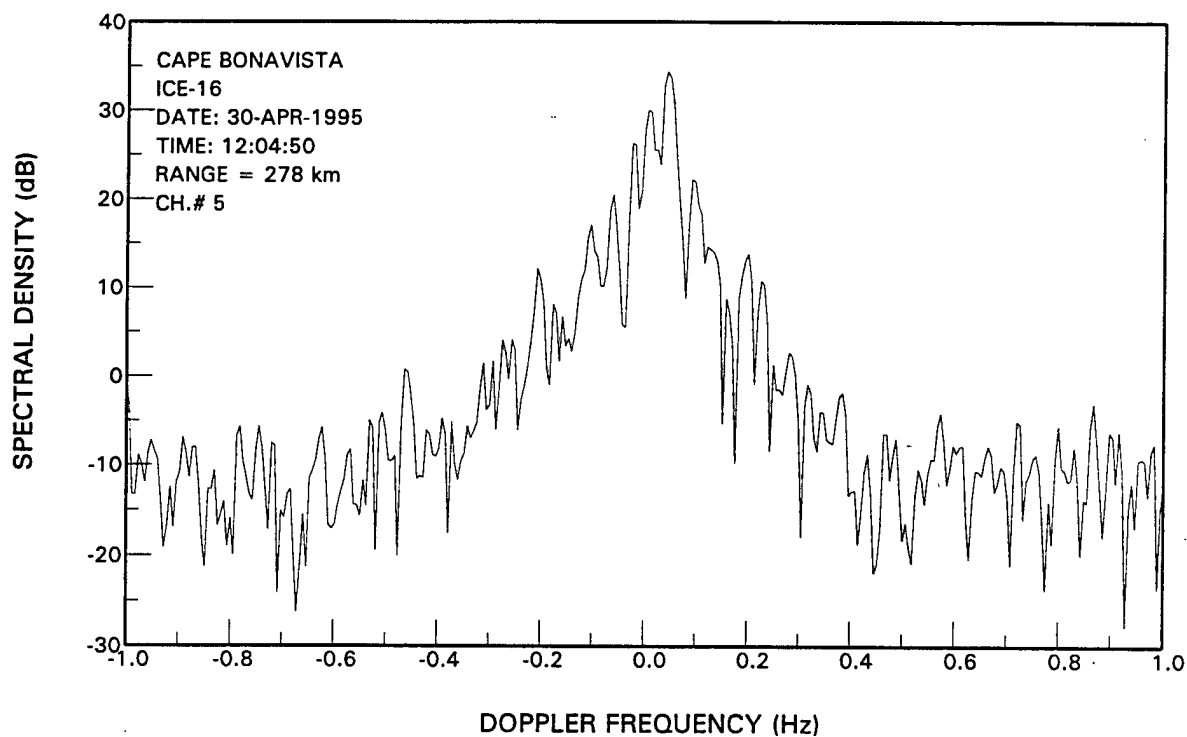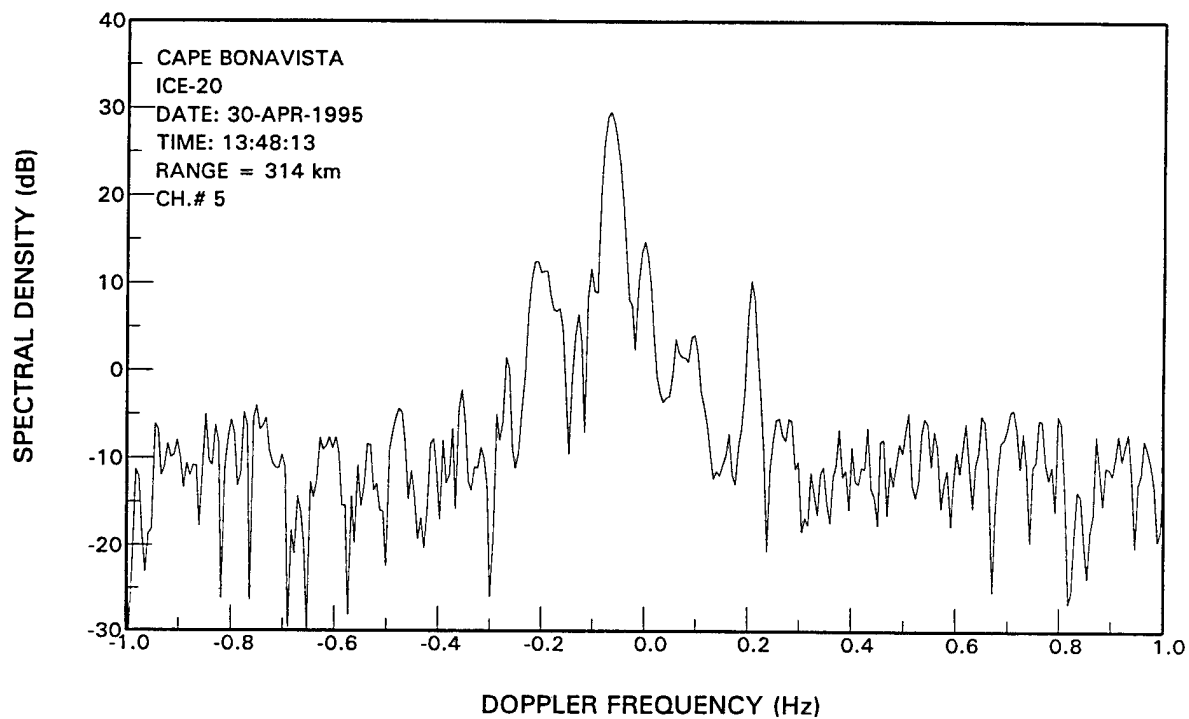
Figure A.2 A typical ionospheric clutter spectrum.

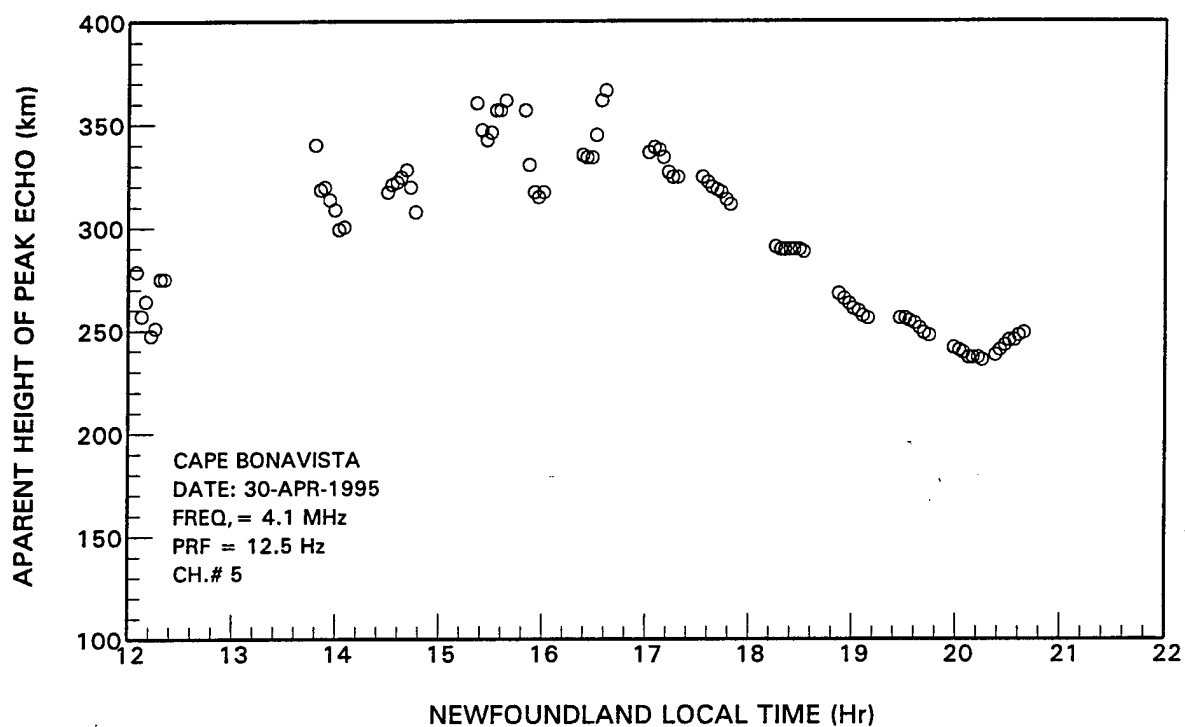Figure A.3 A typical ionospheric clutter spectrum.

60

Figure A.4 Variation of apparent height of ionospheric clutter.
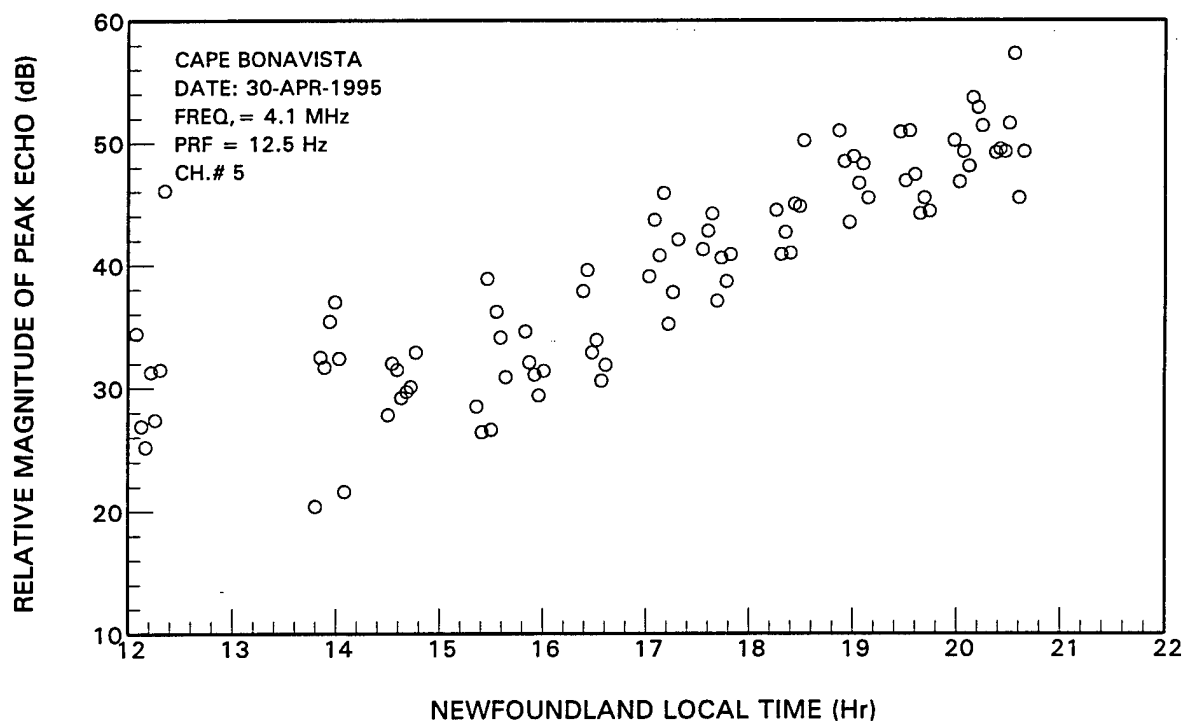

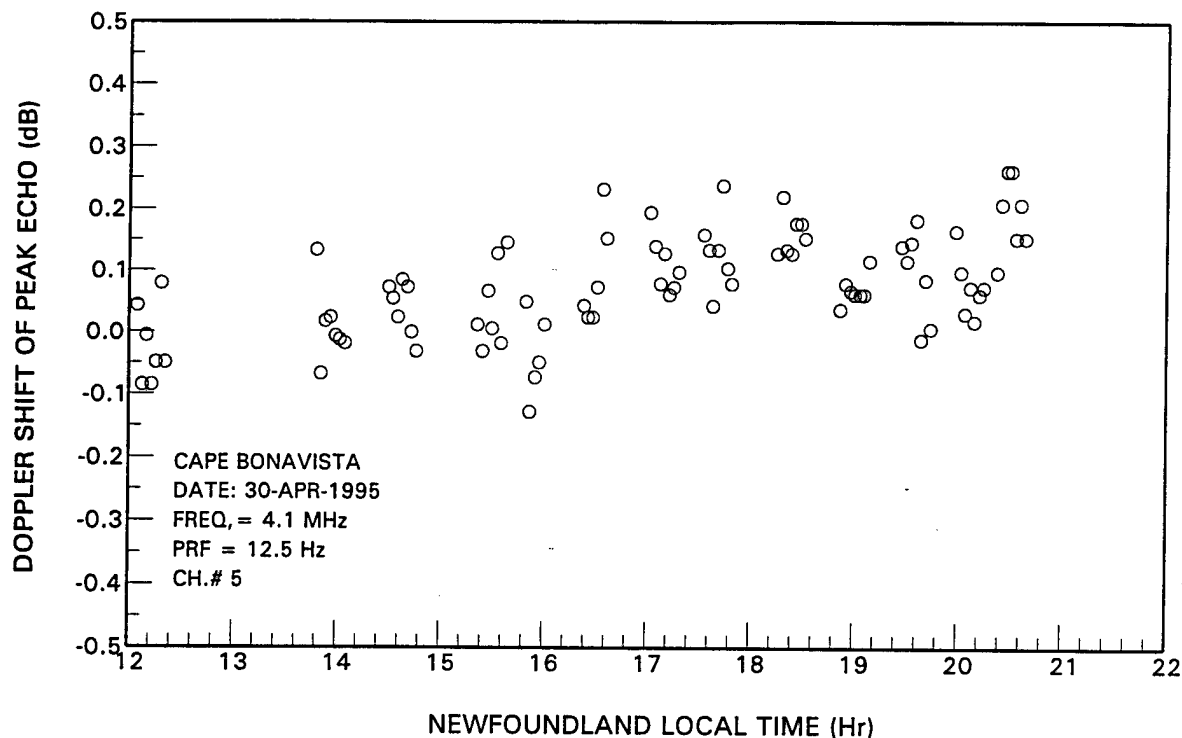Figure A.5 Variation of peak magnitude of ionospheric clutter.

61

Figure A.6 Variation of Doppler shift of the peak ionospheric clutter.

the ionosonde data of 30 April 1995. These results are shown in Figures A.7 and A.8, respectively. Good qualitative agreements between these and the experimental data are observed. In both the prediction and the radar data, the maximum and minimum height occurred at around 1600 and 2000 hours, respectively. The actual maximum range observed by the radar was greater by a few tens of km; however, this could partly be attributed to the normal tolerance of the model and partly to the fact that the prediction assumed a vertical incidence of the reflected signal. The direction of the ionospheric clutter may be at some angle off the vertical axis, thereby yielding a larger slant range.

There was also qualitative agreement between the predicted and observed relative signal strength of the ionospheric clutter. Both were observed to be at a minimum at 1300 hour. The range of variation of the predicted signal strength was much less than that in Figure A.5; however, in Figure A.5, the magnitude was that of the peak Doppler component and not the actual signal power of the total ionospheric clutter.

A.2 Temporal-spatial behaviour of ionospheric clutter.

The temporal behaviour of ionospheric clutter may be observed by examining the time series of a range bin that contain ionospheric clutter. Figure A.9 shows the in-phase waveform of such a time series over a time interval of 20 minutes. It can be observed that a significant level of ionospheric clutter was present in about half of the time. With a typical CIT interval of 200 seconds for ship detection, this implies that ship detection will be affected for 3 or 4 CITs.
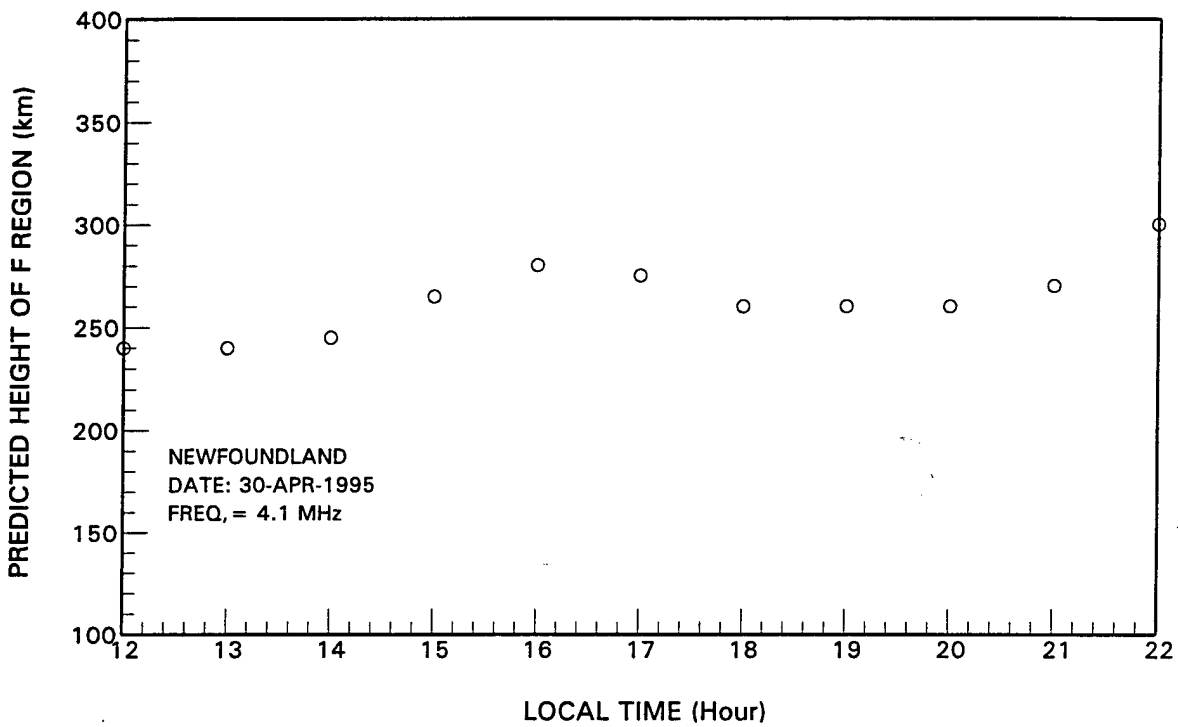
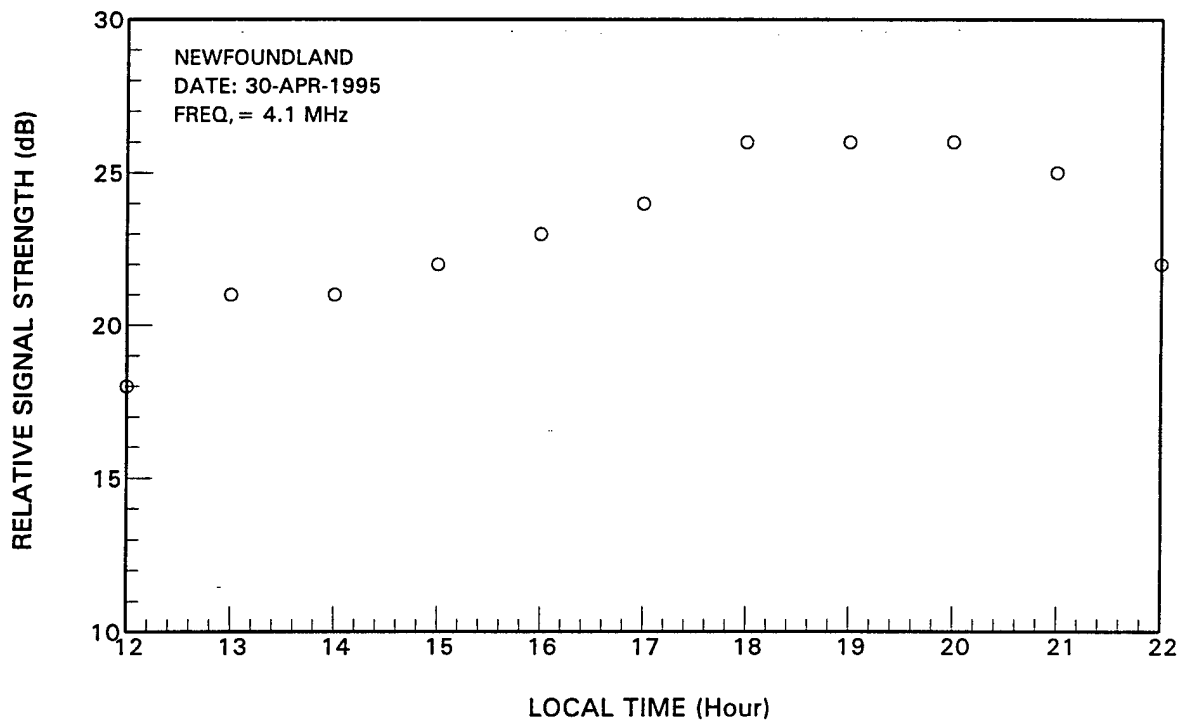Figure A.7 Predicted variation of height of ionospheric clutter.

Figure A.8 Predicted signal strength of F-region ionospheric clutter.
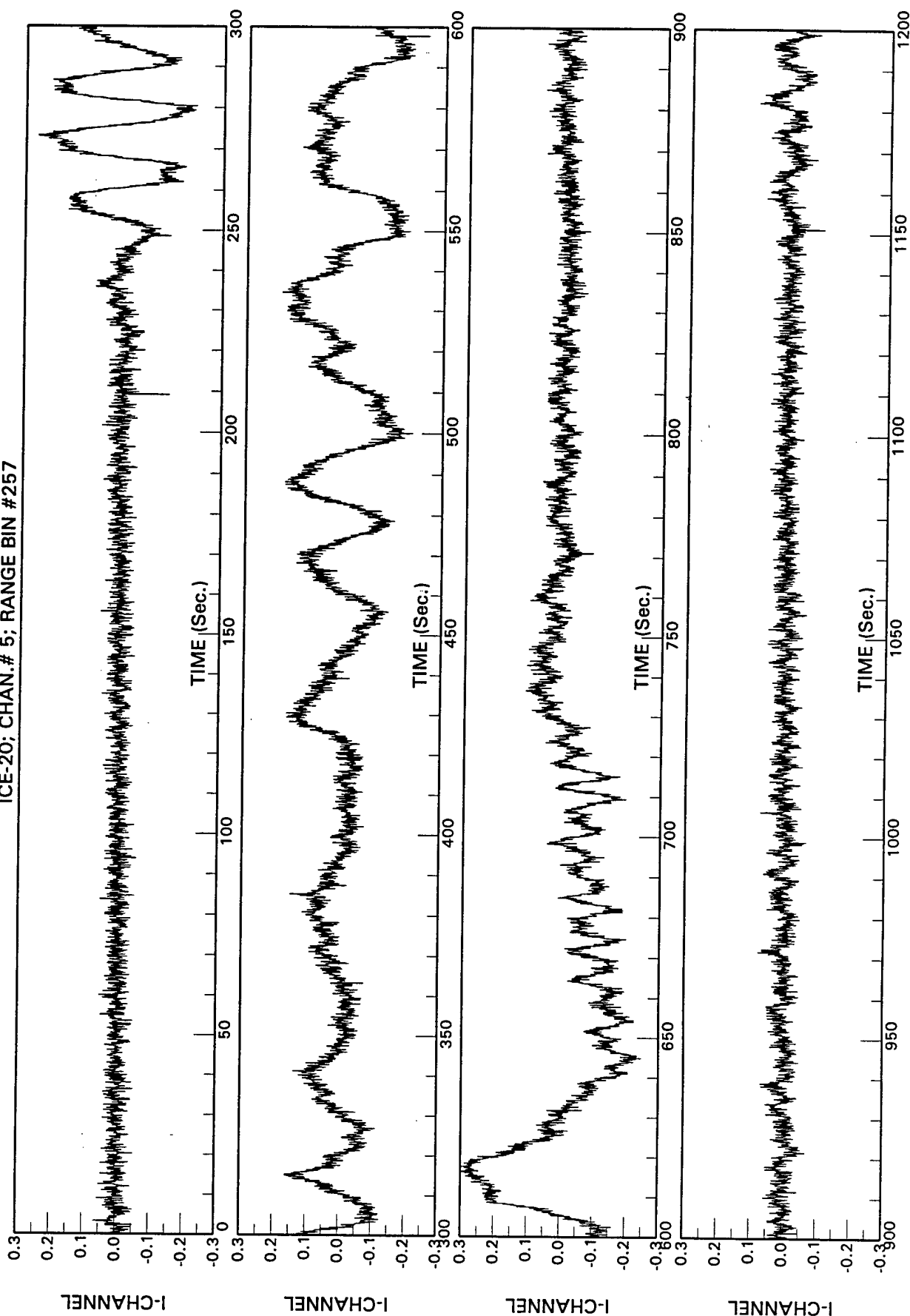
Figure A.9 In-phase waveform of a time series containing ionospheric clutter.

A number of questions are of interest in regard to the development of effective ionospheric clutter suppression schemes. The first is "what are the angles of arrival of the ionospheric clutter and how do they vary with time?" We already know that the direction of the ionospheric clutter is probably near the vertical direction. What is not known is the exact elevation angle and the number of directions in azimuth. To determine the true angles of arrival of a signal, one needs a two-dimensional array. Since we had only data collected from a linear array, we could only examine the apparent angles-of-arrival in azimuth.

To determine the angles-of-arrival of the ionospheric clutter in azimuth, we took the range samples from all the array elements and used the Capon [7] method to compute the angular response. The Capon method has a better angular resolution than the FFT approach for the same number of antenna elements. For the data in Figure A.9, we noticed that the ionospheric clutter began to be visible at time t > 250 sec. We examined 256 contiguous snapshots starting at time t=255 sec. Since the PRF of the radar was 12.5 Hz, the snapshots were 80 msec apart, and total time interval was 20.48 sec. Figure A.10 shows the angular responses of the radar for a particular range (315 km) as a function of snapshot number. It can be observed that, during this 20-second time interval, there were three prominent peaks, located at nominal azimuths of -68°, 5° and 26°, respectively. The mean and standard deviation of these three peaks, over the 256 snapshots, were -67.83°, +4.75°, 25.91° and 1.72°, 1.95°, and 1.91°, respectively. Hence the angles-of-arrival of the dominant peaks did not vary appreciably over the 20-second time interval.

The two peaks near +5° and +26° were not unusual because they could still come from a near-vertical direction but slightly off boresight in azimuth. The peak near -68°, however, was puzzling because of the large apparent azimuthal angle. A linear array cannot provide both azimuthal and elevation information on a signal simultaneously. If the signal is from the vertical direction, then the apparent azimuthal angle (as observed by a linear array) should be close to zero. However, since the linear array employed in the Cape Bonavista was comprised of monopole doublets, it is possible that increased mutual coupling effects could distort the elemental pattern at large squinting angles. Further investigation will be required to arrive at an explanation for this phenomenon.

Another question of interest is whether there is any correlation among the angles-of-arrival of the various Doppler components that constitute the ionospheric clutter spectrum. This is of interest because, if the directional characteristics of one Doppler component are similar to those for another, then the correlation properties estimated from one Doppler component may be used to cancel another Doppler. Figure A.11 shows the Doppler spectra of a time series, at a range of 323 km, for six contiguous CITs of 163.8-second duration. Strong ionospheric clutter components centred about zero Doppler were evident in the spectra. In addition, several spectral peaks were observed whose magnitudes were significantly higher than the clutter continuum.

Figure A.12 compares the angular responses of the largest Doppler components in the spectrum of Figure A.11b. In this figure, the strongest Doppler component was at +0.134 Hz, followed by the ones at -0.006 Hz and -0.195 Hz, respectively. We compared the angular responses of these three Doppler components, together with one (at -0.0916 Hz) selected from the clutter continuum. It can be observed that the correlation of the angular response was not very
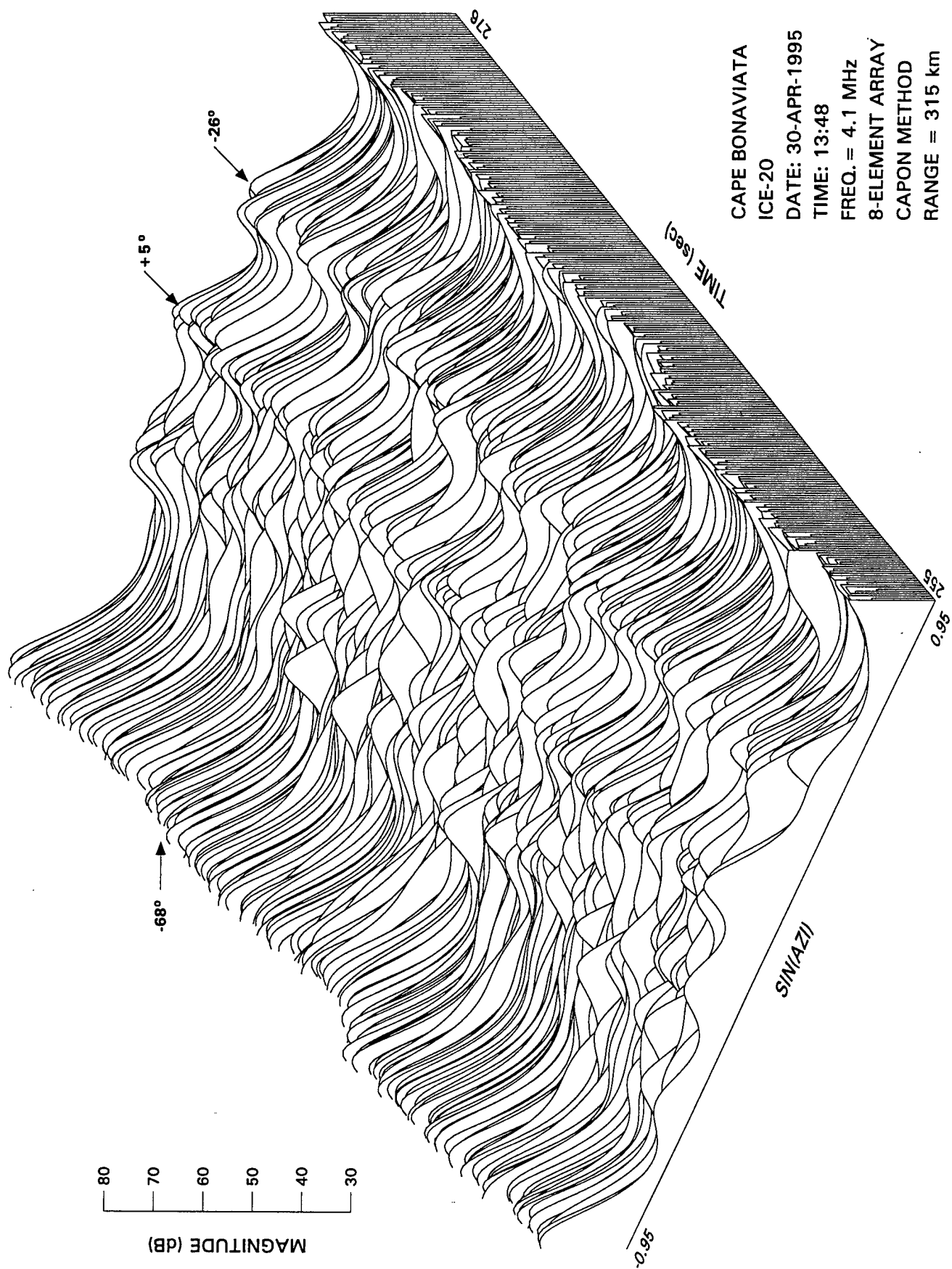
Figure A.10 Variation of angles-of-arrival of ionospheric clutter with time.

CAPE BONAVIATA
ICE-20
DATE: 30-APR-1995
TIME: 13:48
FREQ. = 4.1 MHz
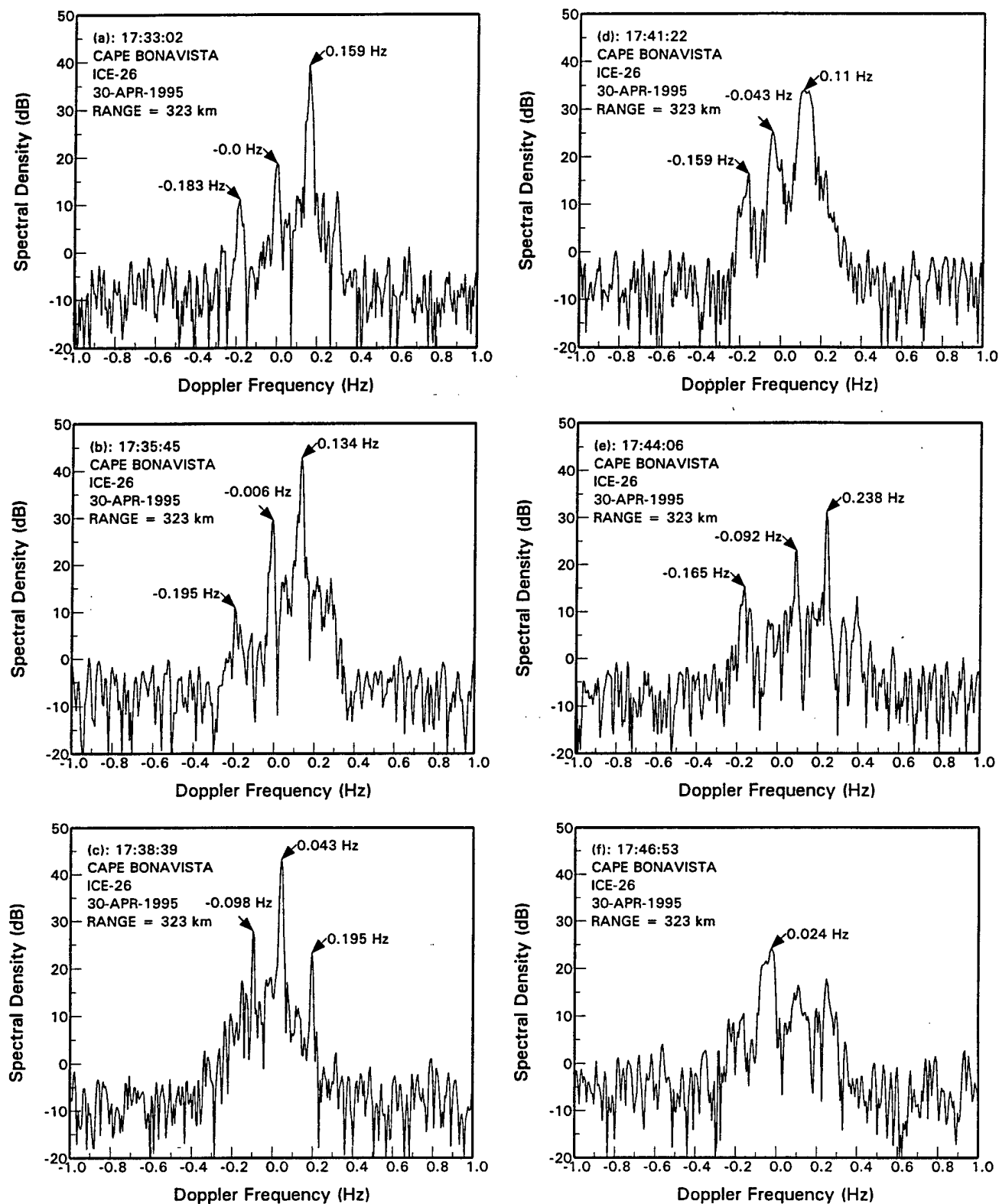8-ELEMENT ARRAY
CAPON METHOD
RANGE = 315 km

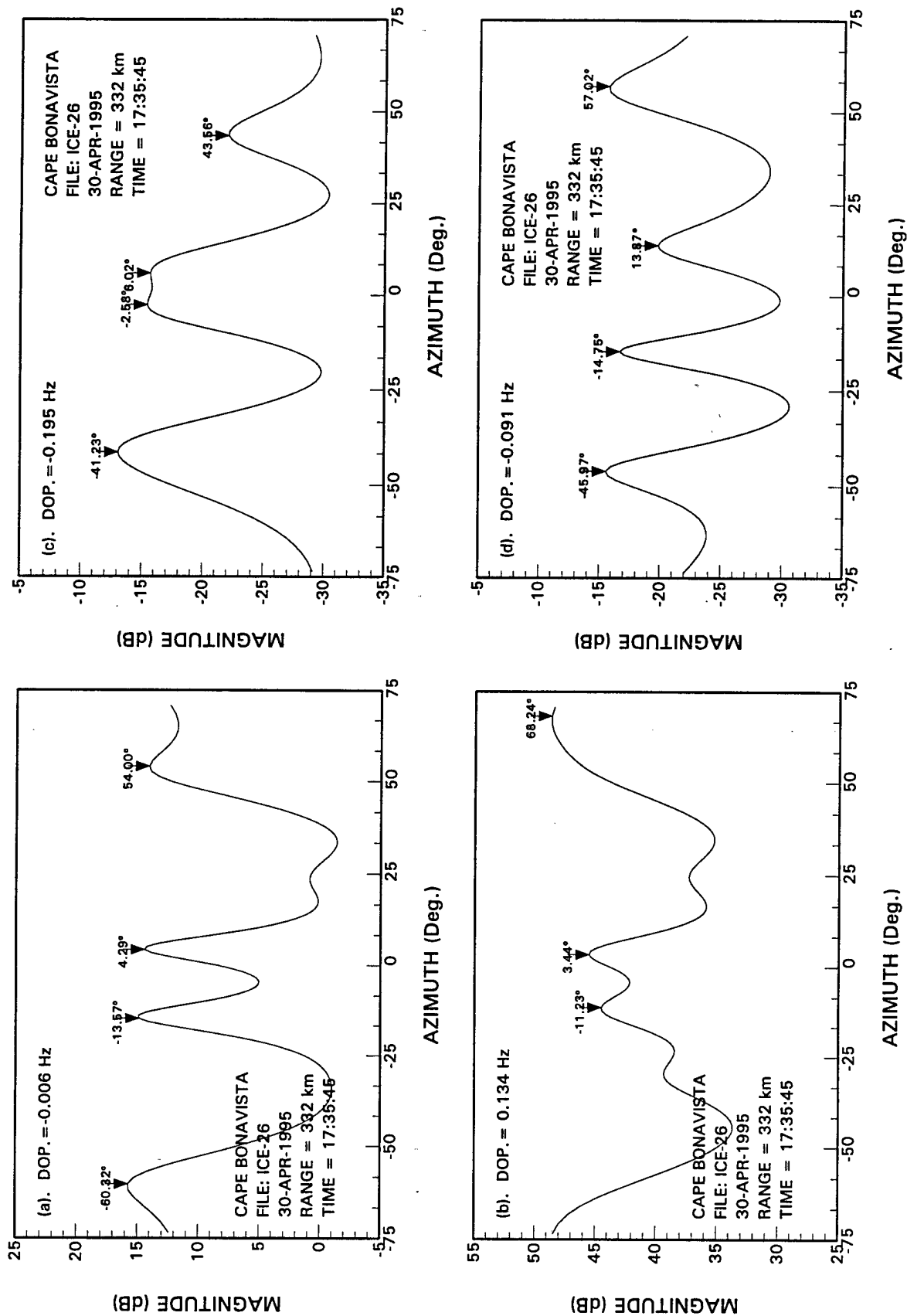Figure A.11 Spectra of ionospheric clutter in consecutive CITs.

Figure A.12 Angular response of different Doppler components of the ionospheric clutter in a particular range bin.

68

good between the four Doppler components. This implies that there is no guarantee that correlation characteristics estimated from one Doppler component can be used to cancel another Doppler component effectively.

DOCUMENT CONTROL DATA
(Security classification of title, body of abstract and indexing annotation must be entered when the overall document is classified)

1. ORIGINATOR (the name and address of the organization preparing the document. Organizations for whom the document was prepared, e.g. Establishment sponsoring a contractor's report, or tasking agency, are entered in section 8.) DEFENCE RESEARCH ESTABLISHMENT OTTAWA	2. SECURITY CLASSIFICATION (overall security classification of the document including special warning terms if applicable) UNCLASSIFIED

3. TITLE (the complete document title as indicated on the title page. Its classification should be indicated by the appropriate abbreviation (S,C or U) in parentheses after the title.)

AN INVESTIGATION IN INTERFERENCE SUPPRESSION FOR HF SURFACE WAVE RADAR (U)

4. AUTHORS (Last name, first name, middle initial)

CHAN, HING C. AND E.K.L. HUNG

5. DATE OF PUBLICATION (month and year of publication of document) April 2000	6a. NO. OF PAGES (total containing information. Include Annexes, Appendices, etc.) 69	6b. NO. OF REFS (total cited in document) 7

7. DESCRIPTIVE NOTES (the category of the document, e.g. technical report, technical note or memorandum. If appropriate, enter the type of report, e.g. interim, progress, summary, annual, or final. Give the inclusive dates when a specific reporting period is covered.)

DREO TECHNICAL REPORT

8. SPONSORING ACTIVITY (the name of the department project office or laboratory sponsoring the research and development. Include the address.)

Defence Research Establishment Ottawa
3701 Carling Avenue
Ottawa, Ontario, K1A 0Z4

9a. PROJECT OR GRANT NO. (if appropriate, the applicable research and development project or grant number under which the document was written. Please specify whether project or grant) 05AB11	9b. CONTRACT NO. (if appropriate, the applicable number under which the document was written)
10a. ORIGINATOR'S DOCUMENT NUMBER (the official document number by which the document is identified by the originating activity. This number must be unique to this document.) DREO TECHNICAL REPORT 2000-028	10b. OTHER DOCUMENT NOS. (Any other numbers which may be assigned this document either by the originator or by the sponsor.

11. DOCUMENT AVAILABILITY (any limitations on further dissemination of the document, other than those omposed by security classification)

(X) Unlimited distribution
( ) Distribution limited to defence departments and defence contractors; further distribution only as approved
( ) Distribution limited to defence departments and Canadian defence contractors; further distribution only as approved
( ) Distribution limited to government departments and agencies; further distribution only as approved
( ) Distribution limited to defence departments; further distribution only as approved
( ) Other (please specify):

12. DOCUMENT ANNOUNCEMENT (any limitation to the bibliographic announcement of this document. This will normally correspond to the Document Availability (11). However, where further distribution (beyond the audience specified in 11) is possible, a wider announcement audience may be selected.)

UNLIMITED

13. ABSTRACT (a brief and factual summary of the document. It may also appear elsewhere in the body of the document itself. It is highly desirable that the abstract of classified documents be unclassified. Each paragraph of the abstract shall begin with an indication of the security classification of the information in the paragraph (unless the document itself is unclassified) represented as (S), (C), or (U). It is not necessary to include here abstracts in both official languages unless the text is bilingual.)

(U)   An evaluation of the performance of the coherent sidelobe cancellation (CSLC) techniques in suppressing nighttime co-channel communications interference and ionospheric clutter in HF surface wave radars operating in coastal regions was carried out. In particular, the optimum order of execution among the three signal processing functions: (i) Doppler processing, (ii) digital beamforming and (iii) interference cancellation was of interest, in terms of signal-to-interference-plus-noise ratio (SINR) improvement and angle accuracy. The optimum order of execution between the above mentioned operations depends on the characteristics of the interference. In terms of ionospheric clutter, there is insufficient information to arrive at definitive conclusions. A preliminary examination of the temporal, spatial and spectral characteristics of ionospheric clutter was carried to aid in the development of mitigating algorithms.

14. KEYWORDS, DESCRIPTORS or IDENTIFIERS (technically meaningful terms or short phrases that characterize a document and could be helpful in cataloguing the document. They should be selected so that no security classification is required. Identifiers, such as equipment model designation, trade name, military project code name, geographic location may also be included. If possible keywords should be selected from a published thesaurs, e.g. Thesaurus of Engineering and Scientific Terms (TEST) and that thesaurus-identified. If it is not possible to select indexing terms which are unclassified, the classification of each should be indicated as with the title.)

RADAR
HIGH FREQUENCY
HF
COHERENT SIDELOBE CANCELLER
SURFACE WAVE
OVER-THE-HORIZON
OTH RADARS
SURVEILLANCE
IONOSPHERE
CLUTTER
INTERFERENCE
NOISE

The Defence Research
and Development Branch
provides Science and
Technology leadership
in the advancement and
maintenance of Canada's
defence capabilities.

Leader en sciences et
technologie de la défense,
la Direction de la recherche
et du développement pour
la défense contribue
à maintenir et à
accroître les compétences
du Canada dans
ce domaine.

DEFENCE **DÉFENSE**

www.crad.dnd.ca